université de BORDEAUX

THÈSE PRÉSENTÉE
POUR OBTENIR LE GRADE DE

DOCTEUR DE

L'UNIVERSITÉ DE BORDEAUX

ÉCOLE DOCTORALE SCIENCES PHYSIQUES DE L'INGENIEUR

SPÉCIALITÉ : MÉCANIQUE

Par Asmae MOUTAOIKIL

Méthodes expérimentales et numériques pour la caractérisation thermique des éléments adaptatifs de l'enveloppe du bâtiment

Sous la direction de : Laurent MORA
(Co-directeur : Christian INARD)

Date de soutenance : 08/07/2026

Membres du jury :

M. DEFER Didier	Professeur, Université d'Artois	Rapporteur
M. ROUCHIER Simon	Maître de conférences HDR, Université Savoie Mont Blanc	Rapporteur
Mme. MAGNIONT Camille	Professeure, Université de Technologie Tarbes	Présidente du jury
Mme. LEPILLER Valérie	Maîtresse de conférences, Université de Franche-Comté	Examinatrice
M. RECHT Thomas	Maître de conférences, Université de Bordeaux	Examinateur
M. MORA Laurent	Professeur, Université de Bordeaux	Directeur de thèse
M. INARD Christian	Professeur, Université de La Rochelle	Co-directeur de thèse

Membres invités :

Mme. VOGT WU Tingting	Maîtresse de conférences, Université de Bordeaux	Co-encadrante
M. DUGUE Antoine	Responsable R&D, Docteur, NOBATEK	Invité

THESIS PRESENTED
TO OBTAIN THE QUALIFICATION OF

DOCTOR OF

THE UNIVERSITY OF BORDEAUX

DOCTORAL SCHOOL OF PHYSICAL SCIENCES AND ENGINEERING

SPECIALITY: MECANICS

By Asmae MOUTAOIKIL

Experimental and numerical methods for the thermal performance characterization of adaptive elements of building envelope

Under supervision of: Laurent MORA
(Co-director: Christian INARD)

Date of defense: 08/07/2026

Jury members:

M. DEFER Didier	Professor, Université d'Artois	Reviewer
M. ROUCHIER Simon	Associate professor, HDR, Université Savoie Mont Blanc	Reviewer
Mme. MAGNIONT Camille	Professor, Université de Technologie Tarbes	Jury president
Mme. LEPILLER Valérie	Associate professor, Université de Franche-Comté	Examiner
M. RECHT Thomas	Associate professor, Université de Bordeaux	Examiner
M. MORA Laurent	Professor, Université de Bordeaux	Thesis director
M. INARD Christian	Professor, Université de La Rochelle	Thesis co-director

Invited members:

Mme. VOGT WU Tingting	Associate professor, Université de Bordeaux	Co-supervisor
M. DUGUE Antoine	R&D Manager, PhD, NOBATEK	Invited

Méthodes expérimentales et numériques pour la caractérisation thermique des éléments adaptatifs de l'enveloppe du bâtiment

Résumé

L'Union européenne vise à atteindre la neutralité carbone d'ici 2050, et le secteur de la construction doit contribuer à cet objectif, notamment car les bâtiments représentent 40 % de la consommation d'énergie finale et 36 % des émissions de gaz à effet de serre de l'Union européenne. L'enveloppe du bâtiment est l'interface principale entre l'environnement intérieur et extérieur, régissant ainsi les pertes de chaleur en hiver, les gains solaires, l'éclairage naturel, *etc.* Elle a donc un impact sur la consommation d'énergie de chauffage et de climatisation ainsi que sur le confort des occupants. Dans ce contexte, l'amélioration des performances thermiques des façades joue un rôle clé. Les façades adaptatives apparaissent comme une solution prometteuse pour répondre à ces enjeux. Ce type de façade est définit comme un élément d'enveloppe de bâtiment capable de changer ses propriétés selon les conditions aux limites ou les systèmes de contrôle utilisés.

Une façade adaptative est caractérisée par un comportement thermique dynamique, qui peut profiter des conditions climatiques pour améliorer le confort de l'occupant et réduire la consommation du chauffage ou de la climatisation. Malgré ce potentiel, l'application de ce type de façade dans la construction se heurte à plusieurs verrous. Les normes et méthodes existantes pour caractériser les performances thermiques des façades reposent sur l'hypothèse des propriétés de matériaux invariantes. L'indicateur de performance (KPI) calculé se résume alors à une seule valeur, qui ne rend pas compte des états dynamiques d'une façade adaptative. De plus, l'utilisation d'un logiciel de simulation pour simuler ces états nécessite la modélisation de chaque état susceptible de changer rapidement selon les conditions environnementales ainsi que les opérations de contrôle, ce qui complique davantage la caractérisation thermique des façades adaptives. Par ailleurs, cette difficulté peut impacter la phase de la conception préliminaire de la façade adaptative, particulièrement le choix du design, de l'orientation optimale de la façade et des opérations de contrôle associées.

À cette fin, la contribution principale de cette thèse est de proposer une méthodologie basée sur des scénarios expérimentaux et un modèle numérique, pour caractériser les performances thermiques de façades adaptatives, avec la finalité d'estimer un indicateur de performance associé. La méthodologie proposée s'articule autour de deux étapes principales. La première étape s'appuie sur la caractérisation de la cellule d'essai extérieure équipée d'une façade de référence, afin d'isoler la contribution propre de l'élément adaptatif. Les mesures expérimentales sont utilisées pour calibrer la cellule d'essai et la validation le modèle numérique. La deuxième étape concerne la caractérisation de la façade adaptative. En effet, cette dernière peut moduler un ou plusieurs phénomènes thermiques qui nécessitent des protocoles expérimentaux spécifiques et un ajustement du modèle numérique.

Cette méthodologie a été appliquée à un brise-soleil à lames orientées en diagonale pour évaluer sa transmittance solaire directe, en utilisant une cellule test équipée d'un double vitrage. Un

modèle RC est entraîné avec ces scénarios expérimentaux pour estimer la transmittance solaire directe. Ces résultats sont comparés avec la transmittance solaire directe calculée par la méthode de lancer de rayons (BSDF, *Bidirectional Scattering Distribution Function*) avec un CV(RMSE) de 24 %. Afin d'évaluer l'efficacité de ce prototype, différentes orientations de façade ont été testées, ce qui a permis de déterminer, dès les premières étapes de la conception, l'orientation plein sud comme la plus appropriée pour la configuration de ce dispositif d'ombrage avec la compaigne experimentale. Ce travail contribue à l'estimation de la transmittance solaire dynamique basée sur les données, en fonction de l'angle d'incidence solaire et de l'azimut local, pour les dispositifs d'ombrage à géométrie complexe.

Mots-clés: Performance thermique des bâtiments; Façade adaptative; Modèle RC; Transmittance solaire; BSDF

Experimental and numerical methods for the thermal performance characterization of adaptive elements of building envelope

Abstract

European union aim to carbon neutrality target by 2050, and the architecture must contribute to achieve this objective, especially that building sector account for 40% of final energy consumption and 36% of greenhouse gas emission of European union. The building envelope façade is an interface between the indoor and outdoor environment. Thus, it is governing the heat loss during winter, solar gain during summer and natural daylight *etc*. which in turn can impact the heating and cooling loads energy consumption as well as occupant's comfort. In this context, adaptive façade appeared to be a promising solution to address these challenges. This façade type is defined as a building envelope element that can change its properties according to boundary conditions and used control systems. However, the thermal characterization of such a system remains challenging.

An adaptive façade is characterized with a dynamic thermal behaviour, and it can take advantage of climate conditions to ensure occupant's comfort and reduce heating and cooling loads energy consumption. Despite this potential, the application in construction of these façade type encounter various challenges. The existing standards and methods to characterize the thermal performance of façade are based on a hypothesis which consider material properties as static. The calculated key performance indicator (KPI) is thus resumed to one value, which does not consider the dynamic states of an adaptive façade. In addition, the use of a simulation tool to model those states require a modelling of each state that may change rapidly according to climate conditions and control operations, which complicate the thermal characterization of adaptive façade. Moreover, these challenges can impact the early-design stage phase of an adaptive façade, particularly the optimal design and façade orientation selection, within the corresponding control operations.

Therefore, the main contribution of this thesis is to propose a hybrid general methodology based on experimental scenarios and a numerical model to characterize thermal performance of adaptive façade, in order to estimate a corresponding key performance indicator. To this aim, the methodology proposed is organized into two main steps: the first step is based on characterizing the outdoor test cell with a reference façade, in order to isolate the main contribution of the adaptive façade. Those measurements are used to calibrate the test cell and validate the numerical model. The second step correspond to characterize the adaptive façade. Since this later can modulate one or more thermal phenomena that require a specific experimental protocols and model adjustment.

To apply this methodology, a case of study was conducted to evaluate the direct thermal transmittance of a shading device with a sunshade with diagonal slats. Using a dedicated outdoor test cell equipped with a double glazing. An RC model combined with experimental measurements is used to estimate the dynamic solar transmittance of the diagonal shading

device. Those results are compared with the theoretical direct solar transmittance calculated by a ray tracing technic: (BSDF, *Bidirectional Scattering Distribution Function*), the resulted CV(RMSE) between both is 24%. To assess the effectiveness of this prototype, different façade orientations were experimented, which leads to an early design stage decision of the south orientation as the best orientation for this configuration and experimental compaign. This work contributes to the dynamic solar transmittance estimation in function of solar incidence angle and local azimuth for complex geometry shading device.

Keywords: Building thermal performance; Adaptive façade; RC model; Solar transmittance; BSDF

Research unit



Institut de Mécanique et d'Ingénierie

CNRS, UMR 5295

http://i2m.u-bordeaux.fr

Département Transferts Fluides Énergétique (TREFLE)

351 Cours de la Libération

33405 Talence

France

Acknowledgements

My sincere gratitude goes first to my director Prof. Laurent MORA for his involvement, and scientific guidance throughout this work. I am also grateful to my co-director Prof. Christian INARD, for his insightful suggestions on research direction, and timely feedback. I would like to thank my co-supervisor Dr. Tingting VOGT WU, for her involvement and availability whenever I need help, and my co-supervisor Dr. Thomas RECHT for his valuable feedback, and positive coaching through the different stages of this PhD project, which helped me move forward.

Thanks to the jury members of this thesis, particularly the reviewers Prof. Didier DEFER, and Dr. Simon ROUCHIER, for taking the time to evaluate this work with care and expertise. Thanks to the examiners Prof. Camille MAGNIONT and Dr. Valérie LEPILLIER for their comments and suggestions, which greatly enriched this research.

I also thank Dr. Antoine DUGUE from Nobatek, for the provided materials for my experiments, and also technical feedback. Many thanks to Dr. Tessa HUBERT who provided me with valuable data analysis library resources and feedback on my work, and to Benjamin VARELA for his help during experimental work. I extend my thanks to the colleagues from ENSAM and Nobatek who kindly gave their help whenever the test cell needed to be moved or handled. I also thank all I2M lab members, the TREFLE department, and E3BUS group, for the provided help through the years. I gratefully acknowledge the Metabuilding project for funding this PhD.

A special thanks goes to my family: parents, siblings, and cats for their unconditional love, and encouragements. I'm deeply grateful for my friends, whom I consider my second family: Jinxia who was my sunshine during my PhD journey, hopefully we met in person again and eat Baozi! Feriel, Zineb, Loubna, Angela, Habiba, Adela, Tinuy, and Zhansaya for their kindness, encouragements, and constant presence. I would also thank my sports class, coach Yannick and all the classmates, for the joyful moments and positive energy.

Finally, I would like to thank myself, for being resilient, and for holding on to my dreams.

Content

General introduction 17
Chapter 1: Adaptive façades and their thermal performance evaluation: a review 20
1.1 Introduction 21
1.2 Adaptive façade: concept and overview 21
1.2.1 Terminology and definition 22
1.2.2 Classification of adaptive façade 23
1.2.3 Control strategies 25
1.3 Building thermal performance evaluation methods and KPIs 27
1.3.1 General functions of building façade 27
1.3.2 Experimental thermal characterization methods 29
1.3.3 Passive façade performance indicators 33
1.3.3.1 Heat transfer characterization 33
1.3.3.2 Indoor air quality/flow characterization 35
1.3.3.3 Daylight characterization 36
1.3.3.4 Acoustic comfort characterization 37
1.4 Focus on adaptive façade thermal performance evaluation approaches 38
1.5 Conclusion and thesis problematic 43
Chapter 2: Methodology for adaptive façade thermal characterization 44
2.1 Introduction 45
2.2 Methodological framework 48
2.2.1 Step 1: Inventory of heat transfer modes and associated KPIs 50
2.2.2 Step 2: Model formulation 53
2.2.3 Step 3: Model calibration and KPI identification 55
2.3 Limitations 60
2.4 Conclusions 61
Chapter 3: Thermal performance characterization of a complex shading device 62
3.1 Introduction 63
3.2 Application of the methodology 65
3.2.1 Description of the studied shading device 65
3.2.2 Experimental setup 68
3.2.3 Inventory of heat transfer phenomena 70

3.2.4 Model formulation: two-steps characterization strategy 74
3.2.4.1 Theoretical solar transmittance 86
3.2.4.2 Instrumentation and sensors positioning 100
3.2.4.3 The RC model validation steps 105
3.3 Conclusion 136
3.4 Limitations 137
General conclusion and perspectives 138
Scientific publications 141
Annex A: Estimation of the interior thermal capacitance of the Hotbox 142
Annex B: Shading ring installation for the pyranometer 143
Annex C: Irradiance transposition 144
Annex D: Glazing and envelope surface temperatures and solar irradiance measurements 145
10 References 146

List of tables

Table 1-1: Designating terms of adaptive facade and their definition 23
Table 1-2: Advantages and limitations of test facility types [37], [38], [39] 30
Table 1-3: Types of outdoor test cells [37], [38], [39] 32
Table 1-4: List of standards for building performance evaluation 40
Table 2-1: Steps of the methodology and the guiding questions 50
Table 2-2: Adaptive heat transfer mode and the corresponding indicators 52
Table 2-3: Example of adaptive façade and associated passive façade that can be used as a baseline for the model 54
Table 2-4: Summary of some protocols that can be used to define the test cell thermal parameters 56
Table 3-1: Description of the shading solution 66
Table 3-2: Detailed RC parameters values and sources 78
Table 3-3: Dimensional characteristics of the glazing 88
Table 3-4: Optical and thermal characteristics of the double-glazing using WINDOW calculations 88
Table 3-5: Radiance convention for BSDF file 96
Table 3-6: Position of experiment sensors 102
Table 3-7: Bounds for each parameter in sensitivity analysis 108
Table 3-8: Obtained metrics values CV(RMSE) and NMBE for co-heating with the ASHRAE guideline hourly metrics criteria for a well calibrated model 111
Table 3-9: Parameters and their variation for sensitivity analysis 116

Table 3-10: Identified values of the parameters: Rinf&tb, Cenv and calibsolar 118
Table 3-11: Obtained calibration metrics alongside with ASHRAE recommended hourly values for outdoor experiment without the shading toward the South 118
Table 3-12: Obtained calibration metrics alongside with ASHRAE recommended hourly values for outdoor experiment with the shading toward South 128
Table 6-1: Inventory of equipment inside the hotbox and their thermal capacitance 142
Table 7-1: Adjustment table for shading ring [151] 143

List of figures

Figure 1-1: overall thesis strategy 19
Figure 1-1: Examples of adaptive façade design [9] 22
Figure 1-2: Adaptive façade general categories proposed by COST project [32] 24
Figure 1-3 : Classification of adaptive façades proposed by COST project [32] 25
Figure 1-4: Closed loop control system [34] 25
Figure 1-5: Open-loop control system [34] 26
Figure 1-6: Interrelationship between physical domains in building [12] 27
Figure 1-7 : The façade as an interface between indoor and outdoor [36] 28
Figure 1-8: European projects aimed at providing test beds, methods for measuring and evaluating thermal performance of buildings 31
Figure 1-9: 3D perspective of the O3BET built in Bordeaux (front and rear view) 32
Figure 1-10: Picture of outdoor test cells [37] 33
Figure 1-11: A schematic overview of adaptive façade technologies and their dominant physical domain [66] 39
Figure 1-12: Linear regression analysis to identify U-value for a conventional and a PCM double glazing unit (DGU) [67] 40
Figure 2-1: Conceptual triangle linking experiment, model and protocol 46
Figure 2-2: The proposed methodology steps 47
Figure 2-3: Classical flowchart of system identification[80] 48
Figure 2-4: Diagram showing the relation between dynamic KPI and triggering variable 52
Figure 2-5: Flowchart of the sub-steps within the KPIs identification step 59
Figure 3-1: Application of the methodological framework 64
Figure 3-2: View of the diagonal shading 65
Figure 3-3: View of the oblong slats shape 65
Figure 3-4: Diagonal shading concept illustration 66
Figure 3-5: Illustration of slat tilt angles of the diagonal shading 67
Figure 3-6: Horizontal or vertical layout of the Hotbox [118] 69
Figure 3-7: 3D schematic view of the Hotbox highlighting the tested façade (front view) and the door (rear view) 69
Figure 3-8: Picture of the Hotbox 69
Figure 3-9: View of the shading inside and outside of the Hotbox 70

Figure 3-10: Metal support to hold the shading in front of the glazed façade of the Hotbox 70
Figure 3-11: Heat transfer inventory of the opaque envelope of the hotbox 71
Figure 3-12: Glazed surface heat transfer inventory illustration 72
Figure 3-13: Components of the solar gain transmitted by the fenestration system 74
Figure 3-14: Simplified heat exchanges used in the RC model 76
Figure 3-15: The proposed RC model 77
Figure 3-16: Linear thermal bridges location in the Hotbox 82
Figure 3-17: Door of the Hotbox insulation 82
Figure 3-18: Illustration of the three phases to determine air leakage using pressure decay method [96] 84
Figure 3-19: Pressure decay installation scheme and experimental setup 85
Figure 3-20: Pressure difference over time during the pressure decay test applied to the Hotbox 85
Figure 3-21: Sun path diagram (Global Solar Atlas, 2025) in Bordeaux 86
Figure 3-22: Solar geometry illustration 87
Figure 3-23: Solar transmittance $\tau \mathrm{direct}, \mathrm{g}$ of the double glazing from WINDOW 7.8 LBNL software [128] 89
Figure 3-24: Solar front reflectance of the glazing in function of solar incidence angle from WINDOW 7.8 LBNL software [128] 89
Figure 3-25: Solar absorbance of the glazing in function of solar incidence angle using WINDOW 7.8 LBNL software [128] 90
Figure 3-26: Time-varying theoretical direct solar transmittance $\tau \mathrm{direct}, \mathrm{g}$ of a double glazing 4/12/4 for a façade toward the south during October 7 in Bordeaux for South orientation . 90
Figure 3-27: Seasonal evolution of $\tau \mathrm{direct}, \mathrm{g}$ for south-oriented 4/12/4 double glazing in Bordeaux 91
Figure 3-28: Profile and front view of the diagonal shading 92
Figure 3-29:Polar and azimuthal angles of incident and exiting directions [135] 92
Figure 3-30: Cosine projection and 3D view of Klems patches 93
Figure 3-31: Difference between specular and diffuse reflectance [138] 94
Figure 3-32: A scheme to illustrate the coordinate system in Radiance 95
Figure 3-33: The objview illustration of the complete system: glazing+shading 95
Figure 3-34: Direct transmittance of the shading with the glazing using BSDF $\tau \mathrm{direct_sh_bsdf}$ 97
Figure 3-35: Direct transmittance of the glazing with shading $\tau \mathrm{direct_sh_bsdf}$ for $\theta = 30°$. 98
Figure 3-36: Direct transmittance of the glazing with shading $\tau \mathrm{direct_sh_bsdf}$ for $\theta = 60°$. 98
Figure 3-37: Decomposition of a reflected solar ray on the shading slats 99
Figure 3-38: the 3D shading model with: (a) total reflectance of 5% and (b) total reflectance of 50% 99
Figure 3-39: Difference of both simulations $\tau 50\%$-$\tau 5\%$ in function of θ and local azimuth φ 100
Figure 3-40 Front view of the test cell and used sensors 101

Figure 3-41: Glazing temperature sensors positioning 103
Figure 3-42: Floor temperature sensors positioning on eastern zone 103
Figure 3-43: Indoor air temperature sensors placement 104
Figure 3-44: Progressive validation steps of the RC model with different experimental protocols 105
Figure 3-45: Difference between the indoor and the outdoor air temperature Tai-Tae (Co-heating test) 106
Figure 3-46: Evolution of the air temperature difference between two indoor air temperature sensors (Co-heating test) 106
Figure 3-47: RC model for the co-heating test 107
Figure 3-48: Total dynamic Sobol indices of RC model parameters influencing Tai (Co-heating test) 109
Figure 3-49: Total dynamic Sobol indices of RC model parameters influencing Tenv (Co-heating test) 110
Figure 3-50: Measured vs calculated indoor air temperature using the identified value of Rinf&tb (Co-heating test) 111
Figure 3-51: Measured vs calculated indoor surface envelope temperature using the identified value of Rinf&tb (Co-heating test) 112
Figure 3-52: Geographical location of the experimental site 112
Figure 3-53: Picture of the experiment without the shading 113
Figure 3-54: Global vertical irradiance (GVI) and diffuse horizontal irradiance (DHI) over time (Outdoor test without shading) 113
Figure 3-55: Interior and exterior air temperature variation (Outdoor test without shading) 114
Figure 3-56: Evaluation of indoor air temperature stratification (Outdoor test without shading) 114
Figure 3-57: RC model for outdoor experiment without shading 114
Figure 3-58: Total dynamic sensitivity analysis of RC model parameters influencing Tai (Outdoor test without shading). 117
Figure 3-59: Total dynamic sensitivity analysis of RC model parameters influencing Tenv (Outdoor test without shading) 117
Figure 3-60:Measured vs calculated indoor air temperature with the identified parameters values (Outdoor test without shading) 119
Figure 3-61: Measured vs calculated indoor surface envelope temperature with the identified parameters values (Outdoor test without shading) 119
Figure 3-62: Experimental set with the shading device 120
Figure 3-63: Measured global vertical irradiance (GVI) and diffuse horizontal irradiance (DHI) over time (Outdoor test with shading) 120
Figure 3-64: Interior and exterior air temperature variation (Outdoor test with shading) 121
Figure 3-65: Evaluation of indoor air temperature stratification (Outdoor test with shading) 121

Figure 3-66: RC model for with the shading experiment 121
Figure 3-67: Geometric relationship between local, surface and solar azimuth angles 123
Figure 3-68:Time-varying angle φ on the 14th October with shading for South orientation 123
Figure 3-69: Time-varying angle θ on the 14th October with shading for South orientation 124
Figure 3-70: Steps to estimate $\tau direct, sh, RC$ from RC model and B-spline function 126
Figure 3-71: Estimation of direct transmittance $\tau direct, sh, RC$ value for South orientation 127
Figure 3-72: Effect of B-spline extremity knots length on the estimation of $\tau direct_sh_RCt$ for South orientation 127
Figure 3-73: Effect of $\tau diff, sh$ diffuse on the $\tau direct_sh_RCt$ estimations for South dataset 128
Figure 3-74: Measured and calculated indoor air temperature (Outdoor test with shading) 128
Figure 3-75: Measured and calculated indoor surface envelope temperature (Outdoor test with shading) 129
Figure 3-76: Schematic representation of the obtention of $\tau direct_sh_bsdft$ derived from BSDF calculations $\tau direct_sh_bsdf\theta, \varphi$ 130
Figure 3-77: The obtained discrete $\tau direct_sh_bsdft$ (South orientation case) 130
Figure 3-78: The obtained smooth $\tau direct_sh_bsdft$ (South orientation case) 131
Figure 3-79: Angular distribution of theoretical direct transmittance of the glazing with shading $\tau direct, shBSDF$ (South orientation case) 131
Figure 3-80: Comparison between $\tau direct_sh_bsdft$ and $\tau direct_gt$ (South orientation case) 131
Figure 3-81: Comparison between $\tau direct_sh_bsdft$ and $\tau direct_sh_RCt$ (South orientation case) 132
Figure 3-82: Transmitted direct heat flux using calculated and theoretical direct transmittance (South orientation case) 132
Figure 3-83: Comparison between direct transmitted solar energy using RC model and BSDF (South orientation case) 133
Figure 3-84: Shading integration and glazing only direct solar transmittance cumulative energy (South orientation case) 134
Figure 3-85: South-West orientation experiment using the shading (Surface azimuth=270°) 135
Figure 3-86: Comparison between $\tau direct, sh, RC$ and $\tau direct, sh, bsdf$ (South-West orientation case) 135
Figure 3-87: Comparison of cumulative energy using BSDF and RC model (South-West orientation case) 136
Figure 3-88: Shading integration and glazing only direct solar transmittance cumulative energy (South-West orientation case) 136
Figure 7-1: Shading ring adjustment to measure the diffuse horizontal irradiance DHI 143

Figure 9-1: Global vertical and horizontal irradiance over time (without shading experiment toward the south) 145
Figure 9-2: Evolution of inner surface temperature for each opaque façade 145
Figure 9-3: Evolution of inner glazing surface temperature 145

Nomenclature

Latin symbols

$A_{env,o}$	Total surface of outer opaque envelope	m^2
$A_{env,i}$	Total surface of inner opaque envelope	m^2
A_g	Glazing surface	m^2
C_{env}	Thermal capacitance of the envelope	kJ/K
C_{in}	Thermal capacitance of the indoor air	kJ/K
$Direct_\gamma$	Direct beam solar radiation for an orientation γ	W/m^2
$Diff_\gamma$	Diffuse solar radiation for an orientation γ	W/m^2
d_i	Thickness of a wall layer number i	m
E	Accumulated solar energy	Wh/m^2
g	Solar gain factor	$-$
h	Solar elevation angle	$°$
h_r	Radiative surface heat transfer coefficient	W/m^2K
h_{cv}	Convective surface heat transfer coefficient	W/m^2K
HLC	Heat loss coefficient	W/K
L	Length	m
P_h	Injected heating power	W
q	Direct solar heat flux	W/m^2
q_i	Secondary heat transfer factor to the interior	$-$
q_o	Secondary heat transfer factor to the outside	$-$
R	Thermal resistance	m^2K/W
S_i	Sensitivity index	$-$
T_{ai}	Indoor air temperature	$°C\ or\ K$
T_{ae}	Outdoor air temperature	$°C\ or\ K$
T_{env}	Indoor envelope surface temperature	$°C\ or\ K$
T_{gi}	Indoor glazing surface temperature	$°C\ or\ K$
T_{RM}	Radiant mean temperature	$°C\ or\ K$
W_i	Weighting coefficient	$-$
U	Thermal transmission coefficient	W/m^2K

Greek symbols

τ	Transmittance	$-$
α	Absorbance	$-$
ρ	Reflectance	$-$
ε	Emissivity	$-$
θ	Incidence angle	$°$
γ	Surface azimuth angle	$°$
γ_s	Solar azimuth angle	$°$
φ	Local azimuth angle	$°$
ω	Hour angle	$°$
δ	Declination angle	$°$

σ	Stefan–Boltzmann constant 5.67×10^{-8}	$\frac{W}{m^2K^4}$
β	Tilt angle of façade from horizontal plan	$^\circ$
Ω	Solid angle	$^\circ$
μ	Tilt angle of the diagonal shading from horizontal plan	$^\circ$
ϑ	Profile tilt angle of diagonal shading	$^\circ$
ϕ	Heat flux density	W/m^2
λ	Thermal conductivity	W/mK
ψ	Linear thermal transmittance	W/mK
Δ	Difference between two variables	

Subscripts

abs	Absorbed
ai	Indoor air
$bsdf$	Bidirectional scattering distribution function
c	Corner
ce	Ceiling
$conde$	Conductive
$conv$	Convective
$direct$	Direct component
$diff$	Diffuse component
env	Envelope
$envi$	Environment
f	Floor
int	Interior
ext	Exterior
$inf\&tb$	Infiltration and thermal bridge
LW	Long wave
g	glass
o	outer
in	inner
ray	Radiative
ref	Reflective
sh	Shading
se	Exterior surface
si	Interior surface
sky	Sky
$surf$	Surface
tr	Transmitted
w	Window

Abbreviation

BSDF	Bidirectional scattering distribution function
BTDF	Bidirectional transmittance distribution function

CV(RMSE)	Coefficient of variation of the root mean square error
DHI	Diffuse horizontal irradiance
GHI	Global horizontal irradiance
GVI	Global vertical irradiance
HTB	Heat transfer coefficient due to thermal bridge
HVAC	Heating ventilating and air conditioning
IAE	Integral of absolute error
MBLabs	METABUILDING Labs Project
MCP	Model predictive control
NMBE	Normalized mean bias error
OSB	Oriented strand board
PCM	Phase change material
RC	Resistance capacitance model
RMSE	Root mean square error

General introduction

In the context of climate change challenges and increasing energy demand, the building envelope plays a major role in strategies implementation to reduce energy consumption. Building façade act as an interface between indoor and outdoor environment, which can directly influence the heat transfer through the building, thus, the energy consumption of Heating, Ventilating and Air Conditioning (HVAC) loads. Consequently, façade performance is a relevant key to consider during early design stage of a building. In this framework, in order to improve energy efficiency of buildings and occupant's comfort, adaptive façades have emerged as a promising solution, they are envelope façades capable to adjust their properties such as: taking advantage of the passive solar gains in winter; protect from those in summer; achieve high air tightness while potentially benefitting from natural ventilation. The adjustment of those properties can be achieved by using control operating system. However, it is necessary to select the suitable optimal adaptive façade design for each building specifics. In addition, this early design stage selection is often a complex process due to the interdependencies between the façade properties and the environmental variables. Simulation tools can be used, but complex modelling, a lack of accurate existing models, or high computational costs often hinder the capacity to do so. Moreover, such an approach might not provide a realistic performance characterization. Thus, there is a need to support the selection of appropriate adaptive façade design at early-stage design and the corresponding control operations under real climate conditions. Outdoor experiments using test cells or in situ buildings are an emerging approach for the performance characterization of building elements. Since the European projects PASSYS (I and II) (1989) and PASLINK (1994), multiple outdoor experimental cells or buildings were constructed across Europe, to characterize building elements in different climate conditions. However, achieving an optimal adaptive design is a challenging task, because there is still a need for a general framework using such an experimental tool to characterize adaptive façades, especially on the thermal performance level. Moreover, the shift from passive to adaptive façades introduces new challenges, and the main complexity of the thermal performance characterization of such a façade type lies in its non-linear adaptive behaviour, which implies that the desired key performance indicators (KPIs) would need a specific pipeline. In terms of control operation, the standard ISO/DIS 52016-3 [1] has already proposed the reference scenarios for control operations to evaluate some types of adaptive shading device, in order to calculate hourly heating and cooling energy needs, either in residential or industrial uses.

Objectives and thesis organization

The objective of this PhD thesis is to propose a general methodology to characterize the thermal behaviour of adaptive façade using experimental and numerical methods, regardless of their specific operating principles and dominant adjustable thermal mechanisms.

To address this objective, the thesis is structured into three main chapters, and the overall thesis strategy is summarized in Figure 1-1.

Chapter 1 presents a comprehensive review of the adaptive façade concept: various definitions, classification, and control strategies integration. It highlights the existing thermal characterization approaches for passive façades, discusses their limitations, and identifies the scientific gap that motivates the need for a hybrid approach for adaptive façade thermal characterization using experimental and numerical methods.

Chapter 2 introduces a methodology for the thermal characterization of adaptive façade based on the findings of the state-of-the-art chapter. It relies on an experimental approach in real outdoor conditions where two experimental scenarios can be conducted: with and without the adaptive façade. The collected measurements can enable the calibration of a previously selected numerical model to estimate the key performance indicators (KPIs) that characterize the adaptive façade.

Chapter 3 applies the hybrid methodology to a diagonal louver. The adaptivity of such a system is due to its seasonal solar gain behaviour. Thus, the objective of this chapter is to determine the dynamical solar gain under real outdoor conditions, using multiple experimental scenarios and a numerical model. A comparison is performed with a theoretical calculated solar gain.

Together, these chapters form a research framework that advances the understanding of adaptive façade thermal behaviour, linking experimental measurements and numerical modelling, toward the development of suitable KPI.

Having presented the content of this thesis, the next section introduces the main research questions which were investigated in this work.

- **What are the limitations** of existing thermal characterization methodologies for adaptive façade?
- **How to propose a generalized methodology** to enhance adaptive façade thermal performance characterization under real outdoor conditions?
- **How to implement the proposed methodology** to evaluate thermal performance of a complex static geometry shading device?
- **How accurately the identified KPI** reproduce the thermal behaviour of the adaptive element?

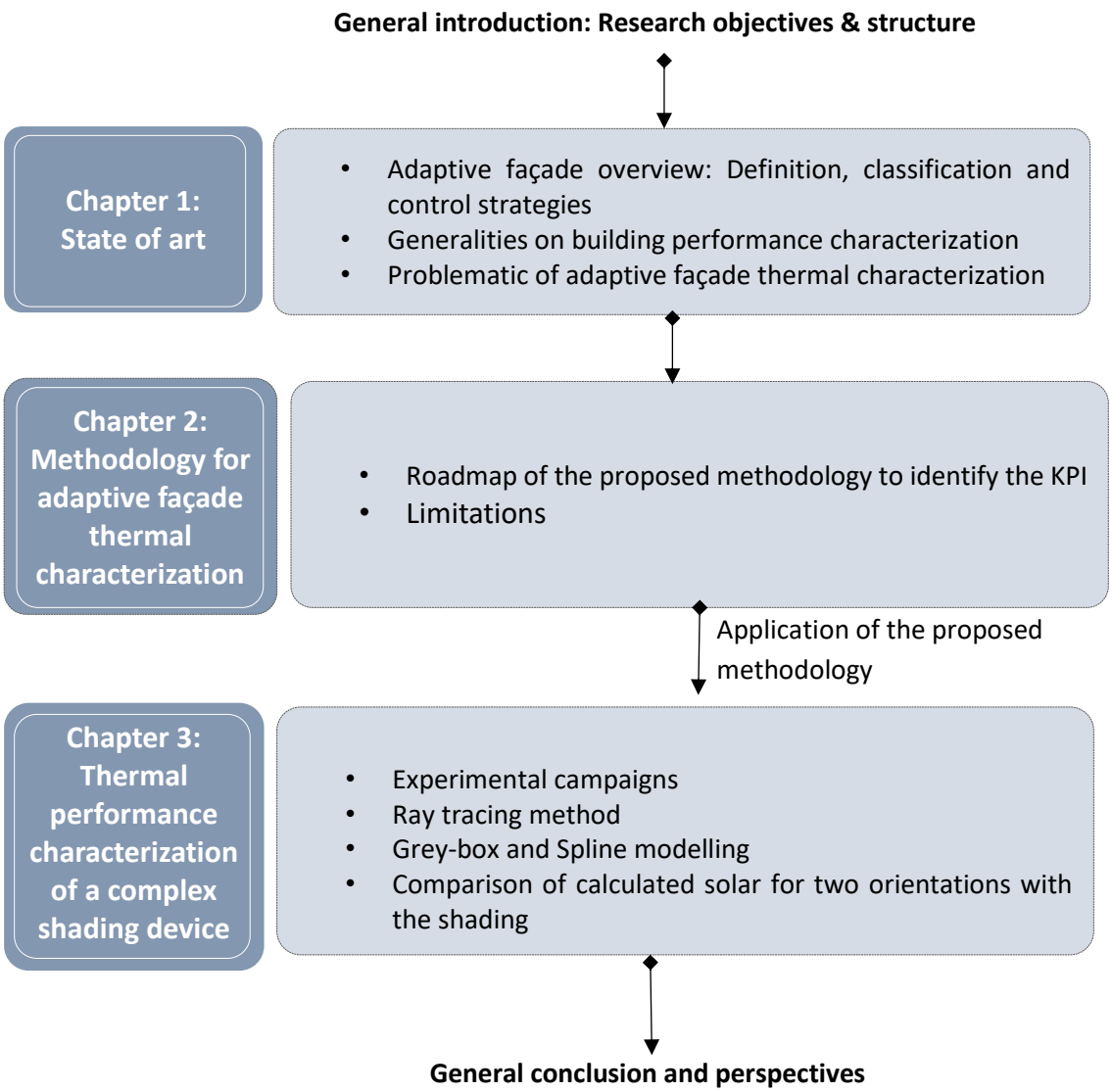

Figure 1-1: overall thesis strategy

Chapter 1: Adaptive façades and their thermal performance evaluation: a review

Summary of the chapter

The purpose of this chapter is to explore the adaptive façade concept, starting with the identified terminologies and classifications (section 1.2), then reviewing existing thermal performance methodologies (section 1.3), and their limitations (section 1.4). Finally, it outlines the main research questions and objectives of this thesis.

Résumé en Français

L'objectif de ce chapitre c'est d'explorer le concept de façade adaptative, à partir des terminologies et classifications identifiés (section 1.2), puis en analysant les méthodologies d'évaluation des performances thermiques existantes(section 1.3), et leurs limitations (section 1.4). Finalement, les objectifs et les principales questions de recherche sont définies

1.1 Introduction

The building construction sector in Europe, including the residential and the industrial accounts for 40% of energy consumption according to European Commission [2]. Moreover, in the year 2020, 62.8% of final energy consumption in the residential sector is due to space heating [3]. The current climate change projection expect a decrease in heating load demand and an increase in cooling load demand [4]. This shift highlights the importance of buildings performance requirements and particularly façades, since they must maximize solar gain in winter to reduce heating load, while minimizing heat solar gain in summer to reduce cooling load demand. A building façade is not only a protective layer from external elements such as weather and noise, but it also contributes to the energy efficiency and building occupants' comfort [5]. The form, orientation, wall composition, wall-window ratio, fenestration glazing type and shading solutions will drastically impact the overall building thermal performance, as well as heating and cooling loads energy consumption. Thus, there is a need to carefully assess those independently and jointly at design stage [4-5].

Adaptive façades are broadly defined as building envelopes that can adjust their properties in response to changing environmental conditions. A unique definition of this term remains elusive (see Section 1.2 for a detailed discussion of terminology). This adaptability can manifest through limiting solar gain to reduce overheating, reduce glare, or maintain air quality. This chapter reviews the adaptive façade concept and classifications, general building façade performance evaluation methods, and related challenges applying those methods for adaptive façade performance evaluation with a focus on the thermal performance, highlighting the need for a more appropriate evaluation methodology.

1.2 Adaptive façade: concept and overview

Adaptive façade is designed to adapt to its surrounding environment and it acts as filter between indoor and outdoor environments, since it can provide a dynamic/seasonal solution that can adapt to changing weather patterns, optimize natural light, regulate heat gains and losses, which in turn can enhance thermal comfort, and improve overall energy efficiency [8]. By incorporating advanced sensors, control operations, and automation systems, adaptive façade technologies can respond in real-time to weather conditions, occupant preferences, and energy demands. These advanced façade technologies not only have the potential to enhance the overall building performance but also contribute to the well-being and productivity of occupants. Figure 1-1 shows some designs of façade building that fall under the adaptive façade category such as dynamic shading solutions.



Figure 1-1: Examples of adaptive façade design [9]

1.2.1 Terminology and definition

Adaptive façades, or climate-adaptive building envelopes [9], can adjust their properties to the dynamic climate conditions. It can be the automatic opening of façade flaps, the changing in chemical properties of a phase change material, or the morphology of plant and stomatal resistance in green façade [10].

In general, a conventional/passive façade is widely applied to building construction; basically, it is a vertical layer that can protect from outdoor climate, such as concrete made wall. However, instead of preventing climate conditions variations, adaptive façade exploits it in favour of the occupant, it is the reason why in literature the terms 'climate façade', 'climate responsive façade', 'climate resilient façade', or 'adaptive architecture' [11] are also used to refer to adaptive façade. The name adaptive façade encompasses a wide variety of technologies that operate under different control strategies and integrate different constructive materials.

Several definitions of adaptive façade are found in literature [7], [12], [13], [14], [15], however, the most complete definition is given by IEA EBC Annex 44 [16] and [12] as: "*A climate adaptive building shell has the ability to repeatedly and reversibly change some of its functions, features or behaviour over time in response to changing performance requirements and variable boundary conditions, and does this with the aim of improving overall building performance*." As stated by the definition, an adaptive façade can change one or more of its properties. Other driving terms can be embedded in adaptive façade concept. The most used terms are: smart [17], intelligent [18], kinetic [19-20], switchable [21-22], interactive [23], biomimetic [24], responsive [25], and active [26]. While those terms are often used interchangeably, a clarification of their distinction must be done. Thus,

Table 1-1 define each of those term according to literature [27], [28], [29].

Table 1-1: Designating terms of adaptive facade and their definition

Term	Definition
Smart [17]	It is constructed from a smart material that can adjust itself due to climate variation, such as phase change material (PCM) or green façade, consequently there is no use of external control mechanisms
Intelligent [18]	It includes at the same time active functionalities and passive strategies for conception, such as venetian blinds with a control system
Switchable [21], [22]	A façade that is transparent and it is constructed from a material that is adaptive, such as smart glass that can regulate the flux of light entering the room
Interactive [23]	A human intervention is necessary to initiate a response
Kinetic [19], [20]	A complex mechanical shading system that can be adjusted with rotation, translation transformation or folding
Biomimetic [24]	A façade that its functionalities are inspired from nature (human skin, plant, animal…)
Responsive [25]	They are limited to the façade that needs an action to react either by changing internal properties of the material or the mechanical behaviour. According to the Annex 44 from IEA [16], a building element is considered responsive, when its features, functions and thermo-physical properties are adapting to various requirements
Active [26]	It contains some non-sophisticated electronic components that can help to adjust the façade components without the intervention of the user

The above-mentioned terms can coexist together, and they must not be treated as synonyms, for example a switchable fenestration system with a selective glazing is considered smart and switchable at same time. Despite these various terms, 'adaptive façade' is adopted in this thesis, since it does not presuppose a specific mechanism, and it englobes all the cited subcategories.

1.2.2 Classification of adaptive façade

In recent years, several initiatives have proposed a classification of the types of adaptive façades. Other classifications of adaptive façade have been identified in literature. In terms of structural concept [30], or in terms of control strategies and movements [31]. A recent and comprehensive one is proposed by the European project COST ACTION TU1403[1] which is a collaborative network of multiple work groups for research and innovation that focuses on adaptive facades. The main objective of this action is to harmonize, share and disseminate technological knowledge on adaptive facade systems across Europe. The work group advocated for an analytical approach, organizing façades into higher-level systems and identifying their constituting lower-level substructures, including components and materials.

[1] https://tu1403.eu/

This method facilitates individual examination of substructures. Façades were accordingly divided into three primary categories as shown in Figure 1-2:

- **Material:** This encompasses various states of material processing, such as raw, extruded, or coated forms, and also materials combined in a way that cannot be separated, like bi-metals. Examples include polymers, bi-metals, steel, wood, and phase-change materials.
- **Component:** Defined as an assembly of materials making up a constructional or functional part of a façade, such as insulated glass units, window frames with glazing, or sun-shading devices.
- **Façade system:** An aggregate of several structural or technical components, both transparent and opaque, that together perform essential technical façade functions including insulation and protection from rain and wind. Examples of façade systems are curtain walls, prefabricated modules, double-skin façades, and ventilated façades.

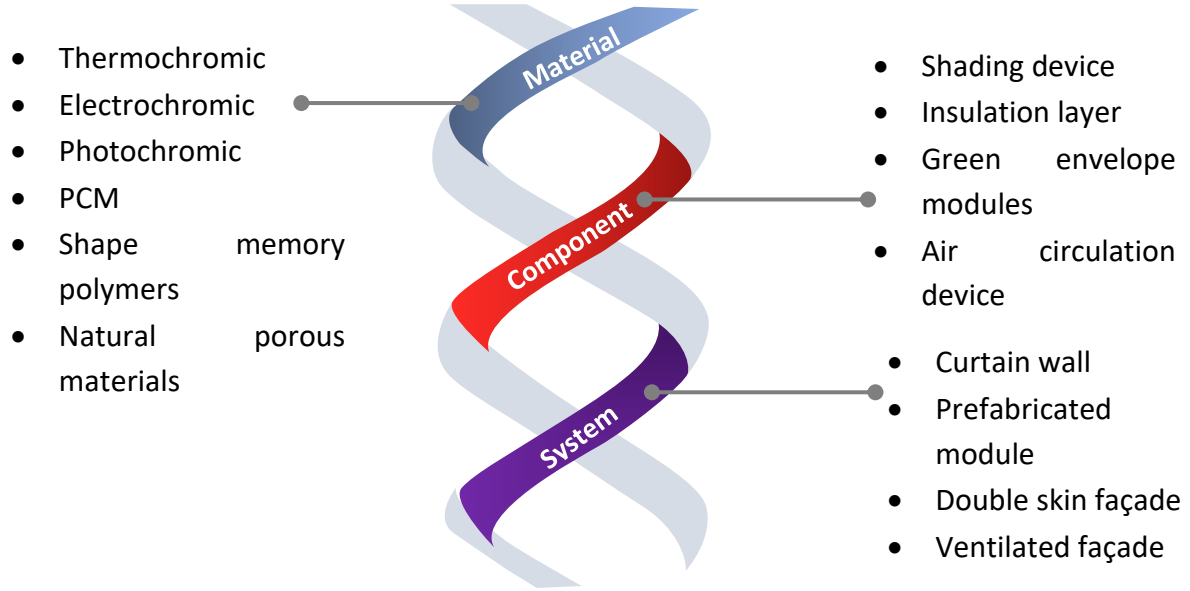

Figure 1-2: Adaptive façade general categories proposed by COST project [32]

Another detailed classification was proposed by the COST project [14] which is based on the triggering event, system of activation and system change. This classification is more accurate and global, also, it is possible to project the new innovative façade technologies using it as shown in Figure 1-3. The essential elements to consider in this proposed classification are: System change, system of activation and triggering event [32]. The system change refers to the response of the adaptive façade, usually it can manifest through the geometry changing. The system activation indicates how the façade response is initiated, and the triggering event is the factor that triggers the response [33].

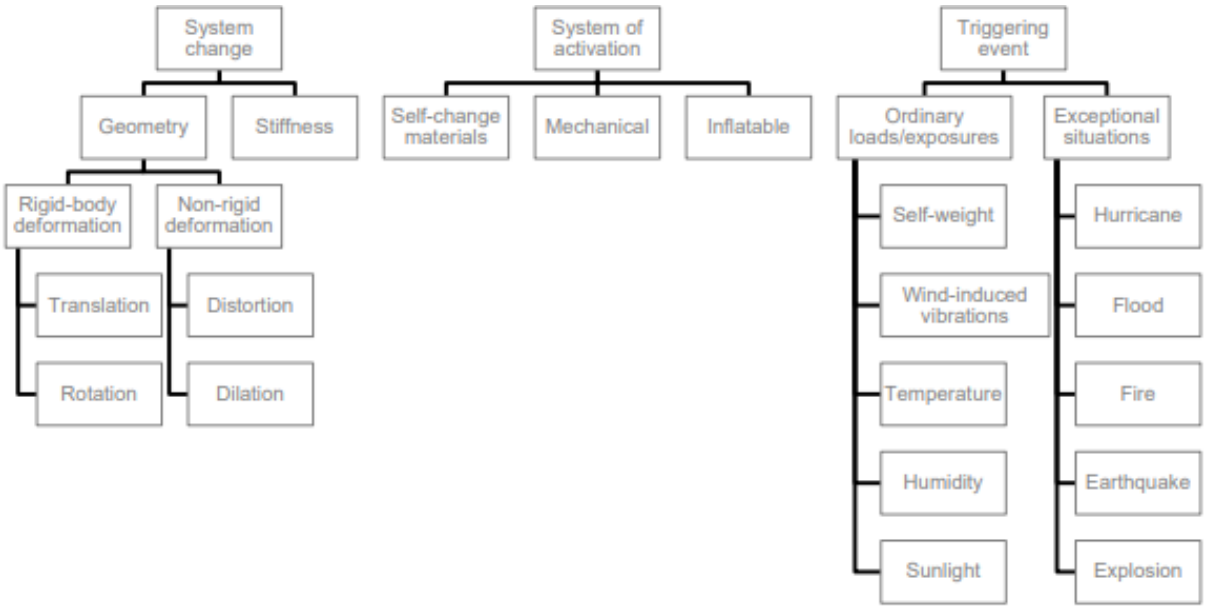

Figure 1-3 : Classification of adaptive façades proposed by COST project [32]

1.2.3 Control strategies

One of the main differences between passive façade and adaptive façade is the integration of control operations in adaptive façade. From Figure 1-3, COST project distinguished three different systems of activation: self-change materials, mechanical or inflatable. This distinction correspond directly to extrinsic and intrinsic control types [34]. When control of the façade uses an actuator, controller and sensors in order to perform operations, such as the opening, rotation, or translation of its own geometry it is called an extrinsic control. The structure of an extrinsic control system consists of three important components as illustrated in Figure 1-4 [34]. The processer or controller, it is the main element that computes the control signals. The sensors that send the signals to the processor. The actuator which is the device to be controlled.

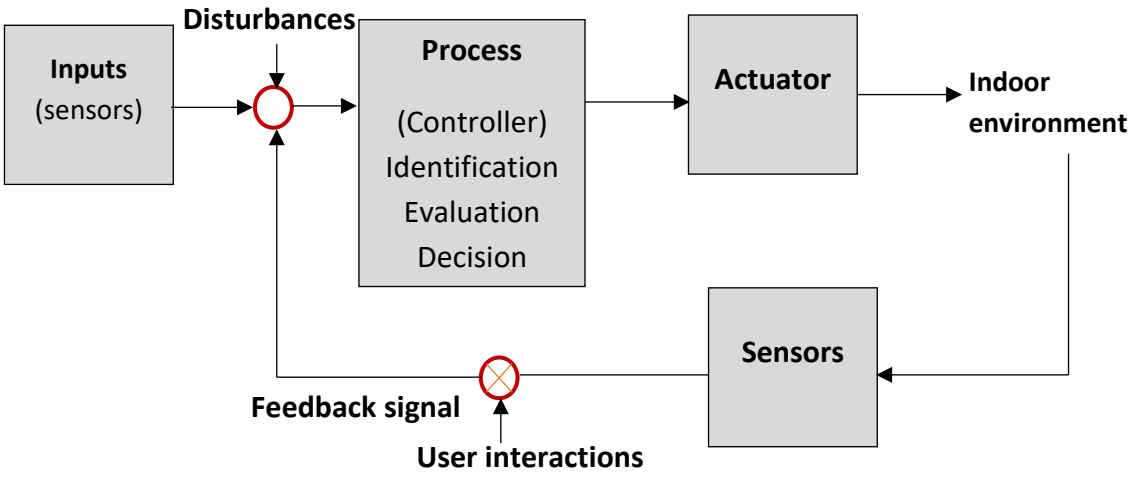

Figure 1-4: Closed loop control system [34]

The intrinsic control on the other hand is an open loop control system, since it does not use a feedback loop. This type of control concerns smart façade, where the material is self-changing with the climate conditions variation, and its internal properties change as a response, like PCM (phase change material) or green façade to climate variation. Moreover, it does not need any other external device. In addition, the PCM and green façade have a low-cost maintenance, despite the end-of-life PCM replacement and green façade irrigation, both does not require regulating using complex equipment's. This control type can be structured as an open loop control system, and it is composed from a processor and an actuator as illustrated in Figure 1-5. In this thesis, Chapter 3 focuses on open-loop controlled adaptive element thermal performance characterization.

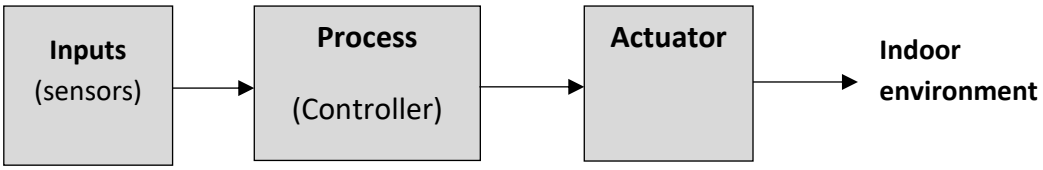

Figure 1-5: Open-loop control system [34]

These control strategies are coupled with the mechanism of adaptability of the adaptive façade. Thus, during early-stage design of adaptive façade it is necessary to choose the optimal control strategy that can align with the following objectives such as assuring: visual comfort, thermal comfort, energy efficiency, and heating and cooling loads energy consumption reduction. The optimal control protocol can achieve the minimization or maximization of a function that characterize the studied physical phenomena [8]. This is possible when the adaptive façade allows user-interaction in order to define the control operations. This decision-making process of control operation for adaptive façade can be achieved in multiple ways, either using classical control such as the rule-based or Proportional-Integral-Derivative (PID) control, which are the simplest to implement, or using advanced control. Model Predictive Control (MPC) is the most used advanced control strategy for buildings, which takes as an input the upcoming states of the adaptive façade and the predicted climate conditions in order to predict the optimal control operation. The MPC consists of the following elements: An objective function, a prediction horizon, decision timestep, manipulated variables, an optimization algorithm and a feedback signal [35]. However, when it comes to façade performance characterization, while this advanced control strategies can potentially offer a high performance, their integration in simulation tools often becomes complex.

However, for adaptive façade such as green façade and PCM, where the façade is triggered by an external environmental factor, controlling the reaction directly is not possible, instead the selection of the right activation drivers is what can be done as an intervention. Thus, the control scenarios can be defined depending of the climate predictions.

A comparison of the performance of adaptive façade elements against a passive one can also be insightful, in order to construct a static baseline to show the benefits of the adaptive

façade. However, to compare them, there is a need to select adequate comparing benchmark, and since an adaptive façade is distinguished by the dynamic behaviour, and relying on the annual heating and cooling load consumptions as an indicator for the comparison can have drawbacks. Thus, the technical and methodological challenge is whether it is possible to characterize an adaptive façade with the same methods as a passive façade. Therefore, in the next section, it is key to recall first, how passive façade performances are evaluated, on many building functions levels, with the related performance indicators.

1.3 Building thermal performance evaluation methods and KPIs

1.3.1 General functions of building façade

Building façade are mainly constructed in order to protect the inside environment from climate events, and to create a comfortable space for the occupant. It is a mandatory that the façade engineer respect strict regulations to maintain the resistance of the façade against climate hazards, by using convenient materials, and a well-established design, while keeping a good aesthetic view of the whole building.

The behavioural performance of a façade is ensured by its main functions. Therefore, it is important to define the building functions at first, and then to define the measurements and evaluation methods to check the target functionality of the façade. In general, the façade act as an interface between the exterior and the interior; to absorb solar radiation, diffuse heat and lighting; allow air circulation, transmit sound, generate energy if the building integrate with renewable energy systems, and sometimes it can allow the occupant to customize the interior environment according to their preferences. In terms of climate or adaptive façade, these functions are often interrelated, as shown in Figure 1-6 where each physical domain is represented with a petal, and the overlapping zones shows the synergies between the different building domains. For instance, a non-ventilated glazed area can address simultanously the two aspects: thermal by transmitting solar radiation and daylight, which correspond to the zone (G).

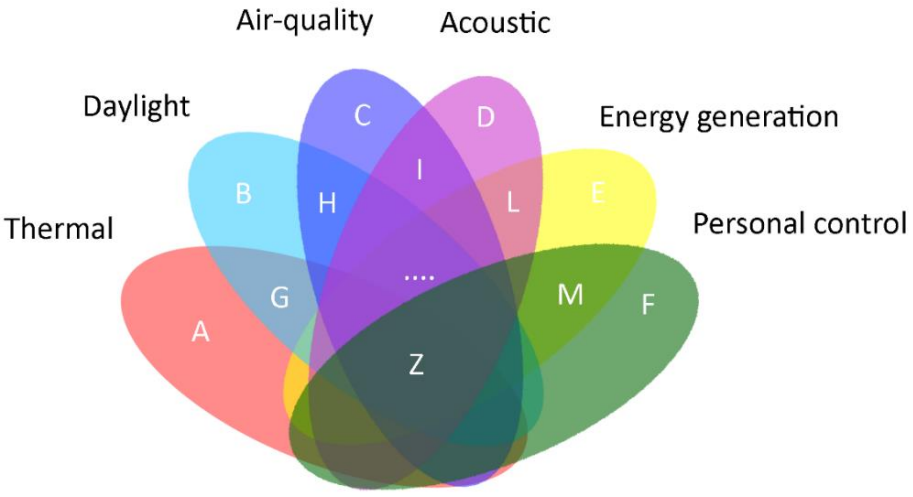

Figure 1-6: Interrelationship between physical domains in building [12]

Those functions can be described as the following:

- **Thermal insulation:** The capacity to limit the heat exchanges between indoor and outdoor environment. The three types of heat transfer are considered (radiative, convective and conductive);
- **Ventilation:** The air renewal which impacts occupant's comfort and health;
- **Daylight:** The visual comfort of the occupant inside the building and the amount of entering light is a very important factor to consider as well;
- **Acoustic:** The façade should also keep the indoor environment isolated from outside noises.

While Figure 1-6 shows the façade objectives as an overlapping domains, and in order to understand how does a façade can achieve those objectives and mediate between indoor and outdoor environment, Figure 1-7 illustrates an interface diagram, listing the physical mechanisms that the building can use such as : absorb/reflect/redirect/diffuse light; dissipate/gain/conserve heat; filter/exchange air; absorb/collect/evaporate the moisture and dampen sound. These actions are impacted by the indoor/outdoor conditions including occupant interactions.

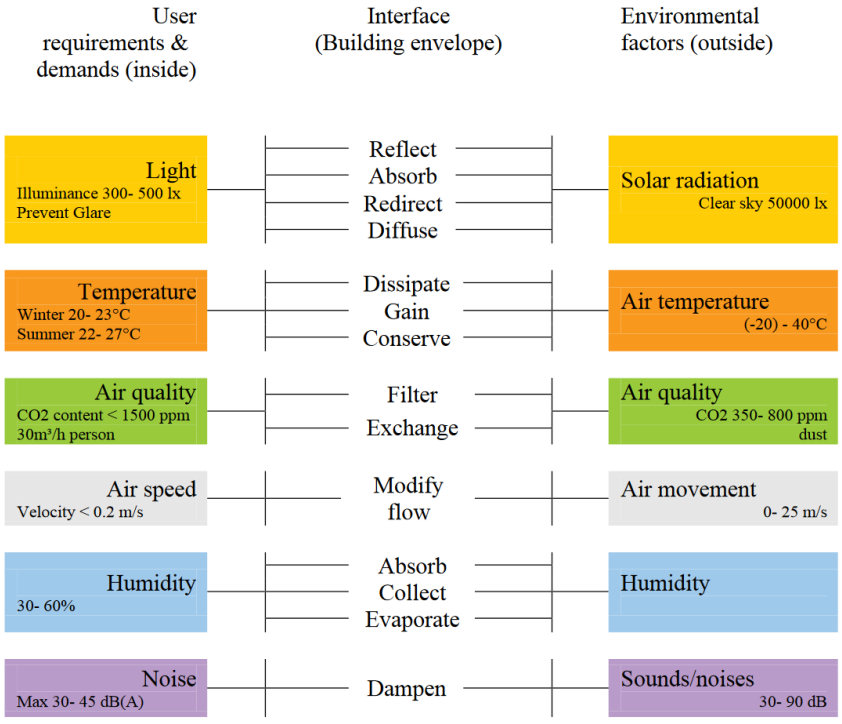

Figure 1-7 : The façade as an interface between indoor and outdoor [36]

This thesis work is focused particulary on the thermal performance caracterization.

In conclusion, performance assessment of building is a very large area that involves many interdependencies between various fields. The evaluation of these performances can lead to quantify key performance indicators (KPIs).

The evaluation of these KPIs can be quantified during experimentation by aggregating the collected measurements into key performance indicators, or using simulation software to get direct evaluation.

1.3.2 Experimental thermal characterization methods

To assess and evaluate a building façade component behaviour and performance, an experimental approach can be used. It relies on an experimental equipment for the installation of the tested element. It can be in a controlled environment namely in a laboratory or exposed to external conditions. The size and therefore the scale of the installation is another characteristic. Often the experimental equipment consists of a cell which is a highly insulated volume with one open side where the tested element is installed. Different kind of installations exist:

- **Indoor test cell:** Conditions of inside environment are controlled;
- **Outdoor test cell:** The indoor environmental conditions are under control, but the outside environment is exposed to the real climate conditions;
- **Outdoor real scale building:** The experiment is done in a real scale building, and it is possible to consider the occupation effect.

Advantages and limitations of such experimental approaches are summarized in the Table 1-2.

Table 1-2: Advantages and limitations of test facility types [37], [38], [39]

Test facility type	**Advantage**	**Limitation**
Indoor test cell	• Control important factors (wind speed, temperature…) • The boundary conditions are controlled by the laboratory	Difficulty to mimic the solar irradiance
Outdoor test cell	• The test cell interior conditions are under control • The outdoor conditions are real climate • Ability to test an element under dynamic conditions • Allows validation of models for simulation • The results can be beneficial for designers, manufacturers, researchers and end-users • The boundary conditions outside are those of the climate	The high variability of climatic conditions leads to the fact that the tests carried out on test cells cannot be replicable
Outdoor real scale	It is possible to consider the occupant's effect	The boundary conditions are defined by the climate and the occupants Average accuracy due to highly variable climatic conditions and occupant's behaviour

The outdoor test cell among can be considered as the most valuable one as it can allow a performance evaluation under real environment. The outdoor test cell was developed in Europe during the 80s, as a part of the PASSYS project standing for PASive Solar System testing as illustrated in Figure 1-8. This project resulted in the construction of 38 test cell facilities in 9 European countries, a number of the test cells were equipped with a rotated platform to be able to change orientation easily [40] such as the Facade System Interactions Lab constructed in the Institute for Renewable Energy in Torino, LABIMED Test Cell constructed in ABITA research Centre in Torino, and TWINS (Testing Window INnovative Systems) constructed in Department of Energy, Politecnico di Torino. The common goal of all those test facilities,

regardless of their size and scope, is to evaluate the performance of building envelope element.

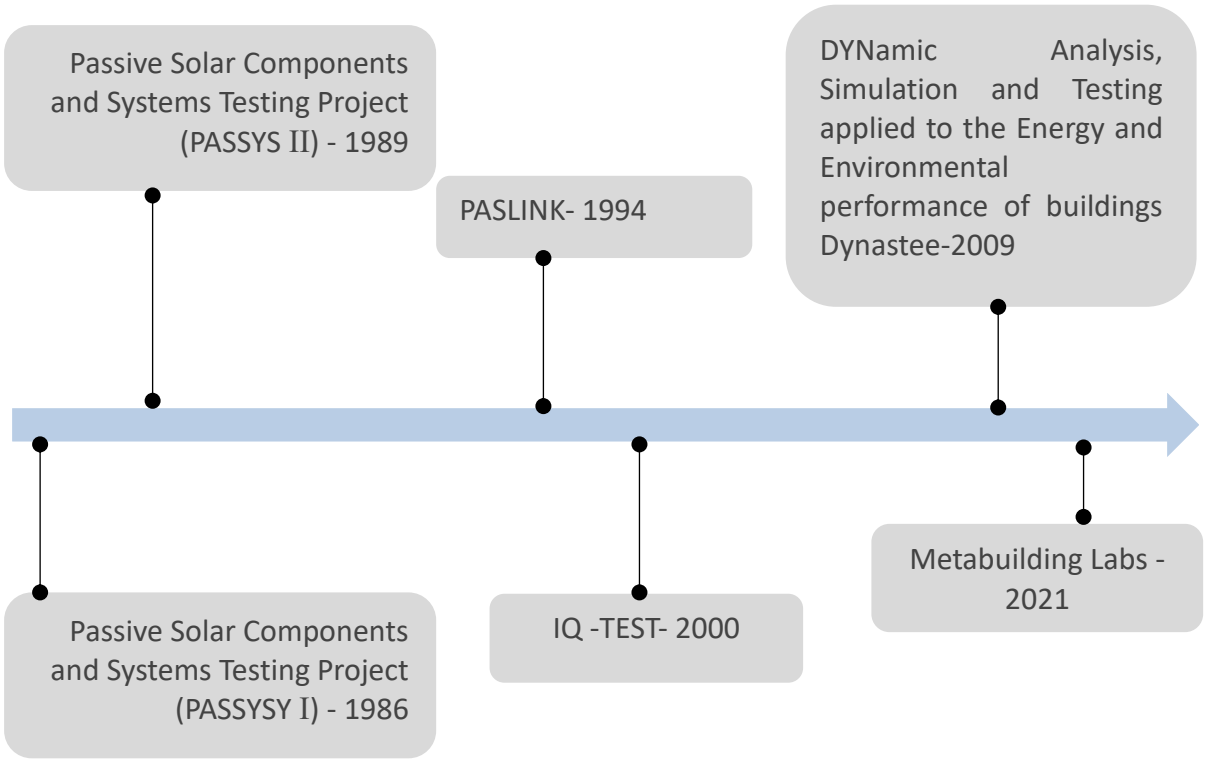

Figure 1-8: European projects aimed at providing test beds, methods for measuring and evaluating thermal performance of buildings

The EU funded METABUILDING Labs[2] Project started in 2021, and involves 40 partners including research institutes and technology providers. It aims to develop a network of capacities and services to assist in the development of innovative envelope systems. One of the objectives is to design and construct outdoor test cells named O3BET across Europe. O3BET stands for Open Source, Open Design, Open access Building Element Testbench. In France, the O3BET is built in Bordeaux city. A 3D visualisation of the test cell is shown in Figure 1-9.

[2] https://www.metabuilding-project.eu/

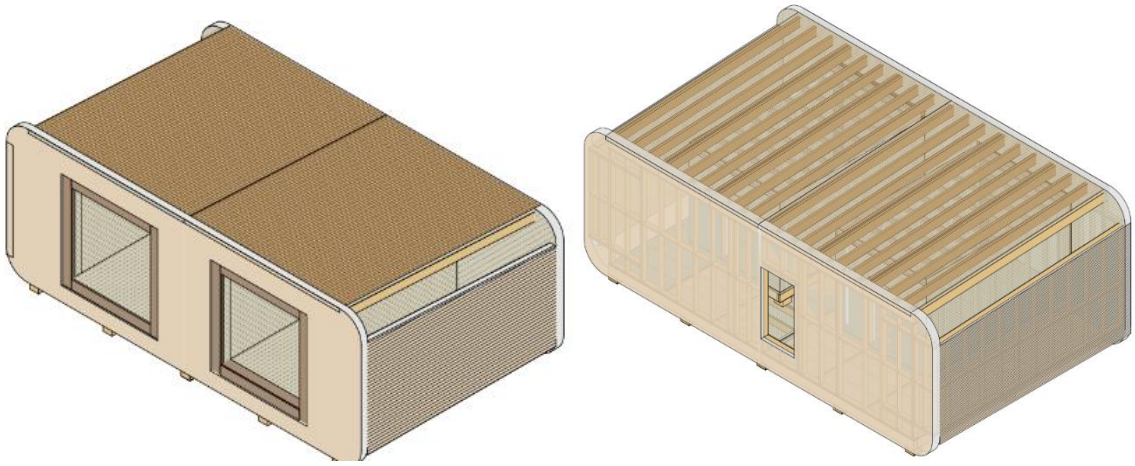

Figure 1-9: 3D perspective of the O3BET built in Bordeaux (front and rear view)

Two types of such outdoor test cells can be identified. They are listed Table 1-3 and illustrated in Figure 1-10.

Table 1-3: Types of outdoor test cells [37], [38], [39]

Test cell	Description
Comparative	The test cell has a reference cell
Absolute	Single cell, it can be guarded and calibrated in same time, when it is not directly exposed to outdoor weather conditions, but is surrounded by a thermally controlled zone to reduce heat loss/gain through the 5 walls, as well as when a thick layer of an insulating material between the tested wall and the other walls is introduced to reduce heat exchange by conduction.

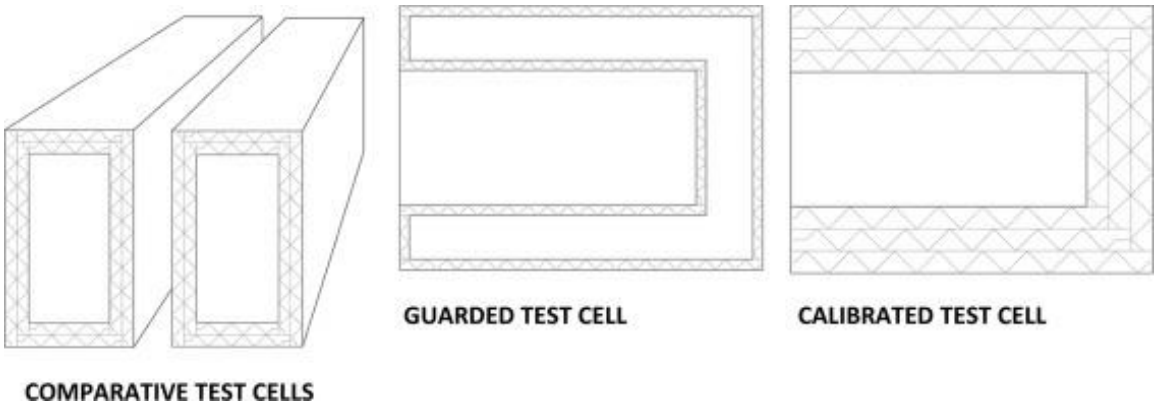

Figure 1-10: Picture of outdoor test cells [37]

The consideration of real climate variation is a great advantage that is offered by outdoor test cells for the performance evaluation of building elements, especially for adaptive building elements characterization. However, these cells represent some limitations [41] such as the dimensional compatibility challenge, because the tested façade must have specific dimensions to be integrated on the outdoor test cell, and this challenge is particularly relevant for adaptive façade where the structure can be possibly movable, and its performance is impacted by the stiffness of the supporting system [42]. The design and regular maintenance cost of the test facility is high due to its exposition to outdoor conditions, which in turn can cause material degradation. In addition, there is a need for long duration tests due to the climate variations. Moreover, the thermal performance particularly is depending on the boundary conditions, which introduce the challenge of repeatability of experimental tests, and the collaboration with other outdoor test cells in other locations.

1.3.3 Passive façade performance indicators

A KPI (key performance indicator) is used to characterize a process or a product, to report its state, understand the occurring problems, and pinpoint areas of improvement. For building characterization, it is necessary to cross all involving physical phenomena, and get the indicators that will be used to evaluate the tested façade. Evaluating the performance of a building façade, requires the identification of relevant KPIs that regulate the different domains listed in Figure 1-6.

1.3.3.1 Heat transfer characterization

In vertical passive façade systems, different steady-state-based technics are used to estimate thermal parameters of building's façade or materials in general. Those technics are based on creating a gradient of temperature with a known thickness of wall, the controlled heat flow on the two sides of the tested wall or material can be assumed to ensure one directional heat flow characterization [43]. The heat transfer characterization can lead to define many factors, such as the heat transfer coefficient U-value, g-value which is referred to the solar heat gain coefficient.

The challenge is to propose through a series of KPIs and associated protocols a clear way to describe the overall thermal performance of a façade element.

During the design process of a passive façade, the theoretical calculation can be done using values of material properties of the façade layers. The calculation procedure is described in standard ISO 6946 [44], and it is based on the analogy with electrical resistance, by considering that the façade is constructed from different layers , and each layer i has a thermal resistance R_i expressed in Eq 1-1.Those thermal resistances are in serial and can be sum up with the internal R_{si} and external R_{se} surface thermal resistances which are already specified in standard ISO 6946 to become a total thermal resistance R_{tot}. Therefore, the expression of heat transfer coefficient U is given by Eq 1-3. Thermal resistance is the amount of resistance that the material offers to the heat flow through the façade, and it depends on the thickness and thermal properties of the material.

The total thermal resistance can be expressed as the following Eq 1-2 [45]:

$$\mathrm{R_i} = \frac{\mathrm{d_i}}{\lambda_\mathrm{i}} \qquad \text{Eq 1-1}$$

$$\mathrm{R_{tot}} = \mathrm{R_{si}} + \sum_{\mathrm{i=1}}^{\mathrm{n}} \mathrm{R_i} + \mathrm{R_{se}} \qquad \text{Eq 1-2}$$

where n is the total number of façade's layers.

$$\mathrm{U} = \frac{1}{\mathrm{R_{tot}}} \qquad \text{Eq 1-3}$$

The application of this norm is limited to the cases where the thermal properties of the used material in the façade are known. Otherwise, it is possible to get those properties using a non-destructive method. The definition of the used physical quantities such as thermal conductivity, and thermal resistance are cited in the standard ISO7345:2018 [46].

Regarding the experimental methods, the heat flow method can be used, and is defined in the standard ISO 98691 [47], and it is held using heat flux sensors and air temperature sensors for indoor and outdoor environment as well. After the experiment and the acquisition of the measurements, data analysis methods must be used in order to estimate the U-value, usually the average method is used. This method assumes that the transmittance of a wall is equal to the mean density of heat flow rate by the mean temperature difference and is expressed by Eq 1-4.

$$\mathrm{U} = \frac{\sum_{\mathrm{i=1}}^{\mathrm{m}} \Phi_\mathrm{i}}{\sum_{\mathrm{i=1}}^{\mathrm{m}} \left(\mathrm{T_{ai,i}} - \mathrm{T_{ae,i}}\right)} \qquad \text{Eq 1-4}$$

Where:

- Φ is the heat flux density in W/m²;
- $T_{ai,i}$ is the indoor air temperature;
- $T_{ae,i}$ is the outdoor air temperature;
- m is the number of measurements.

One of the limitations of the heat flow method is that it considers that wall properties does not change (steady state), also it is tested in real conditions, therefore, results may vary. In addition, a sufficient temperature differential between interior and exterior must be maintained. In order to achieve a stabilised U value, the measurements require a long duration, and it should be performed ideally at night, to eliminate the influence of solar radiation during daytime.

Another experimental method that can be used is infrared thermography. This method is defined in the standard ISO 10878 [48], it can be used *in situ* measurements since it is a non-destructive method, and it requires short duration (2h to 3h) of measurements [49], [50]. Some of the limitations of this method is that resulted images can be affected by the shadow of other buildings or solar radiation during daylight which leads to wrong thermal properties. Also, walls exposure has a relevant influence on the measurement accuracy [51]. Therefore it is usually used for internal surface temperature at night where there is small temperature variation and no shadow due to sunlight at night in order to detect thermal bridge [52].

Other steady state technics can be used such as the hot box technic defined in standard ISO 8990 [53], but the inconvenient of it is that it is a large testing chamber and it is difficult to use in situ. Also, in order to reach steady-state conditions, it requires long testing period (days) depending of the thermal inertia of the tested component [54].

1.3.3.2 Indoor air quality/flow characterization

Various methods are used to keep the indoor air clean, such as mechanical ventilation, chemical purification, and mechanical extraction.

The measurement of air flow rate is considered as a key performance indicator, and it can be calculated using the tracer gas method. The tracer gas method is a non-destructive testing method that aims to introduce a gas in the tested zone, in order to determine the air flow rate. A good tracer gas should be non-toxic, odourless, colourless and inert, such as Carbon dioxide, Nitrous dioxide, and Freon. Also, the gas should not be present in the room before making the test. The standard ISO 12569:2017 [55] defines the following three methods: concentration decay method, continuous dose method, and stationary concentration method. The main principle is the use of a tracer gas in order to evaluate the air flow rate.

According to standard ISO12569:2017 [55], the concentration decay method uses a tracer gas on the evaluated zone, and based on the concentration decay data, the ventilation rate can be obtained from Eq 1-5.

$$\frac{\mathrm{dV_{gas}(t)}}{\mathrm{dt}} = -\mathrm{C_E(t)} \times \mathrm{Q_v(t)} \qquad \text{Eq 1-5}$$

Where:

- t: Time;
- $V_{gas}(t)$: Total gas tracer volume in the zone at time t in m^3;
- $Q_v(t)$: Ventilation rate at time t in m^3/h;
- $C_E(t)$: Average exhaust concentration at time t in m^3/m^3.

In the continuous dose method, the tracer gas in this type of measurement method is continuously added in Eq 1-6:

$$\frac{\mathrm{dV_{gas}(t)}}{\mathrm{dt}} = \mathrm{m(t)} - \mathrm{C_E(t)} \times \mathrm{Q_v(t)} \qquad \text{Eq 1-6}$$

Where:

- $m(t)$ is the dosage of gas at time t in m^3/h.

Finally, the stationary concentration method is used when the stationary state is reached, in other words, the ventilation rate doesn't variate over time, and it can be calculated using the following Eq 1-7:

$$\mathrm{Q_v} = \frac{\mathrm{m}}{\mathrm{C_E}} \qquad \text{Eq 1-7}$$

Where:

- m: Tracer gas flow rate in m^3/h;
- C_E: Exhaust concentration in m^3/m^3.

The study that has been carried out by Jankovic et al. [56], for the characterization of air flow in a double skin façade using different gas tracer technics, showed that there is a strong correlation between the air flow rate measured by all methods and the opening size of the blind. The wind direction effect could not be analysed in this study due to accumulated uncertainties.

1.3.3.3 Daylight characterization

The daylight can help decreases the energy consumption in building, because it can reduce the use of artificial lightning [57]. Using an outdoor test cell experiment, the daylight potential into the building can be characterized using the daylight factor D_a as a metric, which is the quotient of indoor illuminance and outdoor illuminance, and it is defined in the standard ISO 10916:2024 [58] (see Eq 1-8).

$$\mathrm{D_a} = \frac{\mathrm{E_i}}{\mathrm{E_e}} \text{ in } \% \qquad \text{Eq 1-8}$$

Where:

- E_i: Indoor measured illuminance in lx;
- E_e: Outdoor measured illuminance in lx.

The visual indoor quality can also be quantified using a survey dedicated for occupants' satisfaction [59]. For the case of an indoor experiment, an artificial sky light and sun simulator can be used, and the same metric is also used.

1.3.3.4 Acoustic comfort characterization

Façade sound insulation can be measured using various methods. The standard ISO 16823 [60] describes the outdoor measurements that can be used such as the use of loudspeaker as a source of sound or road traffic such as rails and airplanes. The inconvenient of the road traffic sound is that it does not occur often and does not have much energy to help in evaluation process. The loudspeaker should be placed on the ground, with a distance from the façade of 5 m, and an angle between the sound wave and the normal to the façade of 45 degrees. The acoustic performance of a building can be calculated according to the standard ISO 12354-3 using the estimation of sound insulation [61], that can be expressed in three quantities which are determined according to the frequency band. In order to determine the effective sound insulation between two spaces, the apparent sound reduction index can be used in Eq 1-9:

$$\mathrm{R'}_{45^\circ} = \mathrm{L}_{1,s} - \mathrm{L}_2 + 10\log(\frac{\mathrm{S}}{\mathrm{A}}) - 1{,}5\ \mathrm{dB} \qquad \text{Eq 1-9}$$

Where:

- $L_{1,s}$: average sound pressure level on the outside surface of the building element including the reflecting effects from the façade in *dB;*
- L_2: average sound pressure level in the receiving room in *dB;*
- S: area of the building element in m^2*;*
- A: equivalent sound absorption area in the receiving room in m^2.

One of the limitations of the standard ISO 12354-3 [61] calculation method is that it does not provide calculation method of sound insulation for a corner room [62]. Another factor that can be used for the acoustic characterization is the acoustic indoor quality. It can be measured using the sound level meter and the measurement methods are defined in the standard ISO16823-3:2014 [60].The façade resistance against climate hazards is also standardized in terms of fire by the standard ISO 9705-2:2001 [63].

Passive façade by virtue of their static properties, can be inefficient simultaneously for summer and winter seasons, because it cannot respond to changing outdoor conditions, neither to indoor variable thermal gain, which can affect the relevance of its energy saving [64]. Therefore, a series of investigations have been carried out with the objective to integrate adaptive façade systems in buildings and assess their convenience [65], both in terms of energy consumption and thermal comfort. For the comparison to be relevant, the adaptive façade must respect the same building quality criteria as the traditional building.

The standardized characterization methods presented at the beginning of Section 1.3.3 most often use single parameters with a unique value, therefore static, expressed in the technical reports for the characterization of the façade elements. The underlying assumption is that the element responds the same for the exterior climate conditions the whole time. However, this assumption is not totally valid for adaptive façade for which the thermal properties of the material can also vary such as the solar transmittance. Consequently, the KPIs that are once dedicated for passive building façades are not adapted for adaptive façades due to their dynamic nature. Moreover, it is necessary to understand how these control operations are being deployed in the necessary protocols for the thermal performance characterization of adaptive façade. Therefore, more sophisticated KPIs that can take into account dynamic phenomena and the control operations are needed [9]; by using outdoor experiments to have more credible final models [7].

1.4 Focus on adaptive façade thermal performance evaluation approaches

Having established the adaptive façade overview, and building general functions in Sections 1.2 and 1.3, attention now is turned to the adaptive façade thermal characterization approaches.

Often for adaptive façades, multi-physical domain can take place during their interaction with climate, such as thermal, airflow, acoustic and visual. Figure 1-11 illustrates different categories of adaptive façade and their corresponding influential dominant physical phenomena. It is possible that an adaptive façade has more than one dominant physical domains that can have correlated features. Thus, it is important to evaluate them simultaneously [9]. Among these adaptive elements listed, the complex fenestration system is studied in this thesis (circled in red in Figure 1-11), with solar radiation as the primary heat transfer mechanism. To elaborate this section various questions are listed below.

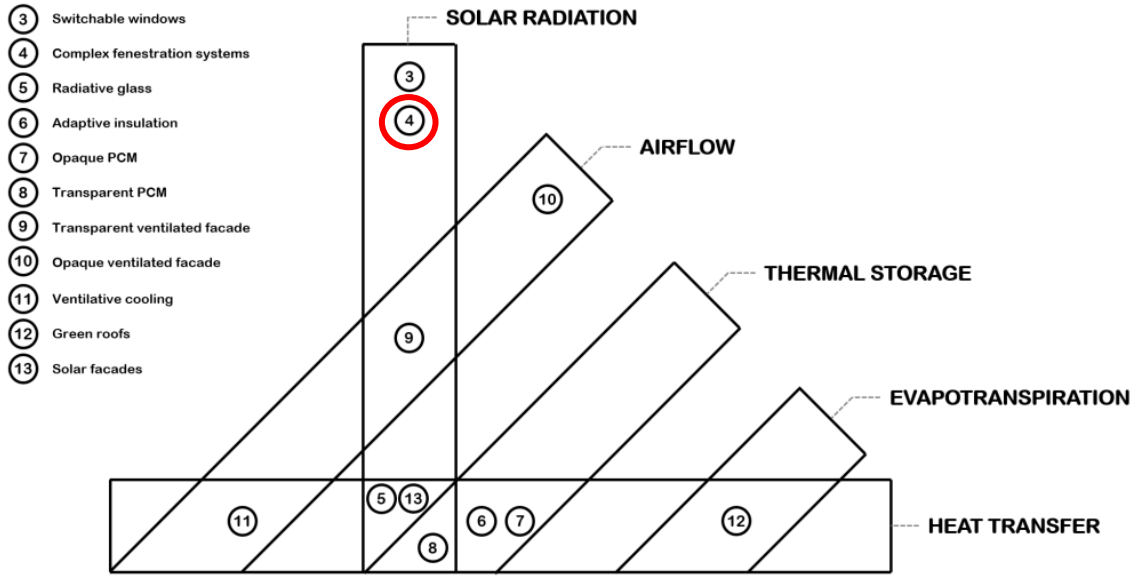

Figure 1-11: A schematic overview of adaptive façade technologies and their dominant physical domain [66]

Why do we need to rethink new metrics for adaptive façade characterization?

The experimental characterization is an important aspect in building performance evaluation since it can validate or even build numerical models. For passive façade, the KPIs are usually physical parameters with static values. An example for passive opaque façade is the single U-value used to characterize the thermal performance. However, for adaptive opaque façade this only value is not sufficient. Limitation for the use of standards dedicated for passive façade to characterize adaptive façade can be summarized in the Table 1-4. This fact is highlighted by the Figure 1-12 [67] , in this study, two glazing units are evaluated, one is conventional and the second is a PCM filled glazing using an outdoor test cell [67], and the graph represents the heat flux through the glazing against the difference between indoor-outdoor air temperature. The U-value can be quantified by the slope of the linear regression line. The DGU (double glazing unit) which is composed of a traditional clear glass (DGU_CG) show a linear behaviour, however, for the DGU_PCM unit the measurements showed a non-linear behaviour, these variable states are influenced by the thermal storage of the PCM. As a result, a single U-value cannot be used to characterize such a system.

Table 1-4: List of standards for building performance evaluation

Phenomena	Test method	Standard	Limitation for adaptive façade characterization
Heat transfer	Theorical	ISO6946 [44]	No measuring device
	Heat flow method	ISO9869 [47]	The core of this method is based on steady-state assumption with one directional heat flow, which is not suitable to characterize adaptive building elements.
	Thermography	ISO10878 [48]	The thermography camera can measure optical properties under fixed conditions, but in case of electrochromic glazing the near infrared transmittance can vary, which make the use of one single state measurement cannot represent the overall thermal characterization.
Acoustic	Sound insulation index	ISO12354-3 [61]	For adaptive façade with movable elements, the acoustic performance varies with the state changing.
Daylight	Daylight factor	ISO 10916 [58]	This standard assumes a fixed daylight factor, which is not the case for adaptive fenestration systems.

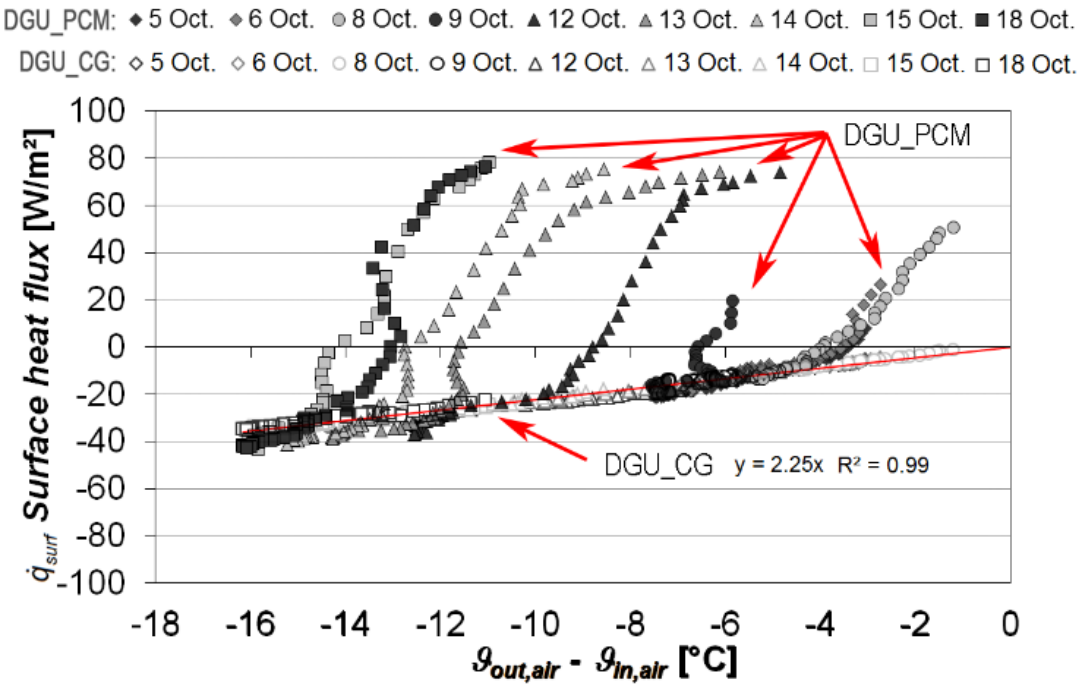

Figure 1-12: Linear regression analysis to identify U-value for a conventional and a PCM double glazing unit (DGU) [67]

Nevertheless, the range of U-value for different operating modes or according to opposite heat flux directions could be used as a characterization approach [68] using laboratory experiments such as guarded hot plate or Hot Box . The challenge of such an approach lies in the characterization of the transient state between the different configurations. Another hybrid approach is to use an outdoor test cell experiment using the adaptive façade, and then to try to identify which equivalent passive façade can reproduce the inner conditions using simulation [69]. Nevertheless, the transitional state between the 'equivalent states' is not again considered. In this context, instead of assigning for each state a model, this thesis proposes a methodology where the KPI can be derived from a single calibrated model while capturing the dynamic thermal behaviour.

In order to identify an adaptive façade thermal characteristics using simulation, the model must support various criteria's such as multi-physical modelling by coupling the equations of different physical domains; the facility to integrate and couple the innovative façade models into the whole building model [70]; the possibility to model time varying properties of the adaptive façade [71]; the possibility to integrate the interactions with the occupant's behaviour [72], [73]; local and global sensitivity analysis integration in the simulation tool in order to understand the influence of the building parameters including the adaptive façade on the occupant's comfort on many levels [74]. About the numerical based approaches for adaptive façade thermal characterization, since the adaptive façade's behaviour is includes its accumulative thermal effect of its different internal states, a straightforward approach is to associate every state of the adaptive façade to a specific model or function [64], and then to calculate the KPI for each façade state [76]. However, it is more complex when the façade behaviour changes quickly, and also this method does not take into account the delayed thermal response [70]. In terms of KPIs, what could be useful in such a case, is either to formulate the KPIs that were once used for passive façade as a dynamic function, or to introduce new KPIs specific for the studied technology [77]. One of the outcomes of the COST project was on some metrics that has been adopted for the characterization of dynamic effects of adaptive façades, such as the capacity of the façade to pre-heat the indoor environment or the ventilated airflow for ventilated façade, or the solar gain efficiency for active insulation. Those metrics are material independent and they are derived from experiment/simulation [78].

What are the needs to satisfy to fairly evaluate an adaptive façade?

When an adaptive façade requires a performance characterization in general, it is usually more useful during the early-stage design phase, so that the best performing façade design can be selected and proposed to the market. However, this adaptive façade characterization approach will need the integration of the control operation of the façade, which will question the validity of this characterization regarding the control protocols. Thus, the choice of the appropriate control operation is crucial. The standard ISO52016-3 [1] already recommended multiple control scenarios to characterize the thermal performance of the active ventilated

façade and for the following shading devices: roller blinds, venetian blinds and chromatic glazing. However, there is a lack in the standards that fully covers adaptive façade control references scenarios [79]. The validity of the characterization approach regarding different climate conditions should also be questioned.

Thus, there is a lack of a generalized methodology and testing suggestion that can cover all adaptive façades [42]. Therefore, to address those challenges, this thesis proposes a hybrid general methodology based on experimental measurements and a numerical model, enabling the derivation of a KPI.

1.5 Conclusion and thesis problematic

The main objectives of this chapter are to i) clarify the adaptive façade definition given the variety of related terminologies, ii) review the current methods used to characterize passive façade performance across the relevant physical domains, and iii) identify the limitations of those methods for adaptive building element characterization.

From this first chapter, it is clear that conventional KPI used to characterize passive façades, such as the heat transfer coefficient, thermal resistance, light transmission factor, and solar factor, are expressed as single static values. Such indicators are not sufficient to capture the dynamic [9], state-dependent behaviour of adaptive façades, whose thermal properties vary with boundary conditions and control operations. The current methodologies poorly describe the transient façade behaviour, since it adopts a state-based approach where a model is attributed for each significant state. Thus, a harmonized methodological framework is needed to characterize such a system linking the real outdoor measurement with a numerical model and a state-dependant KPI.

Therefore, the general objective of this thesis is to introduce a thermal performance evaluation methodology for adaptive façades to overcome the identified limitations, by listing the involving the thermal phenomena, formulating the corresponding model and KPIs, and defining experimental protocols to test how the façade behaves under varying outdoor/indoor environmental conditions. The KPIs are then estimated using a calibrated numerical model. The following requirements must be considered for such a model:

- Consider the dynamic behaviour of the façade (including transient states);
- Model the dynamic control operations;
- Allow integration and coupling of the innovative façade models into a whole building model.

Although the state of the art covered multiple physical domains, the focus of the thesis is on the thermal performance level. The visual, acoustic and airflow performance are not considered.

A specific adaptive shading prototype is used as a case study to validate the proposed methodology. It consists of a diagonal louver with a static geometry, whose adaptivity arises from its seasonal solar gains' behaviour due to the sun position (open-loop control). As such, the control operations are inherent to the system and were not defined in this case. This case study was selected as a proof of concept. The detailed description and experimental application are presented in Chapter3.

Chapter 2: Methodology for adaptive façade thermal characterization

Summary of the chapter

After an introduction and a definition of adaptive façade concept in the previous chapter, the purpose of this chapter is to develop a methodology based on experimental-numerical methods for adaptive façade thermal performance characterization using outdoor test cell. The proposed methodology is based on three steps. The first step (section 2.2.1) corresponds to the inventory of the distinguishing heat transfer modes regulated by the adaptive façade and the related key performance indicators. Those indicators and heat transfer phenomena are incorporated into a numerical model in a second step (section2.2.2). Finally, in order to determine this key performance indicator, a series of experimental scenarios is proposed to: first to calibrate the numerical model using a passive reference configuration, and then to characterize the adaptive façade behaviour. The adaptive façade related KPIs can then be quantified (section2.2.3).

Résumé en Français:

Après une introduction et une définition du concept de façade adaptative présentées au chapitre précédent, ce chapitre vise à développer une méthodologie, basée sur des méthodes expérimentales et numériques, pour la caractérisation des performances thermiques des façades adaptatives à l'aide d'une cellule d'essai placée dans un environnement extérieur. La méthodologie proposée se compose de trois étapes. La première consiste (section2.2.1) à lister les différents modes de transfert thermique régulés par la façade adaptative et les indicateurs clés de performance (KPI) associés. Ces indicateurs et les phénomènes de transfert thermique sont ensuite intégrés dans un modèle numérique pour la deuxième étape (section2.2.2). Enfin, afin de déterminer cet indicateur clé de performance, une série de scénarios expérimentaux est proposée pour caractériser le modèle de façade passive choisi comme référence et le modèle de façade adaptative. Un KPI spécifique à la façade adaptative peut alors être identifié (section2.2.3).

2.1 Introduction

As discussed in Chapter 1, the current existing methodologies to deal with adaptive façade remains incomplete, since they do not consider the effect of transient state of the adaptive façade. In addition, the passive façade related static KPIs are not sufficient to characterize and describe the thermal behaviour of adaptive façade. Now, it is clear that the adaptive façade KPIs plays a critical role in the thermal characterization during façade's early-design stage. However, the question remains: i) how can those KPIs be properly defined and estimated? And ii) given the context of outdoor test cell use, how can the specific contribution of the adaptive element be isolated and evaluated?

Before addressing the above-mentioned questions, regarding the definition and identification of the adaptive façade KPI. One should first ask: what are the key requirements that the proposed methodology destined to characterize the thermal behaviour of adaptive façade must fulfil. The necessary criteria's can be listed as follow:

- *Generalization:* The framework of the methodology should be applicable beyond a single case of study;
- *Modelling adaptive façade behaviour:* The dynamic behaviour must be isolated from surrounding thermal phenomena;
- *KPI identifiability:* The related KPI have to be identifiable from the collected measurements;
- *Robustness regarding boundary conditions:* The framework need to be applicable in different environmental conditions;
- *Modelling adaptive façade operations:* The framework must consider the use of extrinsic control operations.

To meet these requirements, this chapter presents a hybrid methodology combining experimental measurements with a calibrated numerical model. The complementary of experiment, protocols and the numerical model is illustrated by Figure 2-1. This conceptual triangle represents the simultaneous consideration of the three aspects in the proposed methodology: experiments provide real-condition measurements, protocols define the testing scenarios, and the numerical model enables the estimation of the KPIs.

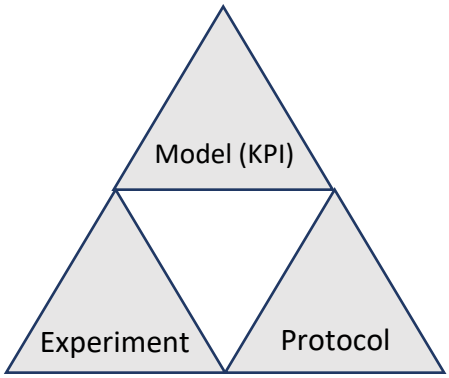

Figure 2-1: Conceptual triangle linking experiment, model and protocol

Importantly, the proposed methodology is not limited to estimate a single KPI, instead, the main focus is its adaptability: once a façade is characterized for a specific configuration (e.g., a given orientation), the same methodological framework can be implemented for other orientations, with the resulting KPIs reflecting the corresponding changes in boundary conditions.

Based on these requirements, the following section 2.2, proposes a hybrid methodology structured into three steps, Figure 2-2 illustrates the summary of the proposed methodology steps starting from the heat transfer inventory, model formulation, and KPI identification.

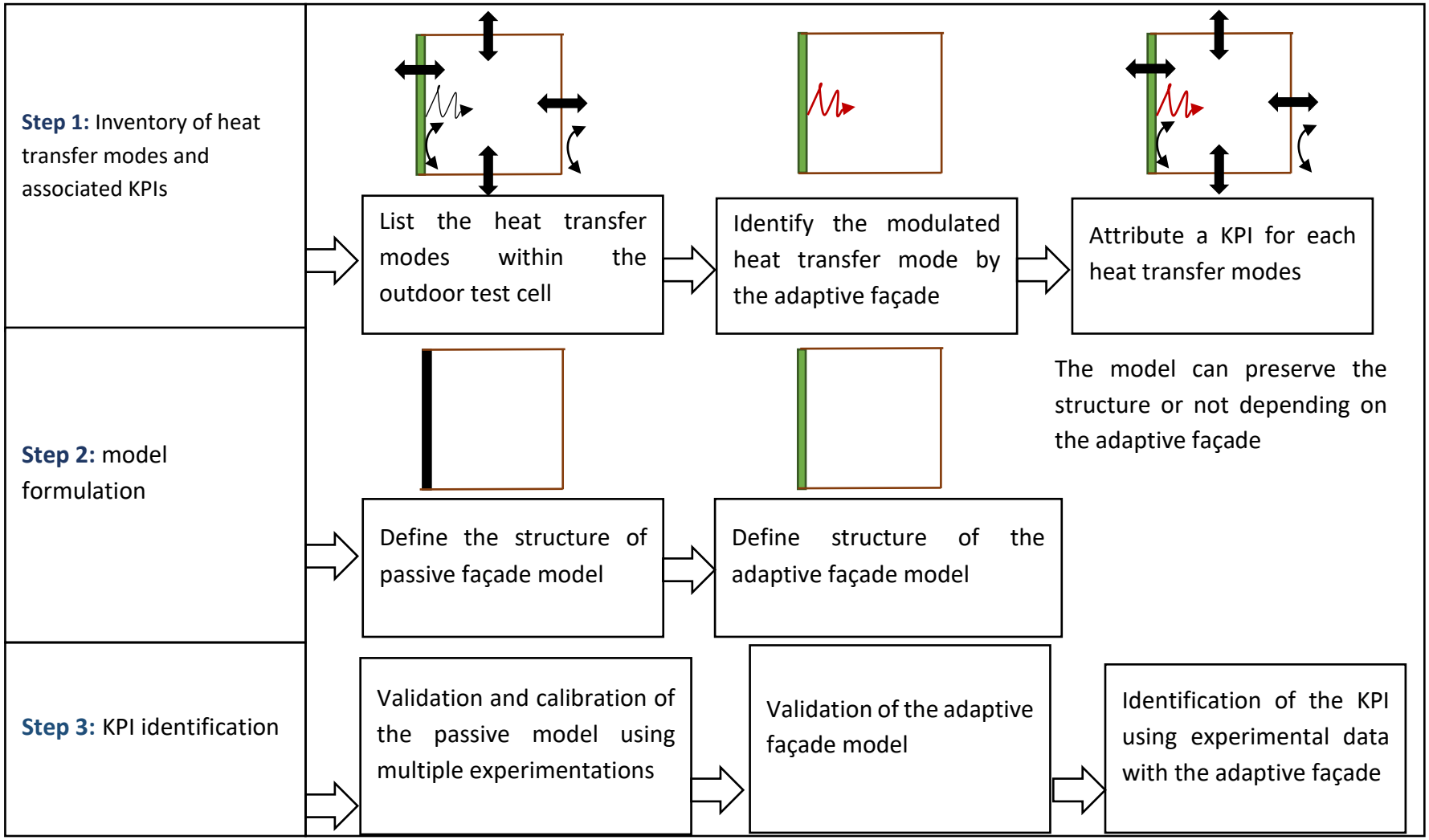

Figure 2-2: The proposed methodology steps

2.2 Methodological framework

A thorough understanding of the adaptive façade functioning is a prerequisite for the thermal characterization under real climate conditions. This understanding can help in building a mathematical model based on measurements, which can enable the identification of KPIs. It is the definition of system identification techniques [80]. In general, the approach of system identification techniques is described in Figure 2-3 .The first step is to design and perform experiments, and after collecting the measurement, a model is constructed and used to estimate the corresponding parameters. This order is often followed in the studies that seek to test new materials and investigate their thermal behaviour.

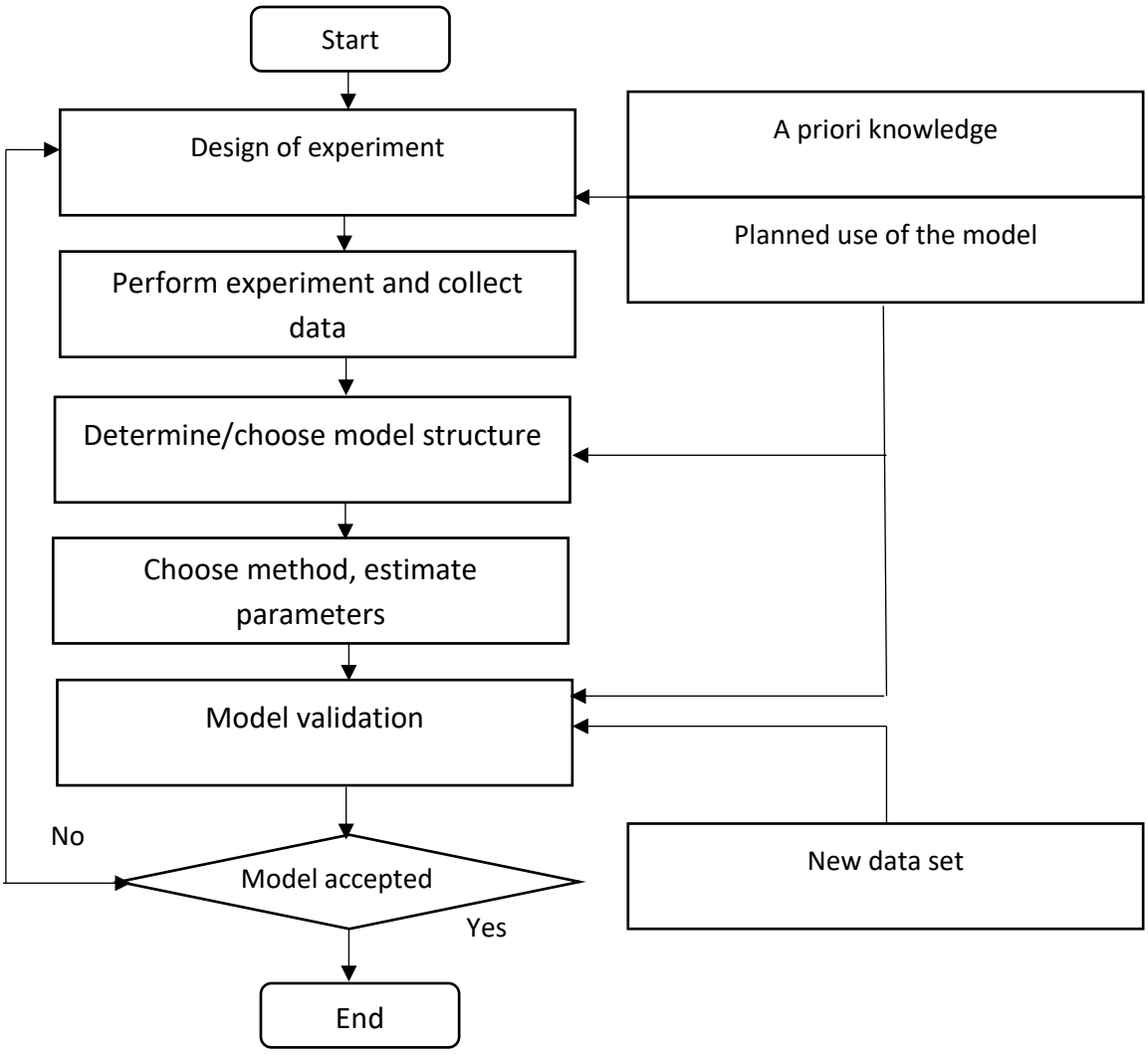

Figure 2-3: Classical flowchart of system identification[80]

Unlike this standard system identification order flowchart for buildings, the considered approach aims to simplify the complex thermal behaviour with a numerical model, which will be validated using the experiment measurements as in studies done by He *et al*. and Zhu *et*

al. [81], [82]. Therefore, the main difference between this approach and the flowchart in Figure 2-3 is that the model structure is detailed before performing experiments. This approach can also serve to list required sensors and their placement, that are necessary for the model implementation in a later step.

Prior to numerical model implementation, it is essential to define the list of all occurring heat transfer pathways governing the building element. This list will allow the definition of the heat pathways modulated by the adaptive façade. Among these, the most dominant ones and those most affected by the dynamic behavior of the façade can be selected. The resulting heat gain or loss can be either measured directly, or estimated and presented as the derived key performance indicator. Lastly, this KPI will then be estimated using a numerical model and experimental data. The proposed research methodology can be broken down into three main phases, namely (1) Inventory of heat transfer modes and the associated KPIs, (2) model formulation, and (3) Identification of the KPI, as schematized in . Each step of the methodology is associated with various research questions that it aims to address. The details of this methodology are presented in the sections 2.2.1 to 2.2.3.

Table 2-1: Steps of the methodology and the guiding questions

Inventory of heat transfer modes and the associated KPIs
- Which heat transfer mechanisms are present? Any heat storage? - Which heat transfer path is modulated by the adaptive façade? - Which performance indicators can better characterize the ongoing phenomena?
Model formulation
- How to model each heat transfer mode? - Where is the equation component that incorporates the variable KPI? - Which parameter can be simplified/neglected? Any hypothesis?
Identification of the key performance indicator
- Which experimental scenarios including control strategies (if they exist) can be performed to calibrate a baseline model? - Which model's parameters are the most influential? - Which experimental scenarios including control strategies can be performed to calibrate an adaptive model?

2.2.1 Step 1: Inventory of heat transfer modes and associated KPIs

The first step of this methodology is to list the heat transfer modes occurring within the test cell integrating the adaptive façade. In general, the building heat transfer can be through three modes: conduction, radiation either short-wave or long-wave, and convection. Those heat transfer modes that occur at the same time have a major impact on the interior heat gain or loss of the building, which in turn impact the overall energy performance. Thus, it is necessary to start with an inventory of those heat transfer modes. Furthermore, the presence of an adaptive façade can modulate one or more of these thermal pathways using extrinsic or intrinsic control strategies. Listing all of these heat transfer modes can lead to selecting the ones that the adaptive façade modulates most significantly. All of the listed heat transfer modes including this selected 'adaptive' heat pathways, should be associated with relevant performance indicators for evaluating the façade. For instance, in the case of shading system

with a glazed area, the dominant heat transfer mode is the short-wave length radiation through the non-shaded parts of the glazing, which introduces a solar gain to the interior environment. This 'adaptive' heat pathway is associated to the key performance indicator called the solar transmittance expressed as $\tau(t)$. This performance indicator is therefore the parameter used to characterize such an adaptive system.

In addition to convection, radiation and conduction, the adaptive façade can also modulate the heat storage, such as with PCM integrated façade. In this case the heat storage through the adaptive façade is the governing phenomenon that can be relevant to the façade thermal characterization. An example of adaptive façades and their associated dominant heat transfer mode and keys performance indicators are listed in Table 2-2. In all cases, the listed key performance indicators that were considered static for passive façade should be considered time-dependent for heat pathways modulated by adaptive façade. This does not deny the fact that even in passive façade a KPI can be time-dependent. For instance the apparent thermal capacitance through an opaque wall depends on the thermal excitation nature and magnitude and how much 'mass' of the wall is engaged thermally [83]. In addition, for an opaque wall exposed to exterior conditions, the thermal capacitance is also highly affected by the solar gain, further illustrating the dynamic nature of even conventional KPIs.

The dynamic KPI associated with the governing modulated heat pathway is the output of the methodology. Thus, it is worthwhile to investigate whether this KPI can be measure directly. Otherwise, an indirect approach is necessary to approximate it using a dedicated model. Although the KPI is time-dependent, in the case of an adaptive façade with extrinsic control, the KPI should be expressed as a function $F(z,u)$ of the triggering variable z (i.e. the external factor that drives the control response) associated with the control strategy u. Figure 2-4 illustrates the cause-effect relationship between the outdoor environmental conditions, the indoor air temperature $\boldsymbol{T_{ai}}$, the triggering variable v, the control operations u, and the dynamic KPI.

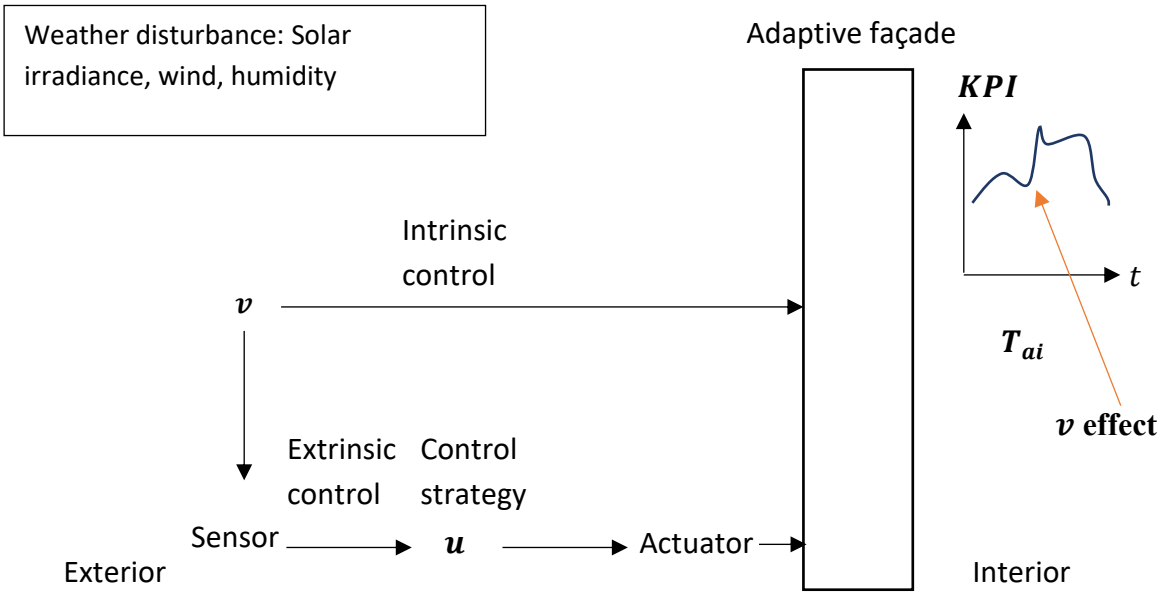

Figure 2-4: Diagram showing the relation between dynamic KPI and triggering variable

Table 2-2 shows the associated variables for the suggested KPIs for various adaptive façades

Table 2-2: Adaptive heat transfer mode and the corresponding indicators

Adaptive heat transfer mode	Adaptive façade example	Suggested indicators	Driving variable and control strategy
Conduction	Opaque adaptive façade	Thermal capacitance $C(t)$ Thermal transmittance $U(t)$	(p, I) Where p is the amplitude of the heat injection, and I is the solar gain
Convection	Double skin façade, ventilated façade, window allowing airflow, ventilated insulation	Indoor convective heat transfer coefficient $h(t)$	(v, α) Where v is the wind speed, and α is the opening area
Short-wave radiation	Shading device, electrochromic glazing	Solar heat gain coefficient $g(t)$ Solar transmittance $\tau(t)$ Solar absorptance $\alpha(t)$ Solar reflectance $\rho(t)$	(θ, β, f) Where θ is the solar incidence angle, β is the tilt façade angle, f the shading system variable
Heat storage	Phase change material (PCM)	Latent heat $L(t)$	(mp) Where mp is the phase changing window

The relationship between the KPI and the triggering variable can be obtained using the outdoor measurements for realistic conditions. However, it is possible to obtain this function using indoor conditions, with a controlled device that can reproduce the triggering variable, such as solar simulator for solar irradiance, or fan effect for wind. The underlying challenge using a controlled device is how well it can mimic the real conditions, especially when many devices should be tested simultaneously to reproduce the outdoor conditions. Besides the reuse of the passive KPIs for adaptive façade, new KPIs can be defined, for example in the case of ventilated façade. It can be characterized using the capacity of the façade to pre-heat the ventilated airflow during winter seasons, or the dynamic insulation and thermal buffer efficiency [84]. For transparent façade, the maximum solar gain ratio and the daily integrated solar gain coefficient can be used [85].

The associated KPIs for the remaining heat transfer modes of the test cell should also be listed. This step of the methodology connects the conceptual inventory of heat transfer phenomena occurring within the adaptive façade and the surrounding envelope with the KPIs. Those KPIs, are therefore, integrated into a selected model.

2.2.2 Step 2: Model formulation

The numerical model aims to provide a simplified representation of the relevant physical phenomena occurring within the façade. After listing the occurring heat transfer phenomena and their associated KPIs as explained in the last section, the next step is to incorporate them into a mathematical model. Thus, the choice of the model and the input parameters should be selected. In fact, three building thermal modeling approaches exist. The physical based models known as “white-box”, the data-based models known as “black-box” and “grey-box” which consists in combining the other two models’ types.

The **white box models** consists of physical based models, solved with numerical equations [86], thus, the interpretation of the parameters is physically meaningful. However, this advantage can work against the model’s accuracy, a significant discrepancy between predicted and actual measurements can often occurs, due to the complexity of the necessary model’s input, besides that the computational cost is higher[87].

The heat flows from a high temperature zone to a lower one, the ability of a material to resist this heat flow is called thermal resistance R, as an analogy with electrical circuit resistance. Whereas a material thermal capacitance C indicate how much internal energy it can store. The less a material’s temperature change when a certain amount of heat is injected to the material the higher its capacitance [88]. A representation of a building using an RC thermal circuit is one of the **grey-box models**. This approach allows the physical interpretation of the parameters using energy balance equations, and also the identifiability based on the measurement data.

The **black-box models**, such as Artificial neural networks (ANN) and Random Forest (RF) can also be used to predict the building's thermal parameters and energy consumption. However those predictor models does not allow the physical interpretation of their hyperparameters, and also they require for the training and validating phases a large dataset that can take long duration to collect [89].

One crucial point here, is that the objective is to evaluate the adaptive façade thermal performance, but if the thermal performance of surrounding envelope, which is the outdoor test cell envelope itself integrating this adaptive façade is unknown, the uncertainties are being accumulated here. Therefore, developing a thermal base model is important to demonstrate the fundamental thermal behavior of the outdoor test cell without the adaptive façade. Thus, at this phase of the proposed methodology, it is necessary to have a two-stage characterization approach: without (with a passive element) and with the adaptive façade. Moving from passive façade model (without adaptive element) to adaptive façade model, the structure of the model does not necessarily need to be modified. In case the adaptive façade modulates an existing heat path already represented in the passive façade model, and does not require additional terms. For example, to test a kinetic shading, a double glazing can be selected as a reference façade, both cases involve the same main heat path: solar radiation, thus the model can remain the same, except that the term representing the solar radiation for kinetic shading model is the KPI to quantify. In order to characterize the outdoor test cell alone, it can be useful to replace the tested façade with a passive façade. The objective behind using a baseline model or a passive façade model is not only the comparison, but to calibrate a baseline model, thus, the passive façade must follow those criteria:

- No discrete operational states;
- No operational energy required for functioning;
- No control operations or user interactions are needed.

As stated above, there is a need for a reference "passive" façade for this methodology. Table 2-3 proposes passive façade types for the evaluation of corresponding adaptive façade.

Table 2-3: Example of adaptive façade and associated passive façade that can be used as a baseline for the model

Adaptive façade to be evaluated	Corresponding passive façade
Adaptive shading device window scale: • Venetian blinds • Roller blinds • Complex geometry shading	Glazing
Adaptive glazing: • Selective glazing • Photochromic glazing • Thermochromic glazing	
Kinetic façade scale	Unshaded façade scale

Ventilated double façade	Unventilated façade
PCM façade	Façade with the same thermal resistance without PCM layer
Green façade	Façade with the same thermal resistance without vegetation
Green roof	Same thermal resistance of the roof without the vegetation

The last later step is described in Section 2.2.3.

2.2.3 Step 3: Model calibration and KPI identification

a. Calibration of the passive façade model: experimental scenarios and sensitivity analysis

Now that the model parameters are defined for both configurations: with and without the adaptive façade, it is necessary to identify the input and output signals. Experimental measurement scenarios and data are therefore required to fit the model for the baseline model calibration first. Then, after the calibration of the model, and after the introduction of the adaptive façade, new experimental campaigns are implemented in order to collect new measurements using outdoor experiment. Those measurements are used to fit the adaptive façade model to identify the corresponding KPI. Those experimental scenarios are dedicated to excite the underlying phenomena that can allow the identification of each KPIs of the model. The experimental scenarios that can provide the needed measurements to fit the model can be categorized into two different types that is to say steady state tests and dynamic experimental tests. The purpose of the steady state tests such as the co-heating test using a constant heating source is to define the heat loss coefficient HLC of the building [90], and the conductive resistance of the building, while avoiding the maximum possible disturbances such as the incorporation of the adaptive façade and if possible, absence of solar gain. Thus, a co-heating test practically involves placing a heater inside an unoccupied building, a fan may also be necessary in the inside of the building to make the temperature homogeneous as possible. This test can be done for a duration of one or more weeks [90]. Applying a controlled dynamic heating injection can also determine the HLC of the building. Methods such as ISABELE [91] and QUB method [92] are used for such a purpose. This later experimental protocol is characterized with a shorter duration test. The dynamic characteristics of the building, require dynamic excitations to the indoor temperature using a dynamic heating source injection such as the ROLBS method which stands for “Randomly Ordered Logarithmic Binary”. This method was proposed during the PASLINK project[93], and it aims to decorrelate the wanted parameter from the indoor conditions, in order to determine the thermal capacitances of the building. Those experimental scenarios are a crucial step for the parameter identification of the outdoor test cell’s model. Outdoor dynamic tests under real conditions should also be performed. All those scenarios, together, can provide the necessary measurements to elaborate the baseline model before the integration of the adaptive façade. Nevertheless, this methodology requires appropriate measurements of indoor and outdoor boundary conditions. The used positioning of sensors is specified in the case study from Chapter 3.

The infiltration and thermal bridges losses are critical parameters to define for any building model. In the perfect case, both losses should be identified experimentally. For the infiltration losses, various methods exist to estimate the air change rate occurring according to an imposed pressure difference to the building. The Blower door test is the most used test for in-situ airtightness test for buildings. This method is defined in the standard ISO 9972 [94]. Other derivative methods also exist for small volume enclosure such as the pressure decay [95], [96] and pulse pressure method . Overall, those pressurization tests technically measure the pressure difference between the inside of the building where a fan is introducing air rate, to the outside pressure within or beyond 50 Pa. Subsequently, the air change rate can be derived from the pressure difference curve. Concentration difference of a chosen gas can also be used for air leakage test according to the gas tracer method defined in ISO 12569 [55] where a gas injector is placed inside a building and its concentration is measured to drive air change rate. For the thermal bridges, the standard ISO 10211 [97] can be used to define a theoretical value. In case the in-situ inspection is required, the infrared thermography method can be used [98]. Table 2-4 summarizes those technics by clarifying which regime is adopted and the main output.

Table 2-4: Summary of some protocols that can be used to define the test cell thermal parameters

Protocol	**Purpose**	**Type of regime**	**Main output**
Co-heating test (unoccupied building)	Global assessment of building heat loss	Steady state (either indoor or outdoor testing)	HLC heat loss coefficient
ISABELE or QUB (unoccupied building)		Dynamic controlled thermal excitation	
ROLBS	Identification of dynamic thermal behaviour	Dynamic controlled thermal excitation	Building thermal capacitance Time constant
Infrared thermography	Detection of thermal bridges	Depend of how and when the measurement is done	Qualitative output: localization of thermal bridge
Gas tracer	Airtightness assessment	Quasi-state	Air change rate
Blower door test		Quasi-state	
Pressure decay		Dynamic	
Pulse pressure			

The experimental scenarios described in Table 2-4 can provide the necessary measurements and some of the identified thermal parameters to fit the baseline model. However, there is a need to know the relative effect of each thermal parameter on the model output. Thus, this is the objective of sensitivity analysis study that should be coupled with the calibration

process. The sensitivity analysis is defined as "*The study of how uncertainty in the output of a model (numerical or otherwise) can be apportioned to different sources of uncertainty in the model input* " [103]. Therefore, it enables the identification of the parameter with the strongest effect on the observed variable. As a result, it can also identify the non-influential parameters which can be remaining constant later. Various methods of sensitivity analysis exist, and they are based on the same general steps namely definition of a variation interval for each parameter, and calculation of the output of the model using those values. The influent parameters will be identified after with an optimization process.

Those sensitivity analysis methods can be classified into two main categories [99]:

- *Local methods:* where only the effect of varying one input parameter within a specific range on the model's output is observed;
- *Global methods:* where all the input parameters are varied at once and as a result it is possible to detect one or a group of parameters that have a mutual effect on the observed output.

Once the sensitivity analysis is performed, a set of influential parameters is selected to be optimized using a dedicated optimization algorithm, the objective function will be the minimization of the error between a predicted variable and its measurement.

While switching between the experimental scenarios, it is essential to note which parameter of the model will remain constant and which one to optimize according to the results of the sensitivity analysis. The infiltration losses, or exterior convective heat transfer coefficient for example are variable between indoor and outdoor experiment, and between variable climate experiments, since they are both affected by the wind velocity. Thus, those two parameters should be identified for each experimental scenario, unless they are not influential on the model's accuracy.

b. Calibration of the adaptive model: Experimental scenarios and the KPI identification

Regarding the calibration of the adaptive façade model, the calibrated passive façade model can be a base for it, since it is already validated during the previous step. Thus, a transfer learning can be performed to reuse the thermal parameters that remain the same or non-influent for both experimental scenarios. Moreover, the control operations are an important aspect to consider in this phase of the methodology, as defined in the introduction listed criteria. When the control is extrinsic, it is important to define which control strategy maximize the observability of the phenomena to be characterized. For example, a closed blind in case of venetian blinds characterization will not be valuable since it does not highlight the contribution of the solar gain. In case of working with solar shading devices such as venetian blinds, roller blinds automated control strategies for residential and office buildings were recommended in ISO 52016-3 [1] to evaluate the energy demand. The application of some of those standard control flowchart was done in [100]. However, those reference control strategies were based on a multicriteria approach that consider the daylight, the occupant's comfort and the energy demand, which means it is dedicated for energy performance

characterization, and at this stage of this research, this thesis work is located at the thermal performance level. Thus, the control strategies should be aligned with final objective of this stage, which is the thermal characterization. To do so, those control strategies should allow the evaluation of the heat transfer path in a more relevant way. For an adaptive façade with an intrinsic control, it is highly climate-dependent. Therefore, a survey of the choice of experiment days with the climate conditions of interest is required. For the outdoor experimental scenarios, it is recommended to save the same sensors location and surface azimuth (orientation) of the passive experimental scenarios. New sensors may be required when introducing the adaptive façade to the test cell. As stated in the passive façade model calibration, sensitivity analysis can also be performed to determine the influence of the new introduced parameters.

c. Hypothesis for model calibration

Both steps, regarding the passive façade model validation, and the adaptive façade model partial validation, can result in obtaining the dynamic KPI. The KPI is the term with the highest uncertainties, and it can be identified directly from the model depending on its type: grey, white or black-box model. During the calibration process, for instance, if the structure of the model is the same, in other words, if the ongoing phenomena was also occurring in the passive façade model, except that now is expressed as a dynamic function $F(z, u)$. In this case, to calibrate the adaptive façade model, as a hypothesis the same thermal parameters of the test cell can be assumed to be identical. For the sake of comparison between the adaptive façade and passive façade thermal performance, the performance indicator should be the same, if not, then the comparison can be on the energy efficiency level, using the heating and cooling load energy consumption for both.

Figure 2-5 summarizes the detailed steps for the dynamic KPI identification.

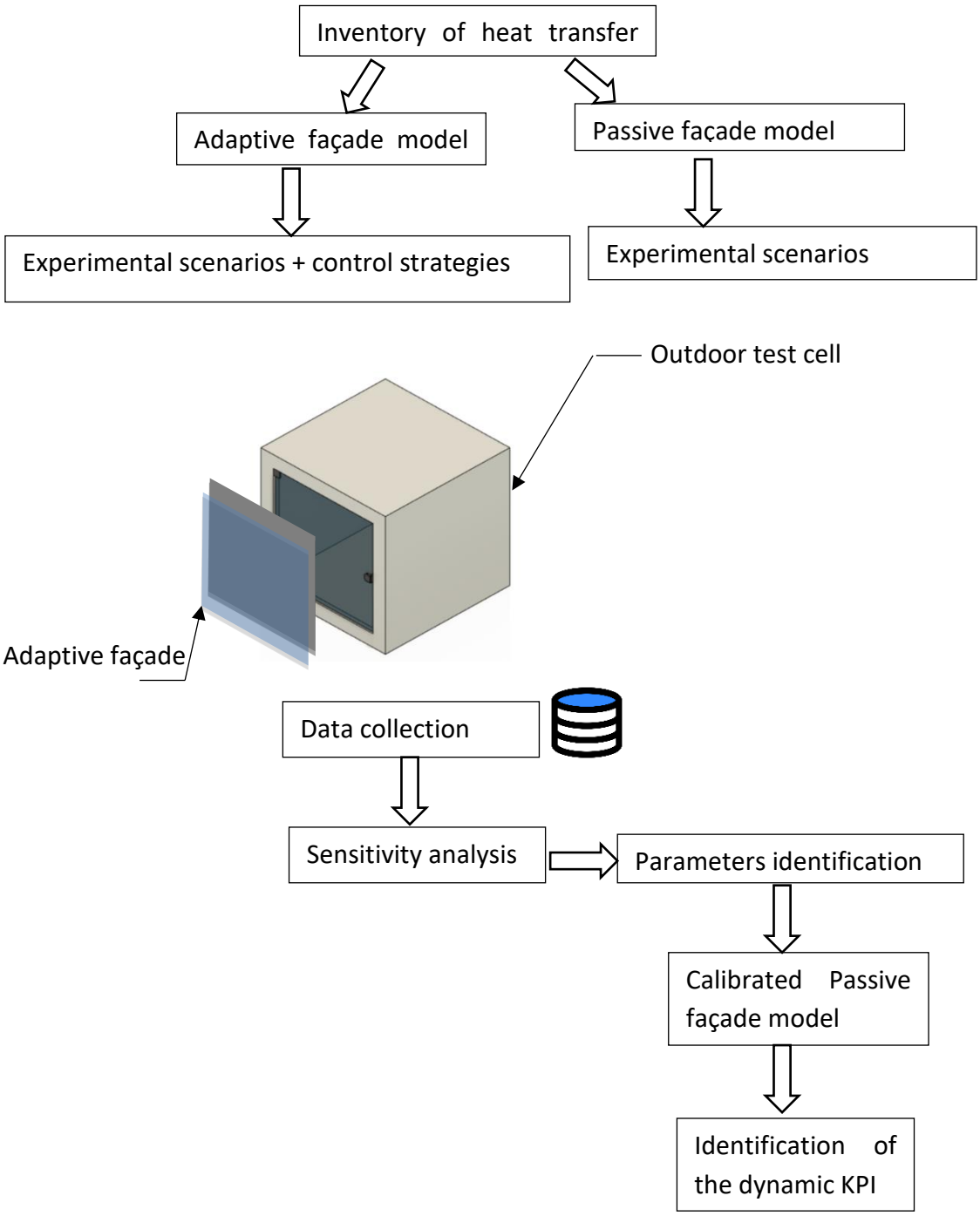

Figure 2-5: Flowchart of the sub-steps within the KPIs identification step

2.3 Limitations

The proposed hybrid methodology for adaptive façade thermal characterization is subjected to several limitations regarding each step of the framework:

1. *Inventory of heat transfer modes:* the listing of occurring heat transfer modes within the test cell and adaptive façade may ignore the inter-dependency of physical domains other than thermal behavior on the KPIs;
2. *Model formulation:* regarding building scale, the characterization framework is designed for outdoor test cell use and not for whole buildings. The step of passive façade testing is difficult to apply to a real building. The dependency of the characterization framework on the passive façade baseline model should also be mentioned. Moreover, the validity of the model when the location is changed must also be questioned. In the context of the MBLabs project, this concerns the applicability of models elaborated at different O3BET locations;
3. *KPI identification:* the dynamic KPI identified using a specific measurements sequence and a selected model must consider the changing meteorological conditions. For instance, a dynamic function that characterizes solar gain as a function of solar incidence angle is not fully reliable for cloudy days data series. Therefore, there is a dependency on the climate context where the data was measured. In other words, since the objective is to identify the KPI when the physical phenomena is dominant (e.g. sunny days for solar gain), this KPI may not coherently applicable to data where this phenomenon is weak (e.g. cloudy days).

Despite those limitations, the proposed methodological framework provides a structured framework to characterize thermal performance for complex adaptive façades, which are often difficult to characterize using simulation tools alone.

2.4 Conclusions

The present methodology chapter aims at proposing a hybrid approach based on experimental-numerical methods to characterize adaptive building elements using outdoor test cells. The proposed approach is based on a two-step characterization: a passive façade model and an adaptive façade model. The passive façade model is dedicated to characterizing the test cell thermal parameters using a selected passive façade configuration. However, the adaptive façade model introduces the parameters that capture the adaptive element performance. Both models are constructed based on a primary inventory of occurring heat transfer modes within the outdoor test cell equipped with the adaptive façade. The calibration of both models is based on experimental scenarios, in order to define the identifiable parameters, and to validate the baseline model. In the case of an adaptive façade with extrinsic control, it is necessary to identify which control strategy can reveal the effect of the heat transfer path modulated by the adaptive façade. For an adaptive façade with intrinsic control, the characterization is more dependent to the outdoor meteorological conditions; thus, the selection of the climate conditions of interest is relevant. One perspective regarding this proposed framework, in the context of outdoor test cell use, is how to transfer the learning from the current model scale to a larger building scale.

Chapter 3: Thermal performance characterization of a complex shading device

Summary of the chapter

The purpose of this chapter is to provide key inputs on the experimental evaluation of the thermal performance of a complex shading device. As a first step, the selected shading device is presented. The second part focuses on the heat transfer, introduces the modes and the model is presented. The third part details measurement campaigns designed to enable model identification from observed behavior for both scenarios: with and without the shading device. Experimental protocols, sensors, and boundary conditions are described for each study case. Results are discussed and this Chapter concludes with recommendations for the methodology.

Résumé en français

L'objectif de ce chapitre est de mettre en œuvre la méthodologie pour caractériser un dispositif d'ombrage complexe. Dans un premier temps, le système d'ombrage considéré ainsi que le dispositif expérimental sont présentés. Ensuite, les transferts de chaleur et le modèle adopté sont définis. La troisième partie détaille les campagnes de mesures conçues pour permettre l'identification du modèle à partir du comportement observé pour les deux scénarios : avec et sans dispositif d'ombrage. Les protocoles expérimentaux, les capteurs et les conditions aux limites sont décrits. Les résultats sont discutés et ce chapitre conclut par des recommandations méthodologiques.

3.1 Introduction

As stated, fenestrations and openings are a key part of the building performance. While their first role is to allow light to enter, they also have to control solar gains. This crucial aspect can serve various functions, such as providing the natural light and solar heating to the inside; allowing air circulation; which in turn can impact the heating and cooling loads [101]. With the window glazing other devices can be integrated such as a shading device, which can be either interior, between the glazing layers, or in the exterior. The use of double glazing with shading device can provide better indoor comfort, and reduce the reliance on the artificial lightening and cooling or heating systems. Many factors play a role on the efficiency of this global window as a system, such as the size of the window and the window-to-wall ratio[102], types and properties of the glazing, the design, the shading device position [103], and the orientation of the building and its exposure to solar radiation.

Heat transfer through windows and other fenestration systems is an important aspect to consider during the thermal performance evaluation of buildings, those elements are regarded as a weakness for the envelope thermal insulation, since they can be responsible for heat loss during winter and heat gain during summer. The thermal performance of glazing systems plays a crucial role in determining the energy efficiency and comfort levels of buildings [104].

Various new technologies in windows glazing market have been introduced, with the aim of reducing energy consumption of heating, ventilation, and air conditioning systems (HVAC) and improving occupant's comfort, such as low emissivity glass coating, new glazing systems resistant to fire, or integrated shading devices in multilayer glazing, that can be automatically or manually manipulated, alongside with gas filled gaps. Those innovative glazing technologies require thermal performance evaluation, for the purpose of measuring the total solar heat flux that is received inside the building, which in turn play a vital role in the sizing and scheduling of HVAC systems functioning. Although advanced existing simulation software can predict glazing performance, and help in decision making process for energy efficiency, such tools still need to be developed to deal with the complexity of unconventional glazing systems.

The key objective of this study, is to investigate the potential of a complex fenestration system composed of a double-glazing with outer diagonal shading devices using an outdoor test cell in Bordeaux (France). This shading system is developed based on an analysis of solar rays' angular characteristics, specifically solar incidence angle and local azimuth which results in a seasonal thermal behavior. The thermal evaluation of adaptive building element methodology as proposed in Chapter 2 starts with a clarification of the heat transfer mechanism, in order to define the dominant heat transfer path modulated by the façade, then the model formulation and the required measurements are collected from experimental scenarios, and the path to the estimation of the desired parameter and model validation using ray tracing technic as illustrated in Figure 3-1.

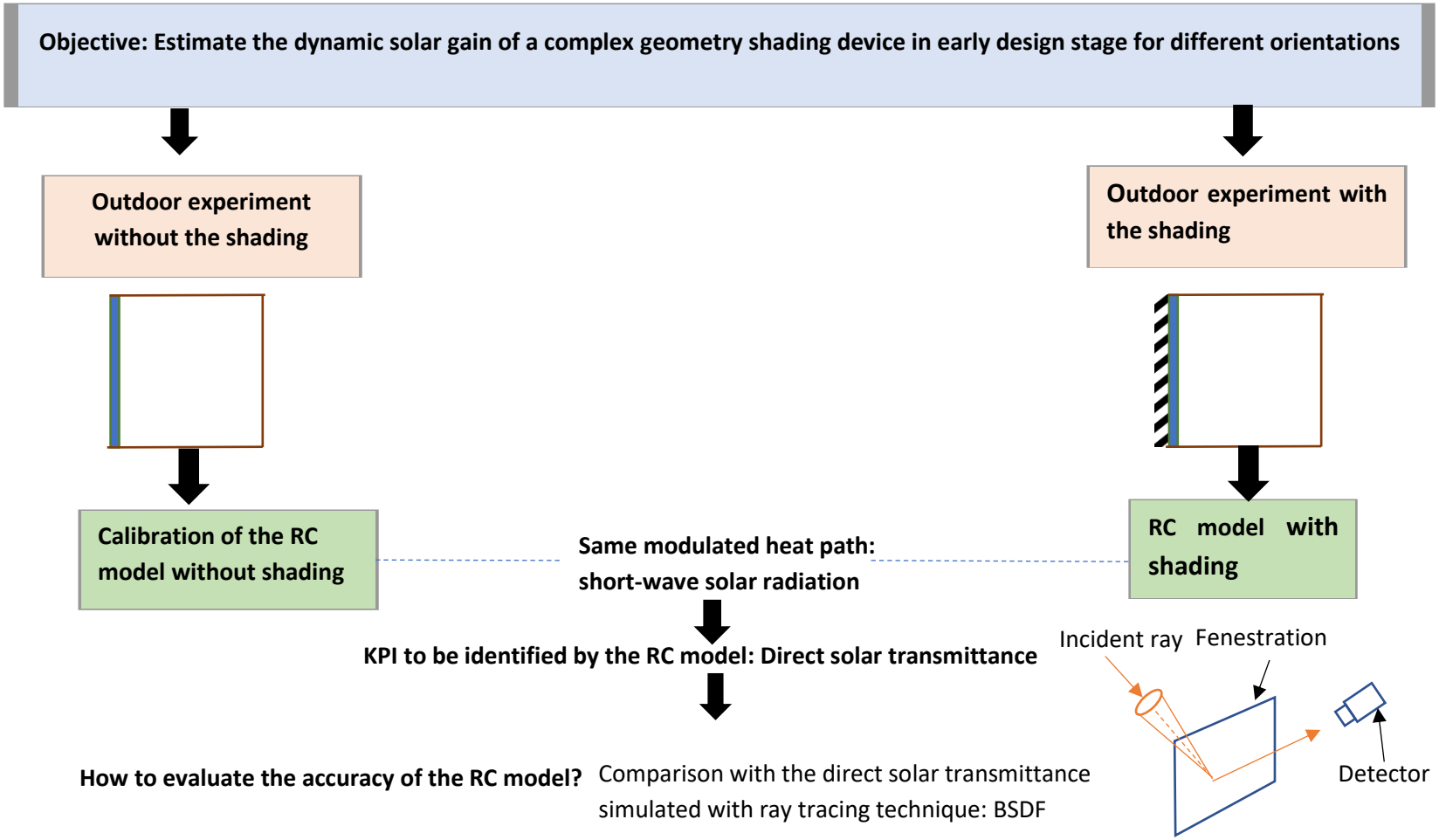

Figure 3-1: Application of the methodological framework

3.2 Application of the methodology

3.2.1 Description of the studied shading device

The shading device that we considered for this thesis can be described as venetian blinds but with fixed external diagonal slats as shown in Figure 3-2. Those stats have been primarily designed to block high altitude summer sun rays while allowing the winter sun rays to pass through (see Figure 3-4). Thus, this seasonal behaviour leads to a dynamic solar transmittance. This shading design depends also of the façade orientation. The tested diagonal shading device shown in Figure 3-3 consists of semi oblong slats made from composite aluminium.



Figure 3-2: View of the diagonal shading

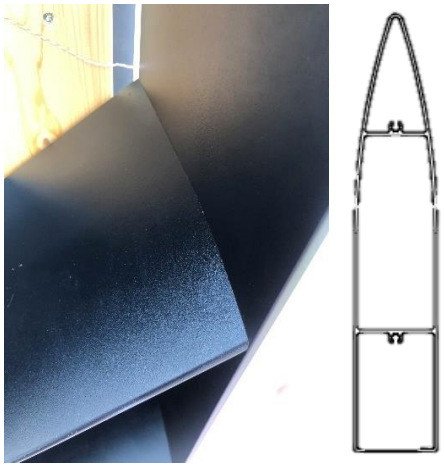

Figure 3-3: View of the oblong slats shape

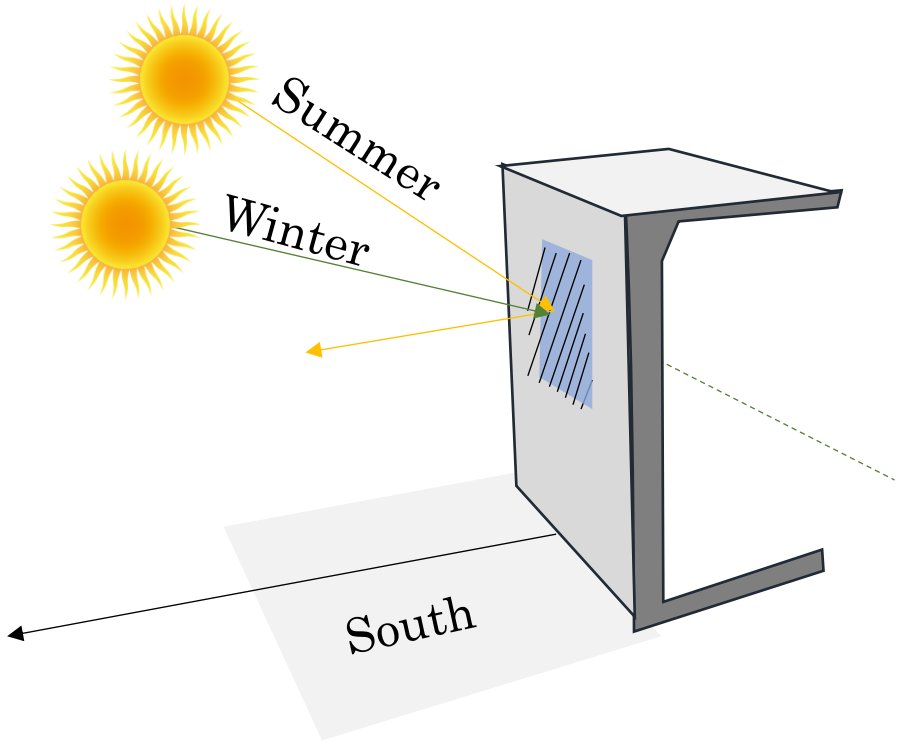

Figure 3-4: Diagonal shading concept illustration

The particularity of this system is that the slats have two design angles: one with the horizontal plan and the second for the tilt profile angle (see Figure 3-5). This shading solution was supplied by a third part company, and the tilt angles were calculated by a propriety confidential algorithm based on solar geometry. The materials used for this prototype and their dimensions are listed in Table 3-1.

Table 3-1: Description of the shading solution

Material	**Composite aluminium with black mat colour RAL 9005**
Slat tilt relative to the horizontal plane	35.4°
Profile tilt angle	+4.1°

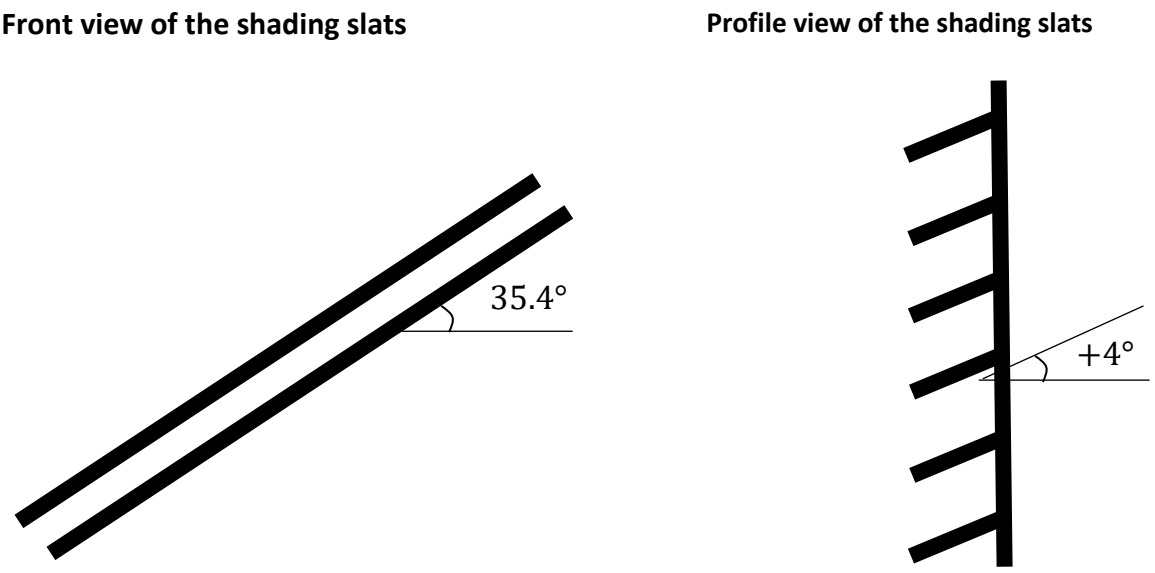

Figure 3-5: Illustration of slat tilt angles of the diagonal shading

Few studies have worked with the diagonal shading device, and they mainly study the daylight effect [105], [106], [107], by using a 3D geometry model to represent the shading. For such as shading device, it is a challenge to evaluate its thermal performance. Current software like EnergyPlus does not include it in the database. Since it is considered as a non-conventional shading device, in contrast with venetian and roller blinds. This shading is considered as a Complex Fenestration System (CFS), which refers to type of systems that redirect rays in a complex way [108]. An accurate model for fenestration system with an integrated shading device's solar gain calculation should be able to represent the optical and thermal properties in two dimensional angular dependency namely solar position and control operation [109]. The direct transmitted short-wave radiation or solar transmittance is a dominant term of the solar gain. There are various technics to evaluate the solar transmittance of conventional shading devices such as screens, shades and blinds. In literature, those technics can be classified into two main approaches: Direct and indirect approaches. The direct approaches mainly use either analytical calculations with the system geometrical characteristics, such as the radiosity method in ISO 15099 [110] for conventional venetian blinds, that is used in many software like EnergyPlus, TRNSYS and WINDOW, or direct on-site measurements. The radiosity based equations take into consideration the geometry of the slat type, and the sun incidence angle. The study in [111] compared the computed solar transmittance thanks to radiosity method with the experimental measurements of solar transmittance using vertical pyranometer. A deviation has been accrued between the estimated solar transmittance with radiosity method and the measured solar transmittance especially when it is mainly the diffused irradiance that is dominated. Moreover, it takes as an assumption that the material is perfectly diffuse, and that the slats have a negligible thickness, which can overestimate the solar transmittance values [112]. In 2015, EnergyPlus and TRNSYS introduced a new method called Bidirectional scattering distribution function (BSDF) to account for the scattering properties of a material. It is based on the work done by Klems [113], and it describes the

optical properties as dependent of solar azimuth and altitude using matrix multiplication. Nevertheless, this method requires a high level of geometry details and the material characteristics of the shading device [114]. The experimental approaches to characterize shading devices can be done either by using multiple fixed vertical pyranometers behind the window, and then taking the average irradiance for the calculation of solar transmittance, such as in the studies [111], [115], [116] or by using moving pyranometers vertically mounted behind the window [117]. However, a pyranometer only presents one measurement point, and it cannot capture the exact interior irradiance when using a shading device. While from the indirect approaches one can deduced the solar gain from dynamic model's energy balance equations. Data-driven approaches such as the RC model serve as an effective way in building energy sector for the estimation of various parameters since they use on-site realistic measurements in buildings. Grey-box RC models, similar to electrical circuits where resistance and capacitance are key parameters, have a physical interpretation, making them effective for identifying model parameters. By prior identification of the influent parameters of the RC model, it is feasible to estimate the time-varying solar transmittance using heat balance equations, by treating the solar gain as the output heat flux of the model and using as inputs temperature measurements and different pre-identified parameters.

3.2.2 Experimental setup

Aiming at characterizing this shading device, we use a test cell called Hotbox which is a 1m*1m*1m insulated box with one open façade on which we can install the tested system. The 5 façades are similar and have same constructive layers: OSB, aluminium profile with an air gap, and polyurethane as illustrated in

Figure 3-6. The test cell includes the door as shown in Figure 3-7, and the opposite side correspond to the façade under test. In our case, in order to test the shading device a double glazing of 4 mm for each layer and a cavity of 12 mm filled with air is installed first. The test cell is equipped with wheels in order to allow the orientation to different surface azimuth. Figure 3-8 shows a real picture of the Hotbox.

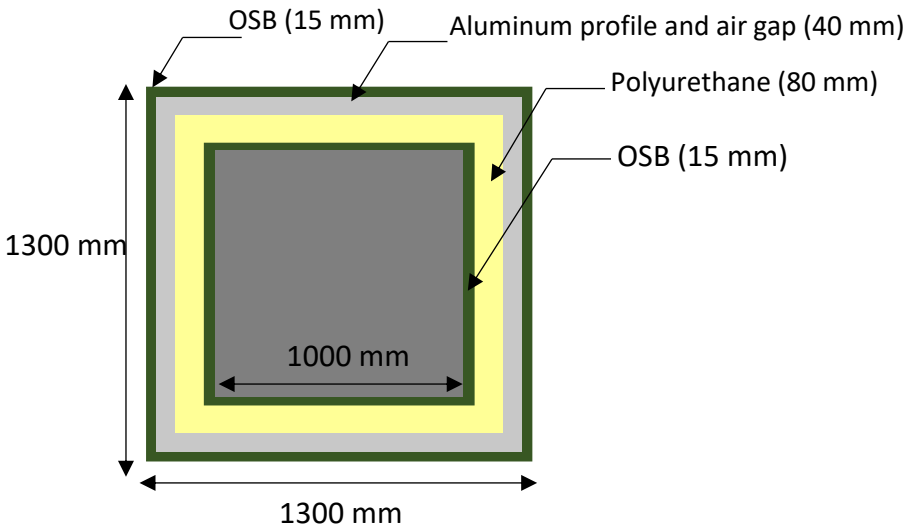

Figure 3-6: Horizontal or vertical layout of the Hotbox [118]

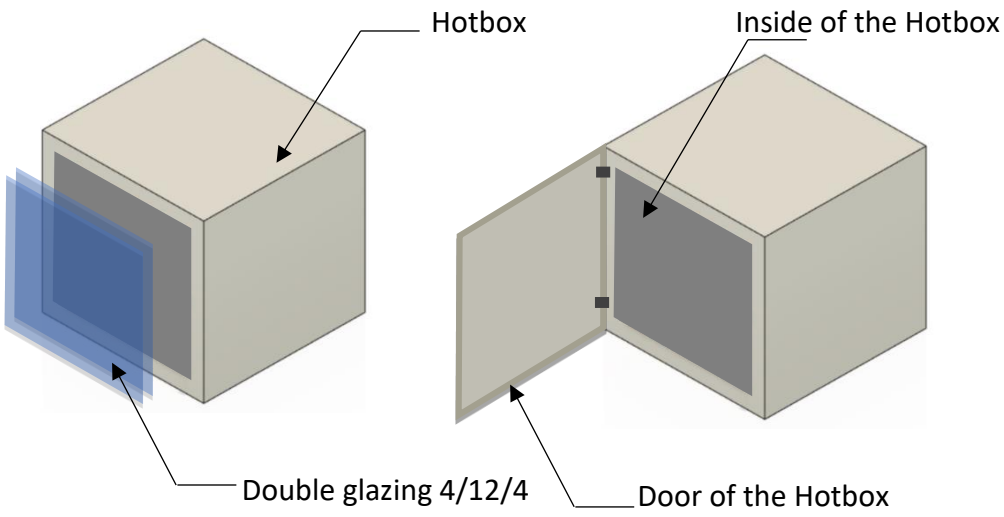

Figure 3-7: 3D schematic view of the Hotbox highlighting the tested façade (front view) and the door (rear view)



Figure 3-8: Picture of the Hotbox

The window is composed from a double glazing Planibel Clearlite 4/12/4 with a cavity filled with air 100%. The shading is therefore placed externally in front of the glazed area as shown in Figure 3-9.



Figure 3-9: View of the shading inside and outside of the Hotbox

The shading structure is positioned on the ground, and to maintain stability under outdoor conditions, especially strong wind, a metal support is fixed on the hotbox rooftop to hold the shading as in Figure 3-10.



Figure 3-10: Metal support to hold the shading in front of the glazed façade of the Hotbox

3.2.3 Inventory of heat transfer phenomena

The heat transfer modes through the Hotbox can be classified into two categories that is to say through the opaque walls and the glazed area, in sunny days conditions those envelope elements subject to multiple heat transfer paths.

Opaque walls

For the outer surface of the opaque walls, the roof is exposed to solar radiation all day, whereas the east, west and rear walls solar radiation exposure depend of the sun trajectory and surface azimuth. The outer surface of the floor is exchange by convection and long wave

radiation with the ground surface. The inner surfaces of the floor, the backdoor, and the east and west façades receive solar radiation during the day from the glazed area. The floor receives such solar radiation during the whole day and for the other vertical façade received solar radiation depending of the sun position. These heated surfaces can release heat to the air by convection. An illustration of those heat paths is presented in Figure 3-11.

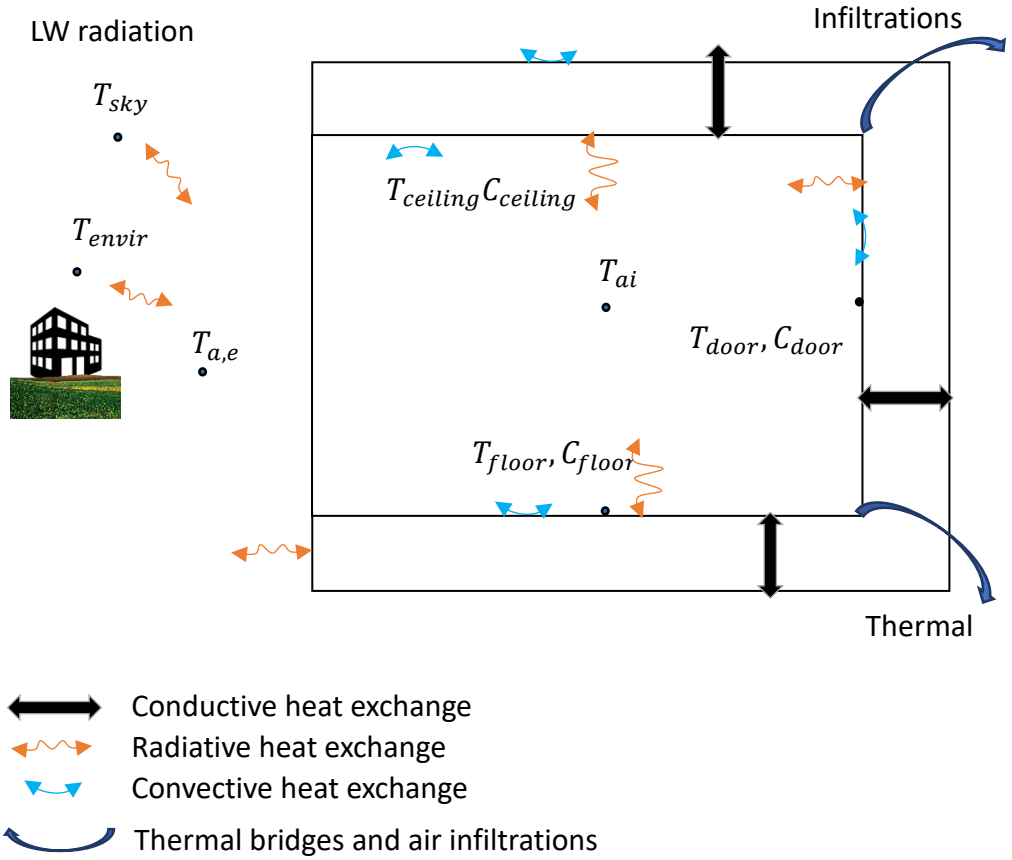

Figure 3-11: Heat transfer inventory of the opaque envelope of the hotbox

Glazed area + shading device

The glazing and shading reflect a part of the exterior solar radiation Φ_{ext} to the outdoor Φ_{ref}, and a part is transmitted filtered by the shading device directly and indirectly through the first glazed layer, air cavity and the second glazed layer to the indoor. The inner surface of the glazing releases the indirectly received solar gain by convection ϕ_{int}^{conv} and long wave radiation ϕ_{int}^{rad}, and the direct part is projected to the inner envelope surface Φ_{tr}, this heat flux first heat up the envelope through absorbed solar radiation, which then exchange with the indoor air through convection and long-wave radiation . Figure 3-12 summarize the heat exchanges within the glazing.

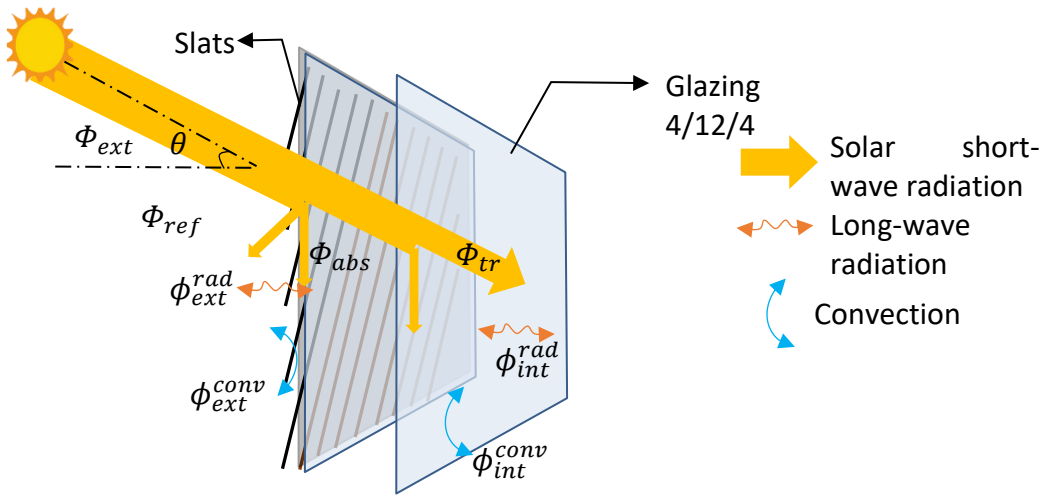

Figure 3-12: Glazed surface heat transfer inventory illustration

The incident solar radiant flux per unit area Φ_{ext} on the fenestration system can be divided into those following parts in Eq 3-1, according to ISO 9050 [119]

$$\Phi_{ext} = \Phi_{tr} + \Phi_{abs} + \Phi_{ref} \quad \text{Eq 3-1}$$

With $\Phi_{abs} = \phi_{int}^{rad} + \phi_{int}^{conv} + \phi_{ext}^{conv} + \phi_{ext}^{rad}$

If we divide the equation above with the Φ_{ext} we can get three optical characteristics in Eq 3-2.

$$\tau + \alpha + \rho = 1 \quad \text{Eq 3-2}$$

Where:

- τ is the short-wave solar transmittance factor of the whole fenestration system;
- ρ is the reflection factor;
- α is the solar absorbance factor, the absorbed quantity of the incidence heat flux $\alpha \times \Phi_{ext}$ is subsequently divided into two parts $q_{int} \times \Phi_{ext}$ and $q_{ext} \times \Phi_{ext}$ which are the energy transferred to the inside and outside respectively as in Eq 3-3.

$$\alpha = q_{int} + q_{ext} \quad \text{Eq 3-3}$$

Where:

- $q_{int}$is the secondary heat transfer coefficient toward the inside by convection and long-wave radiation;
- q_{ext} is the secondary heat transfer coefficient toward the outside by convection and long-wave radiation.

The total solar energy transmittance factor g of the fenestration system is defined by the sum of the direct transmitted fraction of solar radiation and the indirect part released to the inside as a heat exchange by convection and radiation which can be represented by the secondary heat transfer coefficient to the inside q_{int} . g can be defined by Eq 3-4.

$$g = \tau + q_{int} \quad \text{Eq 3-4}$$

Therefore, the total solar energy transmitted to the indoor environment Φ_i is defined by Eq 3-5.

$$\Phi_i = g \times \Phi_{ext} = \tau \times \Phi_{ext} + q_{int} \times \Phi_{ext} \quad \text{Eq 3-5}$$

The dominant heat transfer phenomena in this study case is the short-wave radiation transmitted by the system: shading device + the glazing which is the part $\tau \times \Phi_{ext}$. Therefore, the chosen KPI to evaluate in this case study is the factor τ.

In addition, $\tau_{direct,sh}$ is the solar transmittance factor related to the direct irradiance incident on the fenestration system. This component is the part that holds the dynamic behaviour of the solar gain because the direct incident irradiance on a vertical plan depends of the solar incidence angle as well as the surface azimuth, and $\tau_{diff,sh}$ is used for the factor of the solar transmittance of the diffused irradiance. As a result, the short-wave solar gain across the non-shaded area of the glazing A_g can be expressed using the direct irradiance $Direct_\gamma$ projected at the window plan with the corresponding surface azimuth γ and the projected diffuse irradiance $Diff_\gamma$ from the ground and the sky, as illustrated by Figure 3-13, and it can be defined with Equation 3-6.

$$\Phi_{tr} = A_g \times [\tau_{direct,sh}(t) \times Direct_{\gamma}(t) + \tau_{diff,sh} \times Diff_{\gamma}(t)] \quad \text{Eq 3-6}$$

At this phase, the KPI that capture the dynamic behaviour of the solar gain is $\tau_{direct,sh}$ where the triggering variable in this case is the variable solar incidence angle alongside with surface azimuth. Thus, the fenestration system in this case operates as an open-loop control system, because the short-wave transmittance direct factor $\tau_{direct,sh}(t)$ vary without the interaction with the occupant or any use of an external control device. This leads to conclude that the characterization of the thermal performance of this fenestration system can be done according to the climate solar gain, subsequently, the experimental scenarios will be under sunny climate conditions.

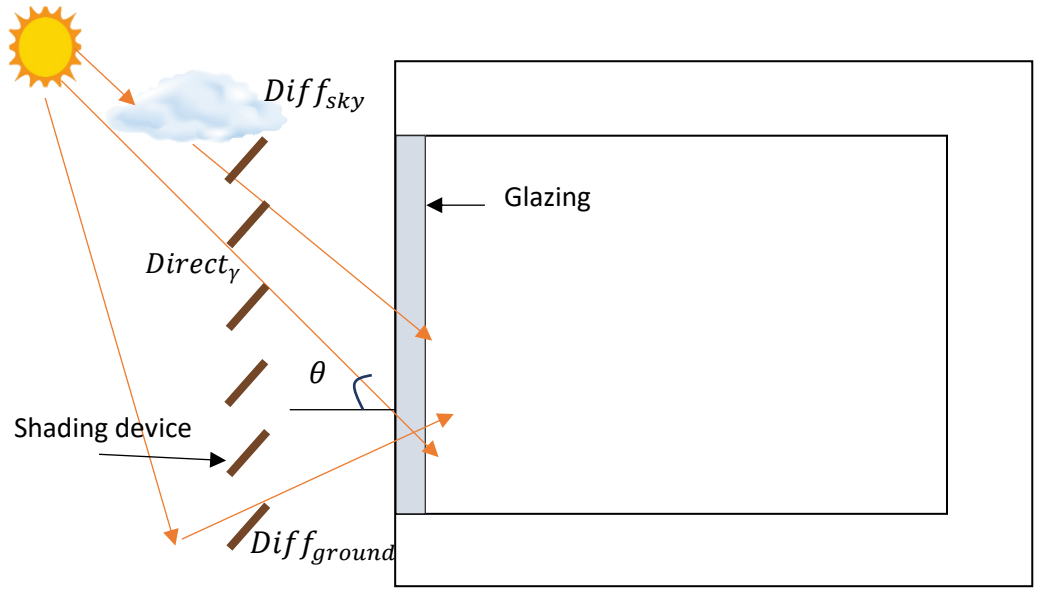

Figure 3-13: Components of the solar gain transmitted by the fenestration system

3.2.4 Model formulation: two-steps characterization strategy

As discussed in the chapter 2, a passive façade model is necessary before the introduction of the adaptive element. This step can serve many purposes: (i) to provide a baseline model to compare with and without shading device effect, (ii) to identify the parameters to consider fixed in both experiments, (iii) to isolate the effect of the adaptive element from the intrinsic properties of the test cell. For the present case study, the double glazing without the shading is considered the passive façade. This case of study is exceptional because the double glazing itself that is considered as a passive façade element exhibits a time-varying solar gain driven by sun trajectory and glazing optical properties. Various studies quantified the angle-dependant total solar gain factor via the double glazing without any shading device by X.ZHANG [120], [121], [122] using outdoor experiments and an RC model with an approximative function: B-spline. Thus, the starting point in this study behaves also dynamically before even introducing the "adaptive element". One may question, if the glazing can also be considered adaptive since its solar transmittance is dynamic, actually, this behavior is governed by Fresnel equations and optical properties of the glazing. In addition, it is a consequence of the solar geometry, rather than intentional, and it does not regulate thermal behavior in response of occupant's comfort during seasons, in contrast of selective glazing or the diagonal shading, more details of the theoretical calculations of solar transmittance of the glazing and shading the solution is in section 3.2.4.1.

The selected model is the RC model; this grey-box model allows the physical interpretability of the parameters unlike black box model where the model lacks physical meaning. In the next section, the RC model is described. The parameters are estimated either using experimental scenarios, simulation, or adopted from standards. Afterwards, a sensitivity analysis is performed to filter the parameters to be optimized for the calibration of the model.

Both for the double glazing and the static geometry shading device, we can model them with a dynamic open-loop control driven by solar geometry. As a result, the RC model named "passive façade model "without the shading device is considered the same, as the "adaptive façade model' with the shading device, with the only difference being the solar gain factor as a control parameter. Next sections detail the RC model and the estimation of its parameters.

To obtain an RC model that represent the dynamic thermal response of the Hotbox, each element should be represented with a network of resistances and capacitors. As a hypothesis, the internal surface of the envelope is represented by one envelope temperature node in the RC model T_{env}. It should be noticed that all the five façades have same constructive materials. Thus, this node is associated with a lumped envelope capacitance C_{env}. The envelope exchanges heat by convection with the interior air temperature $T_{a,i}$ via the thermal resistance $R_{conv,env,i}$ and by conduction with the exterior air temperature $T_{a,e}$ via the thermal resistance $R_{cond,env}$ and by convection $R_{conv,env,e}$. A mean radiant temperature node T_{RM} is also used to represent the long wave radiation exchange with the envelope temperature node T_{env} and with the inner surface of the glazing temperature node T_{gi}. The glazing also exchanges by convection via the thermal resistance $R_{conv,g,i}$ with the indoor air, and by conduction with the outer surface of the second glazing unit via $R_{cond,g}$. This later glazed surface exchanges by long wave radiation with the environmental temperature node T_{envir}, and with the sky temperature node T_{sky}, then by convection with the exterior air temperature node $T_{a,e}$. As a hypothesis, T_{envir} can be considered equal to $T_{a,e}$. The infiltration and thermal bridges losses are important to consider in the model. Therefore, two extra thermal resistance are added to represent these heat losses namely R_{inf} and R_{tb}. Figure 3-14 summarizes the simplified heat exchanges between the hotbox and its environment which are represented in the RC model in Figure 3-15.

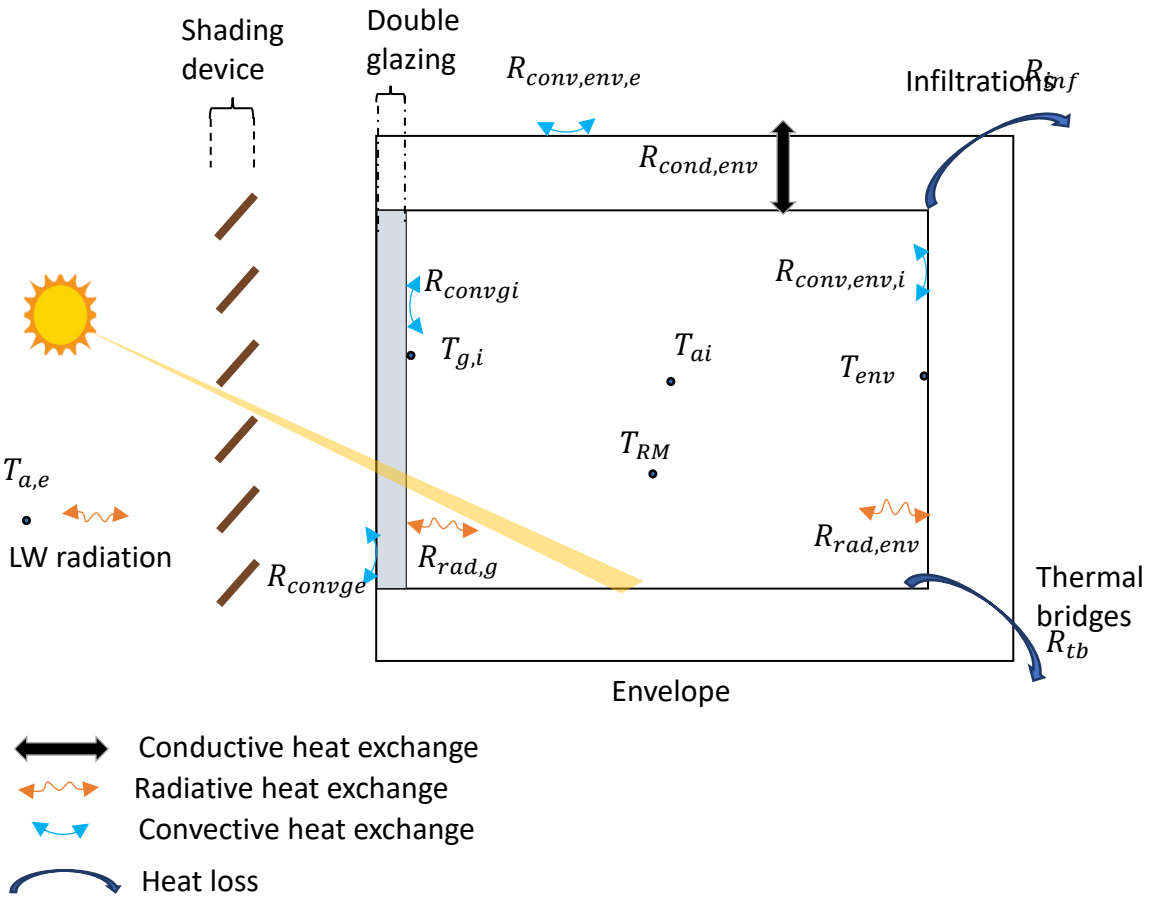

Figure 3-14: Simplified heat exchanges used in the RC model

1) Model and heat balance equations

According to Figure 3-14, the structure of the RC model that can represent the simplified heat exchanges within the Hotbox is shown in Figure 3-15. The exact topology is used for with the shading device experiment calculations. The solar gain is injected on the envelope temperature node, physically the transmitted solar gain into the inside of the test cell is absorbed first by the opaque envelope element, then it releases the heat into the inside of the cell by convection and long-wave radiation and a part is reflected and absorbed by the other surfaces. The part that is absorbed by the glazing effect is already represented by the measurements of the $T_{g,i}$ that are injected into the model.

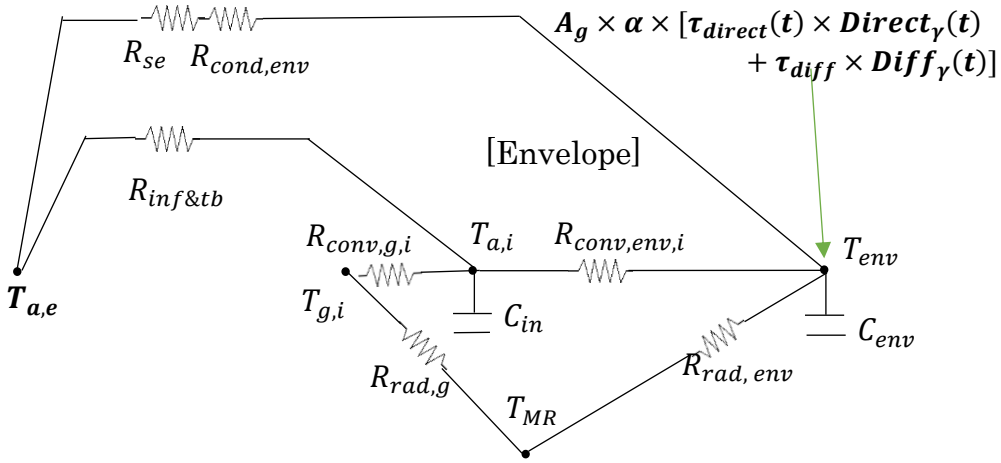

Figure 3-15: The proposed RC model

Indoor air temperature heat balance:

$$C_{in}\frac{dT_{ai}[t]}{dt} = \left(\frac{T_{env}[t] - T_{ai}[t]}{R_{conv,env,i}}\right) + \left(\frac{T_{gi}[t] - T_{ai}[t]}{R_{conv,gi}}\right) + \left(\frac{T_{ae}[t] - T_{ai}[t]}{R_{inf\&tb}}\right) \quad \text{Eq 3-7}$$

Envelope inner surface temperature heat balance:

$$C_{env} * \frac{dT_{env}\,[t]}{dt} = \left(\frac{T_{ai}[t] - T_{env}[t]}{R_{conv,env,i}} + \frac{T_{ae}[t] - T_{env}[t]}{R_{cond,env} + R_{se}} + \frac{T_{RM}[t] - T_{env}[t]}{R_{ray,env}} + A_g \times \alpha \times [\tau_{direct}(t) \times Direct_\gamma\,(t) + \tau_{diff} \times Diff_\gamma(t)]\right) \quad \text{Eq 3-8}$$

Mean radiant temperature:

$$0 = \left(\frac{T_{env}[t] - T_{RM}[t]}{R_{ray,env}}\right) + \left(\frac{T_{gi}[t] - T_{RM}[t]}{R_{ray,g}}\right) \quad \text{Eq 3-9}$$

During the calibration process, measured values of T_{gi} and T_{ae} are injected in the RC model and T_{ai} and T_{env} values are calculated.

2) RC model theoretical parameters definition

The definition of the RC model theoretical parameters is done by means of standards. The Table 3-2 summarizes the used methods in general for the RC parameters, and show the details for each value of the parameter.

Table 3-2: Detailed RC parameters values and sources

Parameter	Meaning and unit	Method or standard
$R_{conv,env,i}$	Interior envelope convective resistance [K/W]	When a fan is placed in the inside, from ASHRAE (2001)[123] the empirical equation can be used: $h_{cv} = 5.65 + 3.9V$ for an air speed V less than 5m/s.For the co-heating test (see Section 2.2.3) air speed is equal to 0.6m/s In outdoor experiment the fan is not used. Thus, the value of convective indoor coefficient from ISO 6946 [44] can be used: $h_{cv} = 2.67 W/m^2K$ Therefore, $R_{conv,env,i} = \frac{1}{A_{env,i} * h_{cv,i}}$, where $A_{env,i}$ is the total surface of the inner opaque envelope which is 5m², then $R_{conv,env,i} = 0.074\ K/W$
R_{se}	Exterior envelope surface resistance [K/W]	From ISO 6946 [44] The thermal resistance is: $R_{\mathrm{se}} = 0.04\ m^2K/W$, if we divide by the total outer envelope opaque surface $A_{env,e}$, then $R_{se} = 0.0061\ K/W$

$R_{\text{cond,env}}$	Conductive envelope resistance [K/W]	The standard ISO 9869-1 [47] defines the thermal resistance of a wall composed from many layers by: $R_{cond,env} = \sum_{i=1}^{2} \frac{e_i}{\lambda_i}$ with e is the thickness and λ is the thermal conductivity for each layer. The wall is composed from: • OSB layers with a thermal conductivity λ of 0.13 W/mK and a thickness of 0.015 m • Polyurethane foam insulation layer with a thermal conductivity λ of 0.025 W/mK and a thickness of 0.08 m The unventilated air layer between OSB and polyurethane have a thickness of 40 mm. the thermal resistance of an unventilated air layer with high emissivity surfaces according to ISO6946 [124] is $R_{air} = 0.18\ m^2K/W$. Therefore, the total conductive resistance is $3.61\ m^2K/W$ for the whole box if we divide by 5 m², it results $R_{cond,env} = 0.72\ K/W$.
$R_{conv,g,i}$	Inner glazing convective resistance [K/W]	When a fan is placed in the inside, from ASHRAE (2001) [123] using the empirical equation $h_{cv} = 5.65 + 3.9V$ for an air speed less then 5m/s. For the co-heating test, the air speed is equal to 0.6 m/s For outdoor experiment no fan is used. Thus, from ISO6946 [124] and for an horizontal heat flux $h_{cv,i} = 2.5\ W/m^2K$, the glazing surface is 0.9 m² thus $R_{conv,g,i} = 0.4\ K/W$
$R_{inf\&tb}$	Infiltration and thermal bridges losses thermal resistance [K/W]	Despite using the pressure decay method, the infiltration losses could not be measured. Therefore, they were combined with thermal bridges losses, and this resistance is identified from the RC model for indoor co-heating, and outdoor without the shading study cases.
C_{env}	Thermal capacitance of the opaque envelope [kJ/K]	According to each façade layer conductivity and thickness, the Hotbox façade is constructed from [125]:

		• Two OSB layers with a thickness of 0.015m, the OSB have a density of 450 kg/m³ and a specific heat capacity of 1200 J/kg.K • One Polyurethane layer with a thickness of 0.08m, the Polyurethane have a density of 32.5 kg/m³ and a specific heat capacity of 1000 J/kg.K • One air gap with a thickness of 0.04 m, a density of 1.225 kg/m³ and a specific heat capacity of 1005 J/kg.K Using the lumped capacitance method, the thermal capacitance for each wall is: $C_{façade} = \sum_{i=1}^{3} \rho_i C_{pi} e_i$= 13.45 kJ/m²K Since it is the same composition for the whole envelope of total interior surface 5 m², the total thermal capacitance is $C_{env} = C_{façade} \times 5$ =67.25 kJ/K
C_{in}	Indoor air thermal capacitance [kJ/K]	The indoor thermal capacitance should account for the air and also interior objects. As a hypothesis, it is estimated to 3 times the thermal capacitance of air with $C_{in} = \mathbf{3} * C_{\boldsymbol{air}}$ Calculations are given in Annex A using tabulated values from ISO 10456 [126]
$R_{\text{ray,env}}$	Long-wave radiative resistance of the opaque envelope [K/W]	ISO 13789:2017 [127] $h_{ray,env,i} = 5.13 W/m^2K$ with an emissivity of ε = 0.9, thus $R_{\text{ray,env}} = \frac{1}{h_{ray,env,i} \times 5} = 0.038 K/W$
$R_{\text{ray},g}$	Long-wave radiative resistance of the glazing [K/W]	$h_{ray,g,i} = \varepsilon \times \sigma \times (T_g^2 + T_{MR}^2)(T_g + T_{RM})$ with ε = 0.84 and using as a hypothesis $T_g = T_{RM} = 20\ C°$, thus $R_{\text{ray},g} = \frac{1}{h_{ray,g,i} \times 0.9} = 0.2 K/W$

τ_{direct}	Solar direct short-wave transmittance factor	Without the shading device, the value of the direct transmittance factor $\tau_{direct,g}$ of the double glazing used for the calibration step of the model is extracted from the software WINDOW from Berkeley Lab [128]. With the shading device, the factor $\tau_{direct,sh}$ is deduced from the calibrated model in the previous step. However, to validate the model the theoretical $\tau_{direct,sh}$ is calculated from ray tracing technique. More details of the theoretical calculations are given in Section 3.1.5
τ_{diff}	Solar diffuse short-wave transmittance factor	In both cases with and without the shading device: the value of the diffuse transmittance factor $\tau_{diff,g}$ of the double glazing is calculated from the integration over the incidence angle of τ_{direct} for without the shading, and for with the shading case, it is also integrated over the local azimuth. More details are given in Section 3.1.5
α	Absorption coefficient of inner surface of the opaque envelope	As a hypothesis the value 0.9 is used as the absorption coefficient of incident rays on inner opaque surface, with the remaining 10% incident radiation is considered as reflected toward indoor environment.
T_{env}	Envelope temperature node	The surface envelope temperature T_{env} that is used in the model is a weighted average of measured interior surface temperatures $T_{surf,i}$, the weight w_i that is used is 1/5 since the surface of one interior façade is $A_{env,i} = 1\,m^2$ and the total interior surface of the opaque envelope is 5 m². The evolution of each envelope surface temperature for the outdoor experimental campaign without shading can be seen in Figure 9-2 (Annex D) $$T_{env} = \sum_{i=1}^{5} w_i T_{surf,i} \;\; with\; w_i = \frac{A_{env,i}}{\sum A_{env,i}}$$

Thermal bridges and air infiltration resistances

- **Thermal bridges losses**

A thermal bridge is a zone of the building envelope where the thermal resistance is not homogenous, due to a discontinuity of the building constructive element which leads to heat losses. Generally, three types of thermal bridges exist. The junction between the façades of the building contains a linear thermal bridge, whereas the junction between three façades is a punctual thermal bridge. The insulation is continuous as shown in Figure 3-17 between the two vertical walls and the floor and the ceiling, but for the door, the order of the construction layers is different, the polyurethane layer is placed in the inner face.

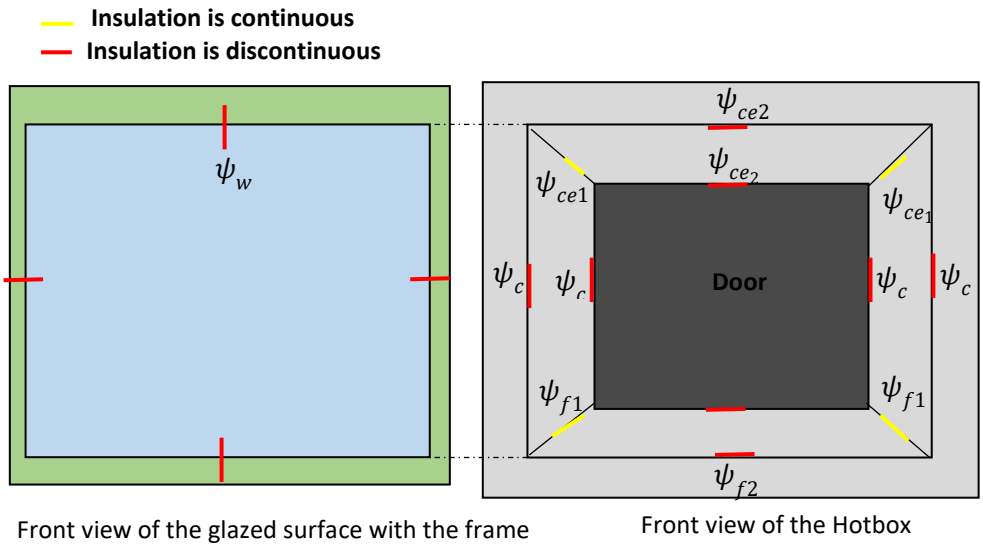

Figure 3-16: Linear thermal bridges location in the Hotbox



Figure 3-17: Door of the Hotbox insulation

The following values are from the standard catalogue ISO 14683 [129]. From Figure 3-16 we can use the following values.

1. Wall–ceiling junction: $\psi_{ce_1} = 0.15\ W/mK$ for the junction between the two vertical walls and the ceiling, for the door and the window that have mismatching materials we can use $\psi_{ce_2} = 0.75\ W/mK$
2. Wall-floor junction: $\psi_{f_1} = 0.15\ W/mK$ (same as wall to ceiling junction because the Hotbox is not placed on the ground, it has wheels) and $\psi_{f_2} = 0.75\ W/mK$ for the junctions with the window and the floor.
3. Vertical corners: $\psi_c = 0.15\ \mathrm{W/mK}$
4. Window junction: $\psi_w = 0.10\ W/mK$ The glazing is mounted in a wooden frame

Lengths:

- 4 vertical corners: L_c = 4 m
- Ceiling perimeter: L_{ce_1} = 2 m for the two matching junctions, and: L_{ce_2} = 2 m for the mismatching junctions
- Floor perimeter: L_{f_1}= 2 m for the two matching junctions, and: L_{f_2}= 2 m for the mismatching junctions
- Window perimeter: L_w = 3.8 m

L is not in the nomenclature

$$HTB = \psi_c L_c + \left(\psi_{ce_1} L_{ce_1} + \psi_{ce_2} L_{ce_2}\right) + \left(\psi_{f_1} L_{f_1} + \psi_{f_2} L_{f_2}\right) + \psi_w L_w \qquad \text{Eq 3-10}$$

It results in HTB equals to $4.58\ W/K$.

- **Infiltration losses**

The air leakage through the building‘s envelope has a significant effect on its energy consumption. In our case of a small-scale test cell $1\ m^3$ the pressure decay method or pulse method can be used. The pressure decay method works by providing an initial pressure difference to the building, and then remove the excitation and measure the pressure decay. This process is illustrated in Figure 3-18.

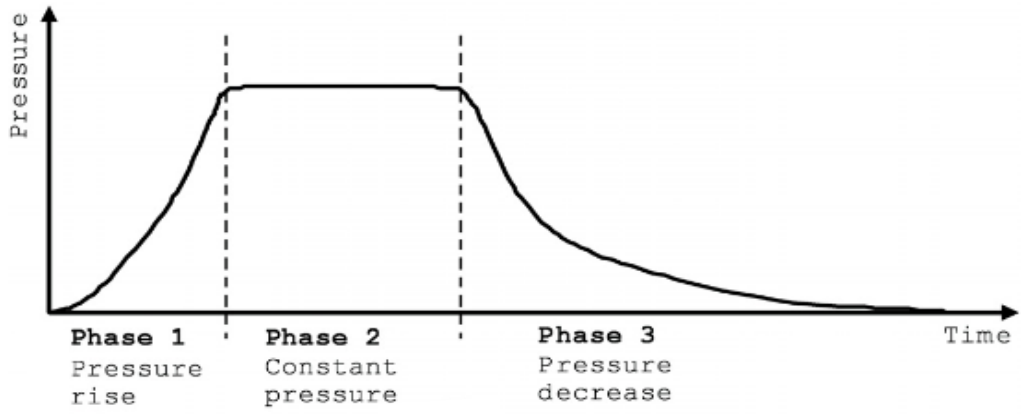

Figure 3-18: Illustration of the three phases to determine air leakage using pressure decay method [96]

On the other hand, the pulse method consists in introducing compressed air [130] inside the building and measuring the pressure changes . This method is more adapted for small size apartments or enclosures, because in large houses, the pressure will not be the same through the volume of the building [131]. To measure the air tightness of the Hotbox, the pressure decay is used. An illustration of the experiment scheme and installation is shown in Figure 3-19. In practice, this method is carried out through three phases. First, the pressure inside the enclosure is increased either with a compressed air tank [96] or with an air supply duct [95]. Once a stable pressure is maintained, the supply source is stopped and the connection with the indoor environment is closed, this third phase measurements of pressure decay can indicate the air leakage. The pressure difference at first is at 0 Pa as shown in Figure 3-20, however, in our case, the maximum pressure difference that was obtained was 20 Pa, and once the fan is stopped the difference pressure decreased instantly close to 0. Therefore, we assume the air tightness was lower than expected, and it was impossible to calculate it through our installation. Either the fan should be more powerful, or the airtightness should be improved. While we addressed this former point, we did not manage to lower it enough.

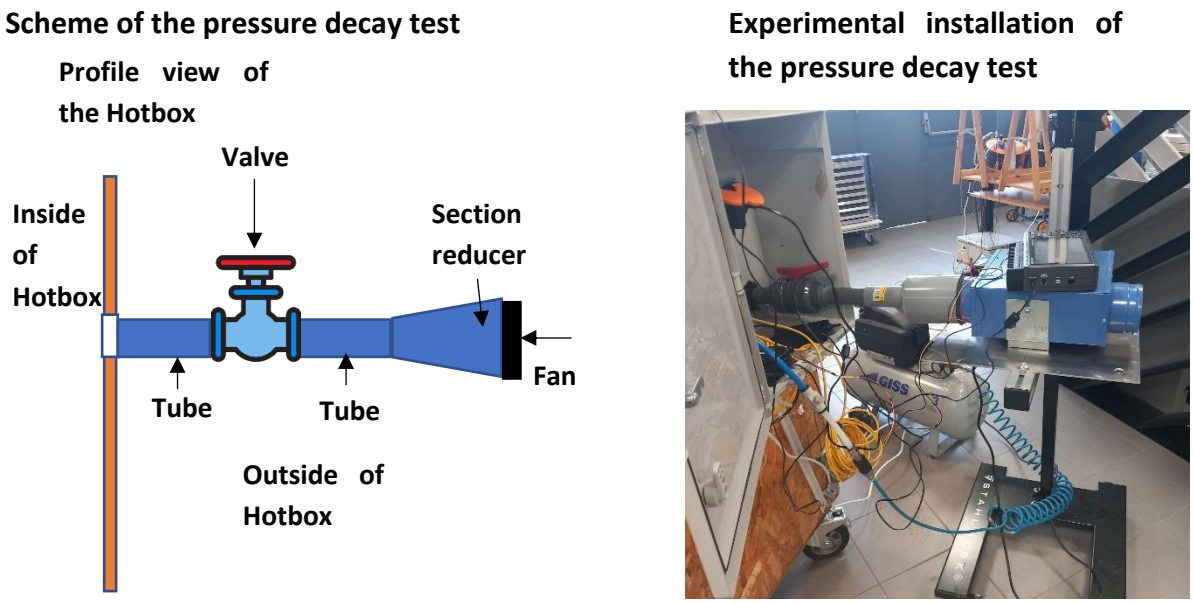

Figure 3-19: Pressure decay installation scheme and experimental setup

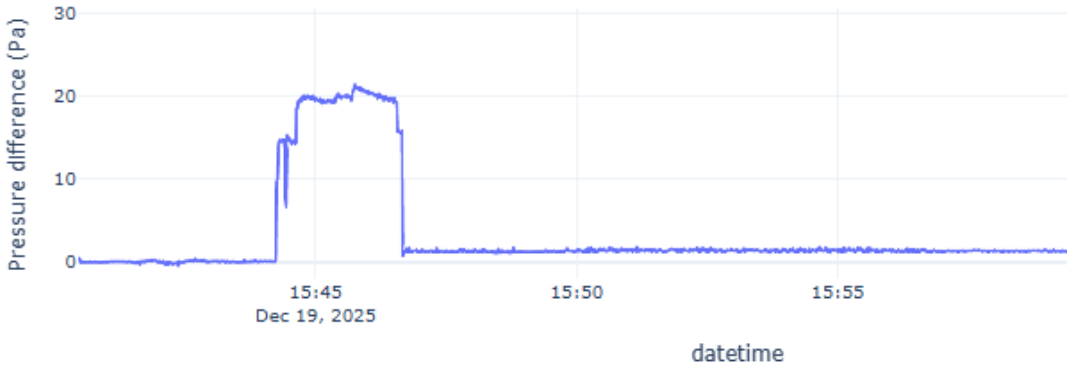

Figure 3-20: Pressure difference over time during the pressure decay test applied to the Hotbox

As a result, it was decided to combine the air leakage and thermal bridges losses in one term for the RC model. This heat loss thermal resistance will be identified during the optimization step for each study case.

3.2.4.1 Theoretical solar transmittance

The theoretical direct solar transmittance is used as an input for the passive façade model (double glazing), but is not an input for the adaptive façade model (with shading). It is only used for comparison with the RC model solar transmittance estimation.

I. Direct solar transmittance estimation without the shading (double glazing only)

Since the solar gain depends on the solar incidence angle and in order to calibrate the passive façade model, it is necessary to estimate the direct solar transmittance factor.

Sun path diagram is a useful visual diagram that can illustrate the position of the sun (solar elevation, azimuth) through the day. In Talence in the south neighborhood of Bordeaux (France), the maximum altitude at the summer solstice is around 68°, while the sun is at a low height in winter with an elevation of 22° during December solstice as shown in Figure 3-21.

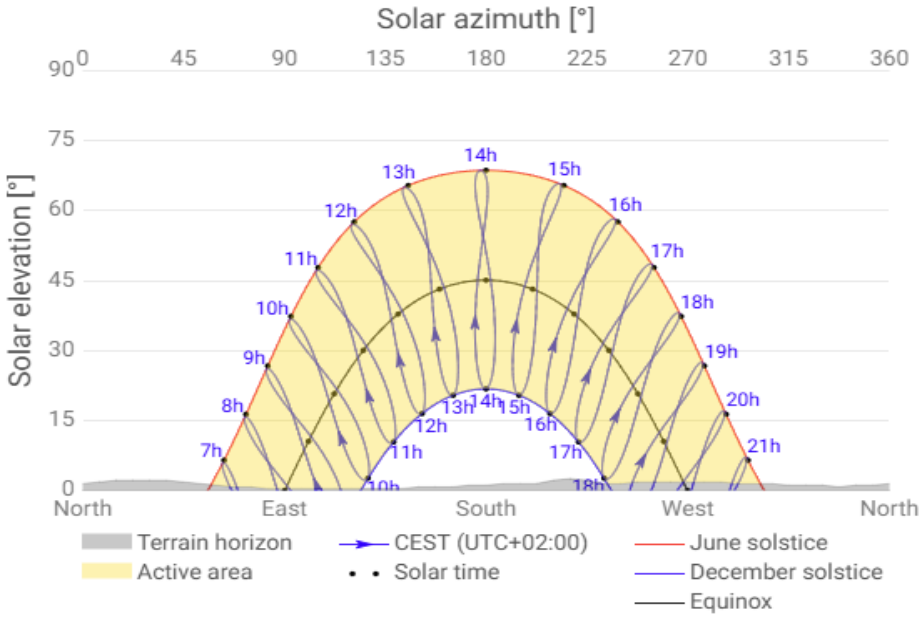

Figure 3-21: Sun path diagram (Global Solar Atlas, 2025) in Bordeaux

The solar azimuth γ_s and the solar elevation angle h, alongside with the surface azimuth γ and tilt angle β of the window are important parameters to define the solar incidence angle of fenestration systems. The solar incidence angle is defined with Eq 3-11 [132] and illustrated by Figure 3-22.

$$\begin{aligned}\cos\theta = {} & \sin\delta sinh\cos\beta \\ & - \sin\delta\cos h\sin\beta\cos\gamma \\ & + \cos\delta\cos h\cos\beta\cos\omega + \cos\delta\sin h\sin\beta\cos\gamma\cos\omega \\ & + \cos\delta\sin\beta\sin\gamma\sin\omega\end{aligned} \qquad \text{Eq 3-11}$$

Where:

- θ: Incidence angle
- δ: Declination which is the angle between solar rays and equatorial plane, and it is defined as

- $\delta = 23.45\ sin\left(360 \times \frac{284+n}{365}\right)$ with n is number of the day $[1, 365]$
- h: Solar elevation angle (°)
- β: Surface tilt (°)
- γ: Azimuth of the surface, as a reference in this thesis work we consider 180° for South, 90° for East, 270° for West, and 0° for North.
- ω: Hour angle related to the Earth rotation and its 15° per hour; morning negative, afternoon positive.

The angle θ may exceed 90◦, which means that the sun is behind the surface.

A simplified form[132] using the solar azimuth angle can be given in Eq 3-12:

$$\cos(\theta) = \sin(\beta)\cos(\gamma - \gamma s) + \sin(h)\cos(\beta) \qquad \text{Eq 3-12}$$

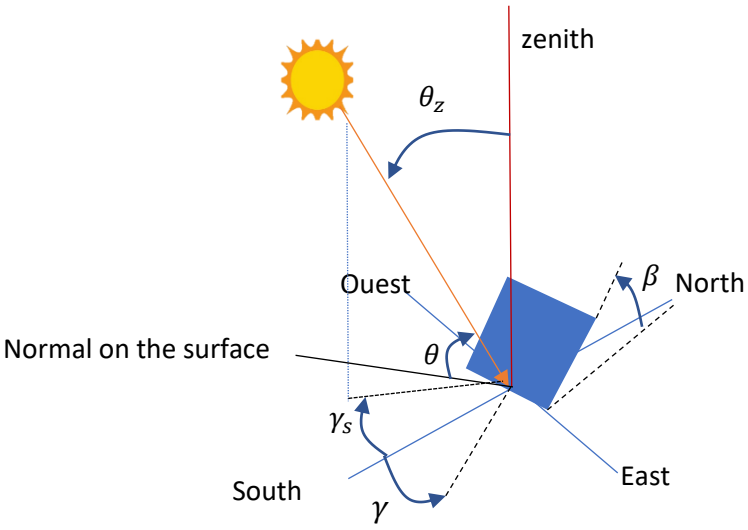

Figure 3-22: Solar geometry illustration

The total transmittance of the double glazing can be expressed as the sum of direct and diffuse component as in Eq 3-13. Both components can be treated separately. Once the solar incidence angle is calculated from Eq 3-11 and 3-12, it can be used to compute the direct transmittance of the glazing which is dependant of the solar incidence angle $\tau_{direct,g}(\theta)$.

$$\tau_{total,g} = \tau_{direct,g}(\theta) + \tau_{diff,g} \qquad \text{Eq 3-13}$$

The values of $\tau_{direct,g}$ for each incidence angle from $[0°, 90°]$ was obtained using the software WINDOW 7.8 from Lawrence Berkeley National Laboratory (LBNL) [128] which is a free public simulation tool to calculate the thermal and optical performances of fenestration systems .
For the calculations, the double glazing was selected from the software database with the dimensional caracteristics listed in Table 3-3 with an environemental conditions according to NFRC 100-2010 [133].

Table 3-3: Dimensional characteristics of the glazing

Height	950 mm
Width	950mm
Thickness of first glass layer	4mm
Thickness of cavity (100 %air)	12mm
Thickness of second glass layer	4mm
Tilt angle of the glazing from horizontal plan	90°
Type of the glass	Planibel clear

The output file of the calculations is a text file with data that can be presented in Table 3-4.

Table 3-4: Optical and thermal characteristics of the double-glazing using WINDOW calculations

Incidence angle [°]	0	10	20	30	40	50	60	70	80	90
Visible transmittance (Tvis)	0.81	0.81	0.81	0.80	0.79	0.76	0.68	0.53	0.26	0
Front visible reflectance (Rfvis)	0.14	0.14	0.14	0.14	0.15	0.18	0.25	0.41	0.67	1
Back visible reflectance (Rbvis)	0.14	0.14	0.14	0.14	0.15	0.18	0.25	0.41	0.67	1
Solar transmittance $\tau_{direct,g}(\theta)$	0.72	0.72	0.71	0.71	0.69	0.66	0.59	0.45	0.21	0
Front solar reflectance (Rfsol)	0.12	0.12	0.12	0.13	0.14	0.16	0.22	0.37	0.61	1
Back solar reflectance (Rbsol)	0.12	0.12	0.12	0.13	0.14	0.16	0.22	0.37	0.61	1
Absorptance of first layer (Abs1)	0.08	0.08	0.08	0.09	0.09	0.09	0.10	0.11	0.11	0
Absorptance of second layer (Abs2)	0.06	0.06	0.06	0.06	0.07	0.07	0.07	0.06	0.04	0
Solar heat gain coefficient (g-value)	0.77	0.77	0.77	0.76	0.75	0.72	0.65	0.50	0.26	0

From Table 3-4 we can observe that the front and back reflectance are the same, which is logical since the glass is uncoated. The curve $\tau_{direct,g}(\theta)$ can be obtained as shown in Figure 3-23. With a null incidence angle the direct solar transmittance $\tau_{direct,g}(0°)$ is equal to 0.72.

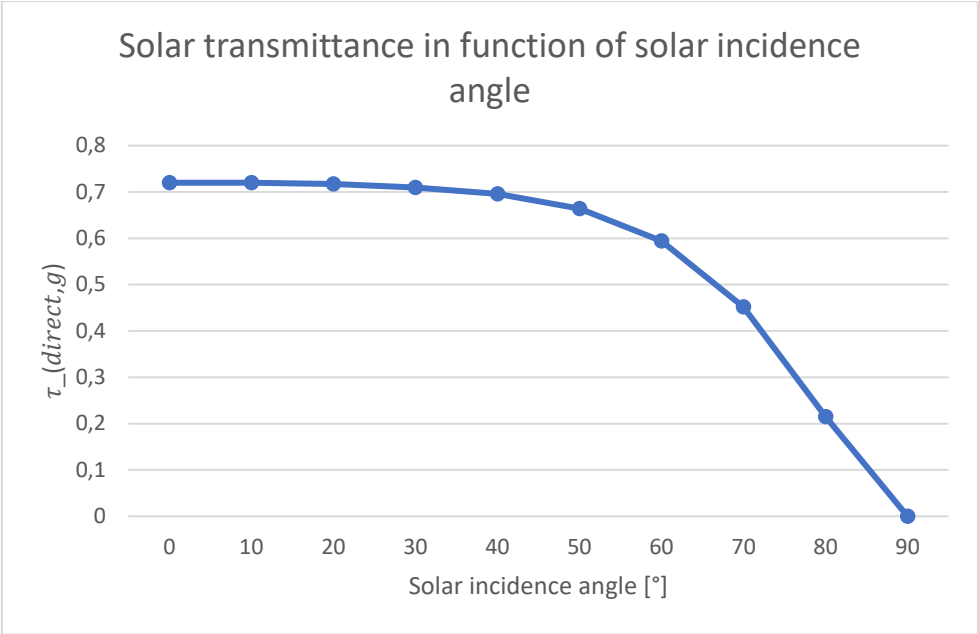

Figure 3-23: Solar transmittance $\tau_{direct,g}$ of the double glazing from WINDOW 7.8 LBNL software [128]

Figure 3-24 shows the front solar reflectance which refers to the fraction of incident solar radiation that is reflected by the front side of the glass namely exposed to the exterior environment. It appears that it increases while solar incidence angle increases, until it arrives to a total reflectance at an incidence angle of 90°.

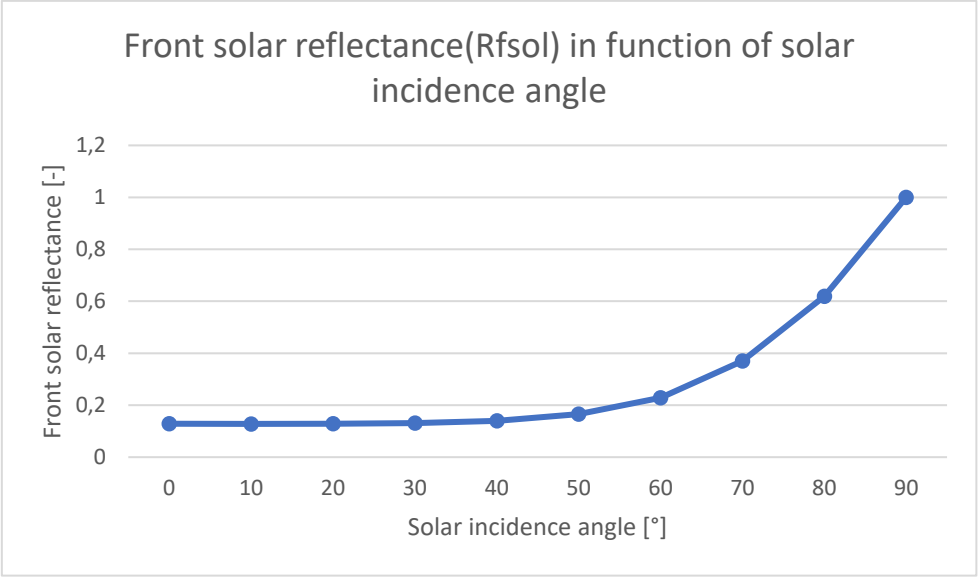

Figure 3-24: Solar front reflectance of the glazing in function of solar incidence angle from WINDOW 7.8 LBNL software [128]

The absorbtance in function of solar incidence angle is also plotted from the Table 3-4 for both glazing layers as illustrated in Figure 3-25. It can be ibserbed that glass layer 1 exhibit higher absorbance then the inner glass layer, as it directly intercept solar rays.

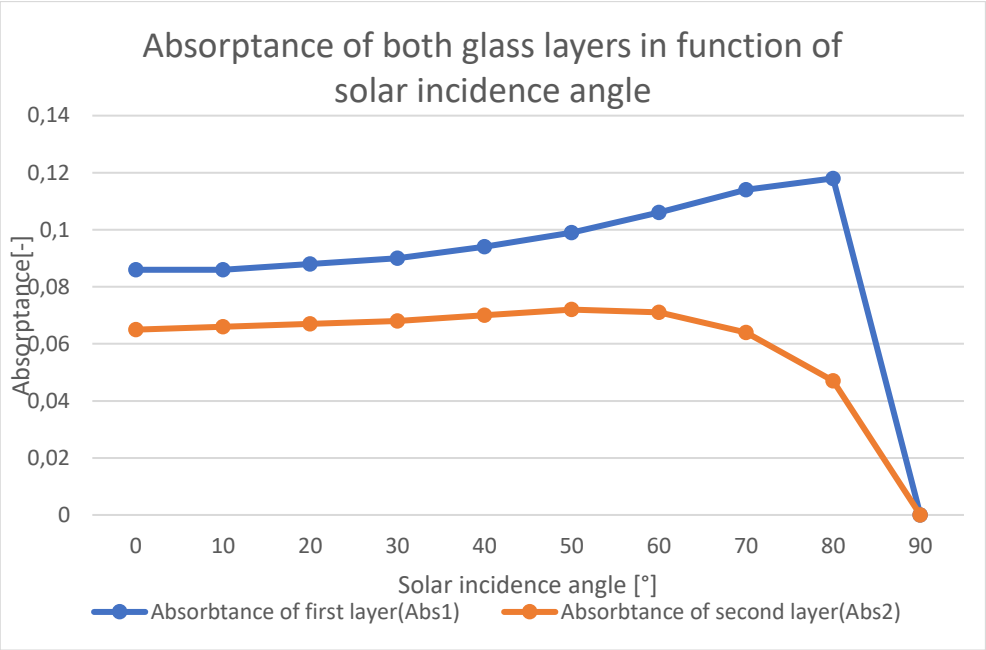

Figure 3-25: Solar absorbance of the glazing in function of solar incidence angle using WINDOW 7.8 LBNL software [128]

We can split the variation of $\tau_{direct,g}$ as a function of θ into three angular regimes in Eq 3-14:

$$\tau_{direct,g}(\theta) = \begin{cases} 0.71 & if\ \theta < 30° \\ -0.0003\theta^2 + 0.0226\theta + 0.2478 & if\ \theta > 30° \\ 0 & if\ \theta > 90° \end{cases} \qquad \text{Eq 3-14}$$

Using the calculations above, we get time-varying solar transmittance of the double glazing $\tau_{direct,g}(t)$ toward the south for a day in October as shown in Figure 3-26. During October the solar incidence angle is above 30° for a South oriented façade, therefore, only the polynomial expression is used in Eq 3-14, with an enforced transmittance to zero when $\theta > 90°$.

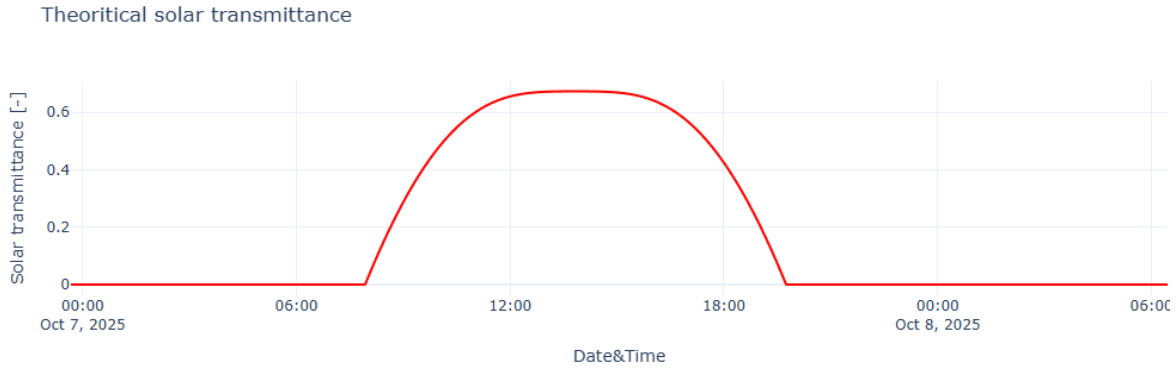

Figure 3-26: Time-varying theoretical direct solar transmittance $\tau_{direct,g}$ of a double glazing 4/12/4 for a façade toward the south during October 7 in Bordeaux for South orientation

From Figure 3-26 we can notice a flat top near noon of the direct transmittance, which is due to the slow angular change of sun path. As illustrated in Figure 3-27 , for a south oriented

vertical glazing, during April and June, and using the same equation of Window LBLN driven solar transmittance, the peak can be sharp because the sun moves 'faster' in angle space since the incidence angle is larger in summer.

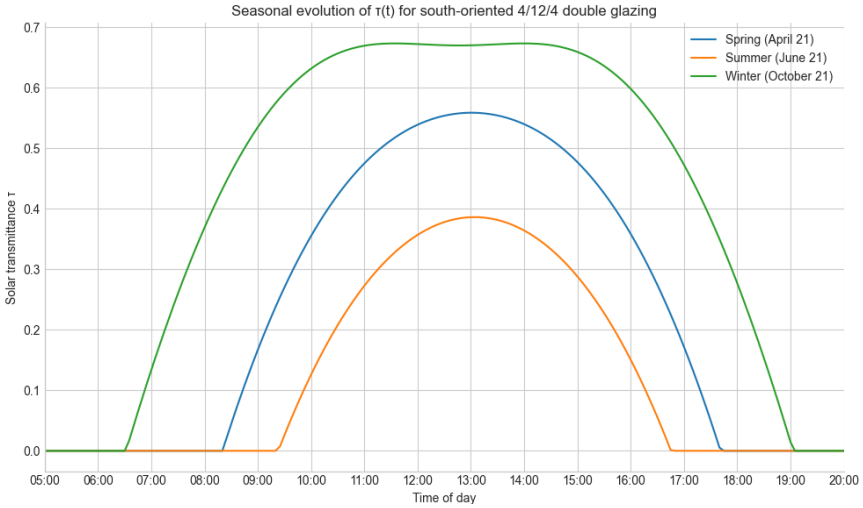

Figure 3-27: Seasonal evolution of $\tau_{direct,g}$ for south-oriented 4/12/4 double glazing in Bordeaux

For the diffuse solar transmittance which includes the diffuse reflections from ground and sky, it was computed using the equation of hemisphirical value of a property $P(\theta)$ from EnergyPlus documentation [134] in Eq 3-15.

$$P_{hemispherical} = 2\int_0^{\frac{\pi}{2}} P(\theta)\cos(\theta)\sin(\theta)\,d\theta \qquad \text{Eq 3-15}$$

Considering that $\tau_{diff,g}$ is the hemispherical distribution of $\tau_{direct,g}(\theta)$ we can obtain Eq 3-16:

$$\tau_{diff,g} = 2\int_0^{\frac{\pi}{2}} \tau_{direct,g}(\theta)\cos(\theta)\sin(\theta)\,d\theta \qquad \text{Eq 3-16}$$

Those calculation resulted in a $\tau_{diff,g}$ of 0.6.

II. Direct solar transmittance with the shading and the double glazing

To understand the behaviour of the solar transmittance of the diagonal shading device, it is necessary to visualize the effect of the angle from the horizontal plan μ and the tilt angle ϑ as shown in Figure 3-28. Theoretically, if we visualize the diagonal slats, the slats will receive rays from all the directions, among all the rays that may hit slats, a certain percentage will be absorbed or reflected by the slats, or transmitted directly by entering the non-obstacle area. The rays that will be directly transmitted by the non-shaded area are characterized with a direction that is parallel to the slats angle μ (rays in colour red) as illustrated in Figure 3-28.

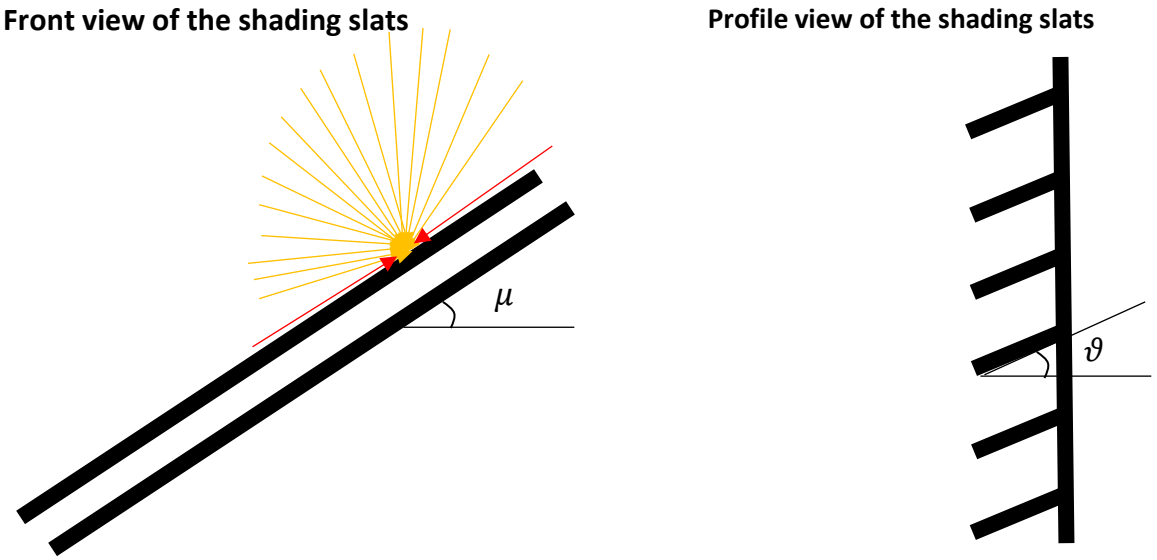

Figure 3-28: Profile and front view of the diagonal shading

One of the methods that can be used to simulate the transmittance of such a complex geometry shading is the ray tracing using Bidirectional Scattering Distribution Function (BSDF) which describes the behaviour of an optical system to transmit or reflect a quantity of radiation within a given incidence angle and a direction. The BSDF have a unit of sr^{-1}, steradian as a unit of solid angle. Geometrically, BSDF quantify the amount of radiation transmitted or reflected from an incident direction (θ_1, φ_1) with a solid angle $d\Omega_1$ to an outgoing direction (θ_2, φ_2), with a solid angle $d\Omega_2$ as seen in Figure 3-29. The local azimuth φ corresponds to the angle of the ray rotation around Z axis with $\varphi \epsilon [0°, 360°]$.

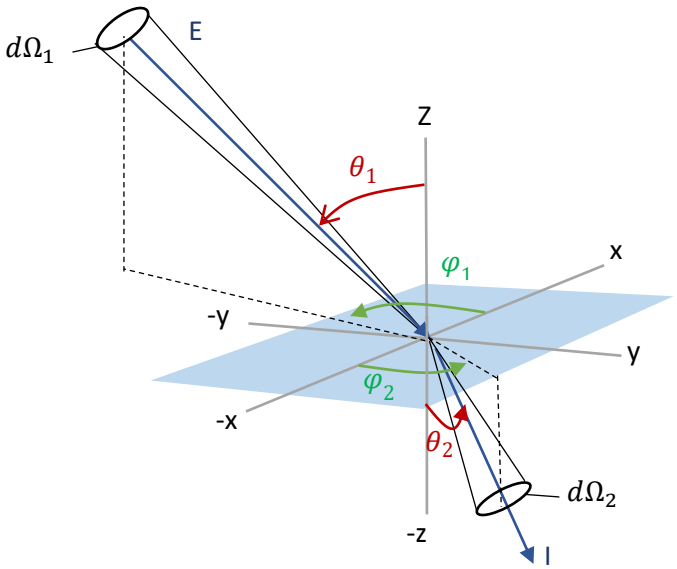

Figure 3-29:Polar and azimuthal angles of incident and exiting directions [135]

We can distinguish Bidirectional Transmittance Distribution Function (BTDF) and Bidirectional Reflectance Distribution Function (BRDF). A BSDF of a complex fenestration system can be

measured using a goniometer or a large integrating sphere [114]. For a simulation based ray tracing calculations, *genBSDF* can be used, which is a free open source program compatible with Radiance [136] as a ray tracing software that works with complex fenestration systems using a Monto Carlo method.

The BSDF exhibit the three following properties [135]:

1. Positivity: $f(\theta_1, \varphi_1, \theta_2, \varphi_2) \geq 0$
2. Helmholtz reciprocity: $f(\theta_1, \varphi_1, \theta_2, \varphi_2) = f(\theta_2, \varphi_2, \theta_1, \varphi_1)$,
3. Energy conservation: $\alpha(\theta_1, \varphi_1) = \int_0^{2\pi} \int_0^{\pi} f(\theta_1, \varphi_1, \theta_2, \varphi_2) |cos\theta_2| sin\theta_2 d\theta_2 d\varphi_2 \; 1 \; for \; all \; (\theta_1, \varphi_1)$

The resulted BSDF is discretized using a discretization scheme. A widely used discretion method in CFS simulation is Klems distribution [137]. In this distribution, the incident hemisphere is subdivided into 145 patches with 9 incidence angles θ rings, and each patch is defined with θ and a ray direction angle which is the local azimuth φ.

Each ring corresponds to the same incidence angle θ. The first patch number 1 correspond to rays that are normal to the fenestration surface with $\theta = 0$ as shown in Figure 3-30. The last ring patches contain rays which have an incidence angle $\theta = 82°$. Thus, for the same incidence angle and depending on the fenestration system, the transmittance can be different from a patch to another due to the local azimuth φ variation.

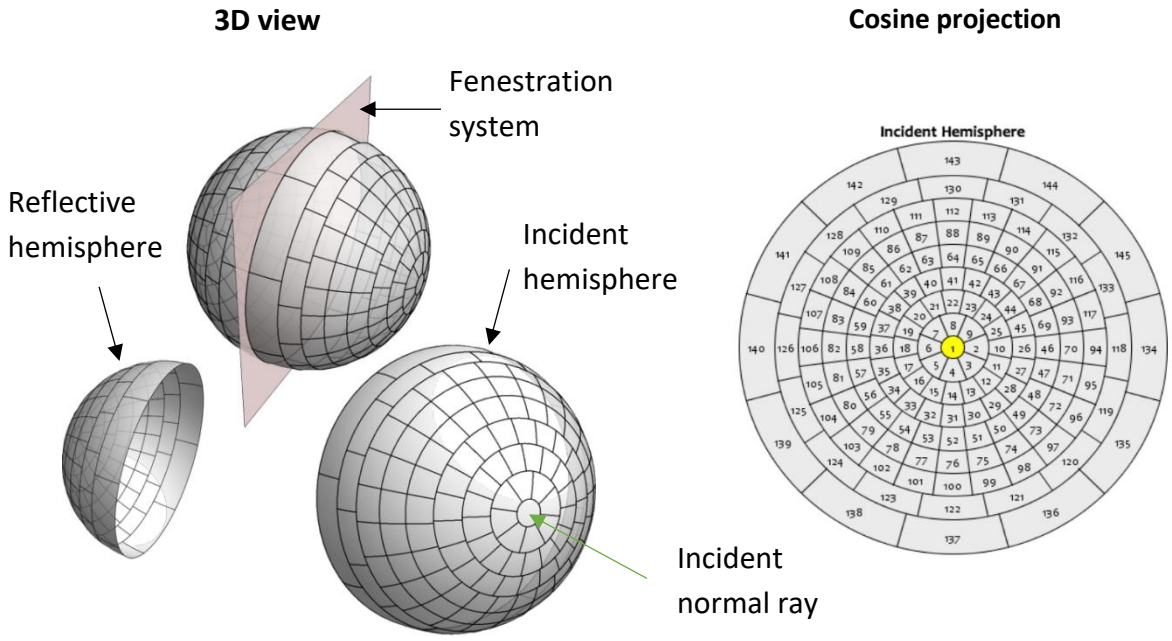

Figure 3-30: Cosine projection and 3D view of Klems patches

In order to generate the BTDF for the shading system, the following steps are followed:

1. Generate and import a 3D model for the system;
2. Combine the shading with a glazing;

3. Use *genbsdf* to produce a tabulated BSDF;
4. From BTDF density to direct transmittance;
5. Extract the corresponding direct transmittance for each time step of the studied time series.

Those steps are detailed in the following.

1) Generate and import the 3D model

The 3D model of the shading is exported as an *.obj* file from Rhino, and then converted to a *.rad* file using *obj2rad* function. The 3D model was explicitly modelled without the frame, as the shading dimensions $(1300 \times 1300\ mm)$ extend the glazed area surface $(950 \times 950\ mm)$ of the Hotbox. Moreover, the frame is supposed to block the lateral incident angles radiations, however, these angles are already excluded by BSDF calculations since it stops at an incidence angle of 82°.

For the shading material, plastic was used for the simulation. The shading was painted with a black mat colour reference RAL9005. The coefficients for diffuse and specular reflectance must be defined for the shading. A specular reflectance occurs when the ray reflects, in a single, mirrored-like direction of the incidence angle, as the case for metal. On the other hand, the diffuse reflectance describes a reflection of an incident ray in many directions. An illustration of the difference between the two reflection types is in Figure 3-31.

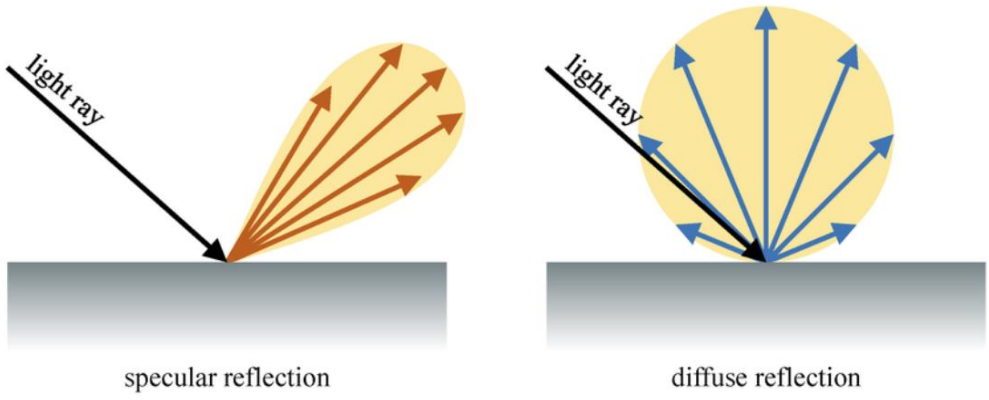

Figure 3-31: Difference between specular and diffuse reflectance [138]

Due to the lack of reflectance coefficient of slats measurements, a coefficient of diffuse reflectance of 4% and specular reflectance of 1% were used as a hypothesis from the slat coating manufacture's catalogue [139].

2) Combine the shading with a glazing

The direct transmittance to incorporate in the RC model should consider the glazing transmittance as well, therefore it was necessary to generate a glazing in Radiance with the command *void glass* using same optical properties of double-glazing. Radiance uses Fresnel equations for the calculation of transmittance and reflectance of the glass, by default, the refraction index is 1.5. Thus, the transmittance at normal incidence of 0.72 which was

calculated using WINDOW LBNL[128] for 4/12/4 double glazing was used in the glass definition. BSDF calculations require dimensional conformity of the system layers, means that the shading and the glazing must have same dimensions: height and width, therefore, both had a height and width of 1300 mm for those calculations.

A distance between the glazing and the shading was defined using *xform* command and it was specified according to the real distance which was 5 cm.

3) Use *genbsdf* to produce a tabulated BSDF

To generate the BTDF, it is expected that the model is contained in a rectangular profile. A special attention must be paid to the positioning of the shading, it must be in the exterior, and the complete system namely shading and glazing must be in the -Z half space, since *genbsdf* tool uses Klems coordinate and the +Z direction points toward the inside as shown in Figure 3-32.

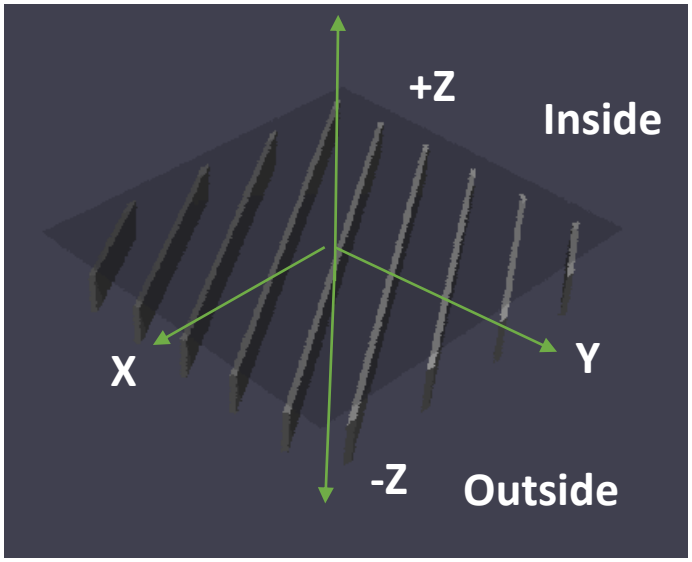

Figure 3-32: A scheme to illustrate the coordinate system in Radiance

To visualize the complete system on Radiance, the command *objvew* is used (Figure 3-33).



Figure 3-33: The objview illustration of the complete system: glazing+shading

Next, once we have the complete defined system, the ray tracing can be launched using *genbsdf* command, by default Radiance use 2000 rays' samples for each incidence angle, in our case 4000 rays are used for higher precision, and the forward transmittance calculation were performed with the parameter *+f*.

```
genbsdf +f  -c 4000 -geom meter system.rad > system_bsdf.xml
```

The output file has an XML extension, and it is structured as blocks: the BSDF data is provided as a matrix of 145 x 145 elements for the four components: "Transmission Front", "Transmission Back", "Reflectance Front", and "Reflectance back". Table 3-5 shows the incident and exiting hemisphere convention for each component according to Radiance convention:

Table 3-5: Radiance convention for BSDF file

Blocks of the xml file	Incident hemisphere	Exiting hemisphere
Front transmission	Outdoor	Indoor
Back reflection	Indoor	Indoor
Back transmission	Indoor	Outdoor
Front reflection	Outdoor	Outdoor

The same software WINDOW LBNL that was used to calculate direct transmittance of the double glazing cannot be used for the shading and glazing, because even if it gives a possibility to import an ".xml" file of the BSDF of the shading, and after combining with the double glazing, it cannot output a dynamic transmittance for this system. Thus, it was necessary to extract from the xml file the corresponding dynamic transmittance. According to Table 3-5, the component that is extracted from the xml file is the "Front transmission".

4) From BTDF density to direct transmittance

According to IEA SHC Task 61/EBC Annex 77 [135] the corresponding direct transmittance for each incidence angle θ and azimuth direction angle φ can be calculated from BSTDF density using Eq 3-17.

$$\tau_{direct_sh_bsdf}(\theta_1, \varphi_1) = \int_0^{2\pi} \int_0^{\frac{\pi}{2}} BTDF(\theta_1, \varphi_1, \theta_2, \varphi_2) cos(\theta_2) sin(\theta_2) d\theta_2 d\varphi_2 \quad \text{Eq 3-17}$$

It is integration on each output patch, that contains rays coming from same incident patches.

With the hypothesis of a total coefficient of reflection of slats equal to 5%: diffuse reflectance of 4% + specular reflectance of 1%

, we can obtain the direct transmittance for each incidence angle and corresponding local azimuth as shown in Figure 3-34. It can be observed that transmittance of the complete

system namely glazing with shading is higher when the rays have a lower incidence angle, and a lower transmittance when the incidence angle is higher. This dynamic behaviour was destined mainly for seasonal changing of sun altitude during winter and summer. In addition, two lobes are distinguished, both appear during the alignment between the incident rays and the diagonal slats tilt angle.

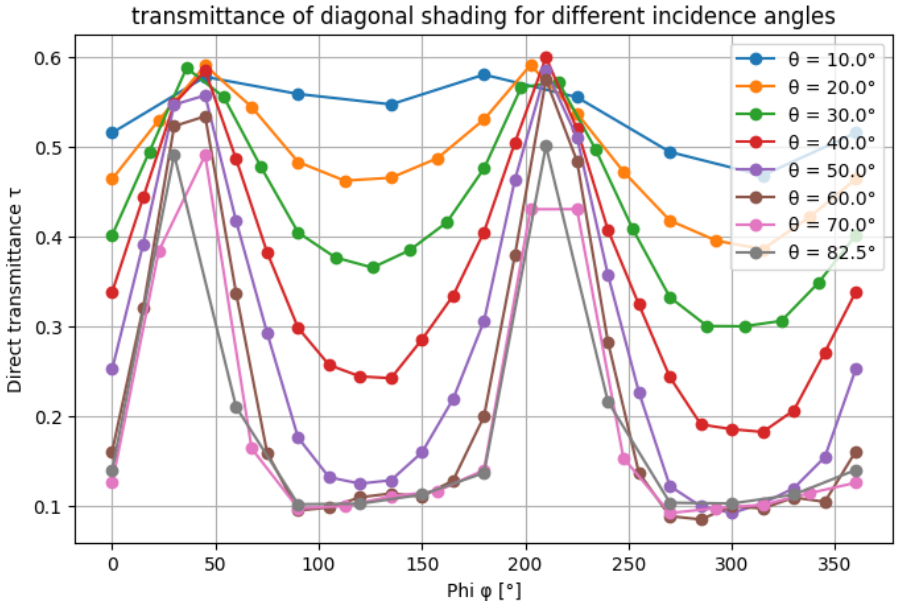

Figure 3-34: Direct transmittance of the shading with the glazing using BSDF $\tau_{direct_\mathrm{sh_bsdf}}$

Polar charts are used to show clearly the behaviour of the shading for low θ in Figure 3-35 and for high θ with Figure 3-36. The distance from the centre represents the transmittance values. The angle of rotation of the circle is the local azimuth φ.

From the polar charts we can note several remarks:

1. As expected from the start, the highest transmittance values occur twice, when the rays are aligned with the slats tilt angle, and in the opposite side with approximatively 180° which create a certain symmetrical profile on the polar plots.
2. An increased value of transmittance in the lower incidence angles.
3. A lower transmittance values occur with the lateral incidence angle.
4. The effect of θ can be linked with the width of the transmittance profile.

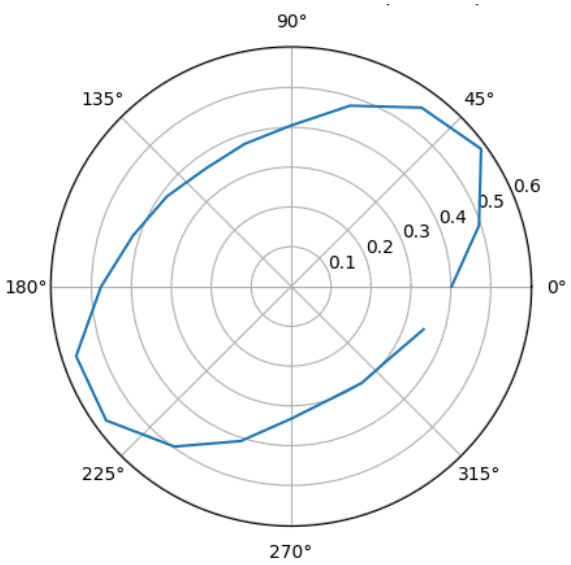

Figure 3-35: Direct transmittance of the glazing with shading $\tau_{direct_\mathrm{sh_bsdf}}$ for $\theta = 30°$

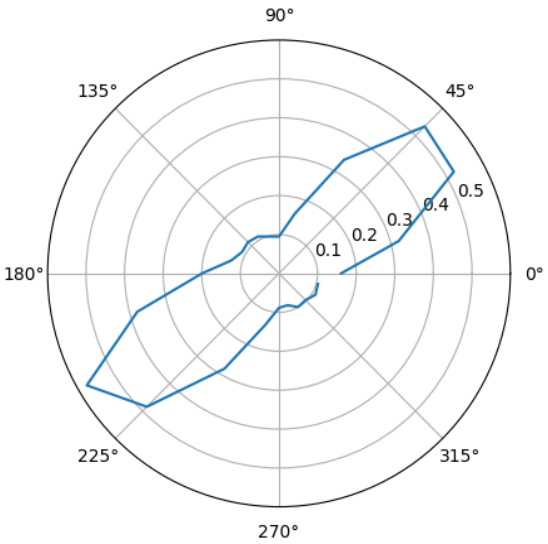

Figure 3-36: Direct transmittance of the glazing with shading $\tau_{direct_\mathrm{sh_bsdf}}$ for $\theta = 60°$

When a solar ray is hitting the shading slat, and depending of the slat reflectance coefficient, a percentage of the rays will be reflected either to indoor or outdoor, and a percentage will be absorbed as illustrated in Figure 3-37. Thus, the direct solar transmittance can be written as the sum between the transmitted direct-direct rays, and the transmitted direct-diffuse rays in Eq 3-18.

$$\tau_{direct} = \tau_{direct_direct} + \tau_{direct_diff} \qquad \text{Eq 3-18}$$

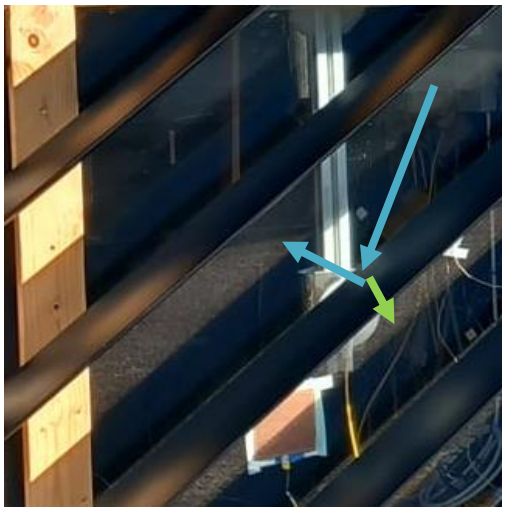

Figure 3-37: Decomposition of a reflected solar ray on the shading slats

Hence, the reflection coefficient of slats must be evaluated, but since the measurements of specular and diffuse component of the shading system reflectance are not available, and in order to make sure of how full spectrum reflectance of the shading can impact the direct transmittance, two simulations were run with *genbsdf:*

- A total solar reflectance of 50% composed of diffuse coefficient of 40% and specular coefficient of 10%, the 3D model is illustrated in Figure 3-38 (a)
- A total solar reflectance of 5% composed from: diffuse coefficient of 4% and specular coefficient of 1%, the 3D model is illustrated in Figure 3-38 (b)

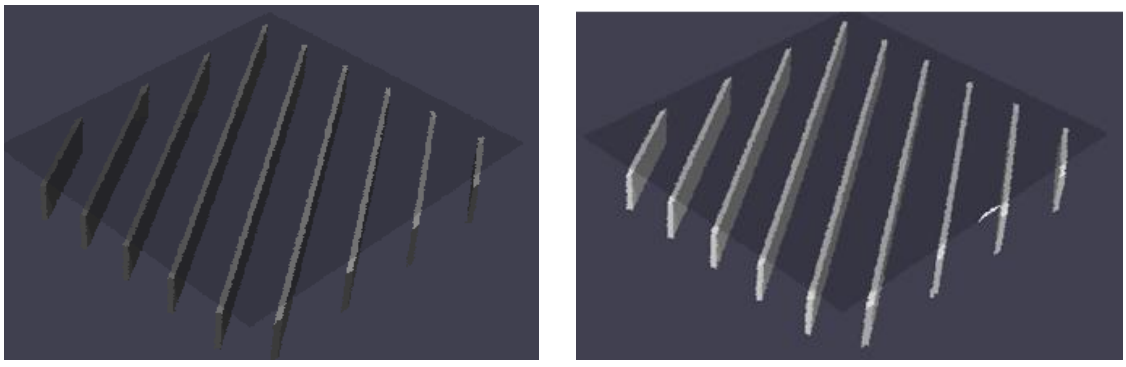

(a) (b)

Figure 3-38: the 3D shading model with: (a) total reflectance of 5% and (b) total reflectance of 50%

The objective with these two simulations is to evaluate the difference of direct transmittance for both, to verify the contribution of reflected rays using Eq 3-19:

$$\Delta\tau = \tau_{50\%} - \tau_{5\%} \qquad \text{Eq 3-19}$$

After running both simulations, the minimum difference of direct transmittance between both is 0.001, and the maximum difference is 0.1, which is shown in Figure 3-39. The difference is positive. This low $\Delta\tau$ suggest that the shadng transmission profile is mainly through direct transmission, and the reflected rays are directed toward the outside.

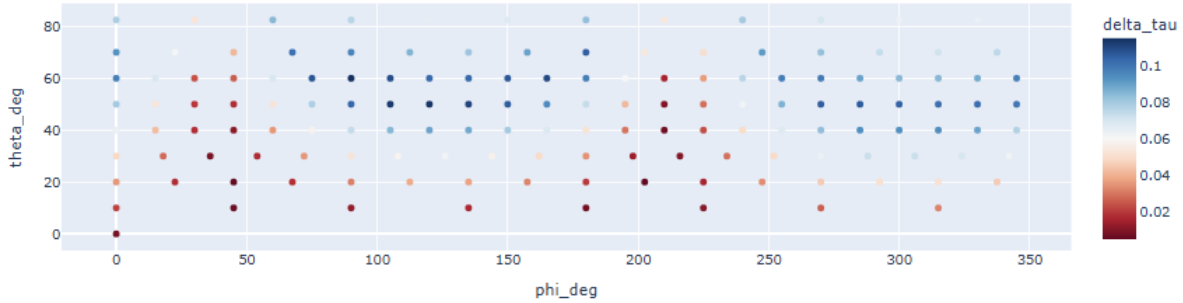

Figure 3-39: Difference of both simulations $\tau_{50\%} - \tau_{5\%}$ in function of θ and local azimuth φ

For the diffuse transmittance $\tau_{diff,sh}$ in the case of shading, it can be calculated with integrating over θ and φ with Eq 3-20 [135].

$$\tau_{diff,sh} = \frac{1}{\pi}\int_{-\pi}^{\pi}\int_{0}^{\pi/2} \tau_{direct,sh}(\theta,\varphi)cos(\theta,\varphi)sin(\theta)d\theta d\varphi \qquad \text{Eq 3-20}$$

The obtained diffuse transmittance is $\tau_{diff,sh} = 0.27$, which is a reduction of 55% when compared to diffuse transmittance of glazing alone ($\tau_{diff,g} = 0.6$).

The last step which is to extract the corresponding direct transmittance for each time step of the studied time series is applied for each case of study with the shading.

3.2.4.2 **Instrumentation and sensors positioning**

The project Annex 58 was developed by the International Energy Agency, in order to provide necessary tools and methods to evaluate façade performance by using study cases [140]. This annex has defined some regulations for the building performance evaluation phase, for example it was recommended the use of a fan to avoid the stratification of temperature inside the testing area. The fan in turn can help to homogenize the indoor air temperature and therefore the measurements are practically acceptable. The shielding also is a critical practice for temperature sensors, in order to be protected from solar radiation that can cause high unrealistic peaks in indoor air temperature measurements. Also, it was recommended that the observation and measurements period of a certain phenomenon should be selected when the phenomena under study clearly observable. In order to gather a strong value of its variation. For example, if the objective was to measure solar irradiance, it is better to perform it while there is strong solar radiation. Based on the guiding recommendations, the experimental setup of the hotbox is developed and illustrated in Figure 3-40.

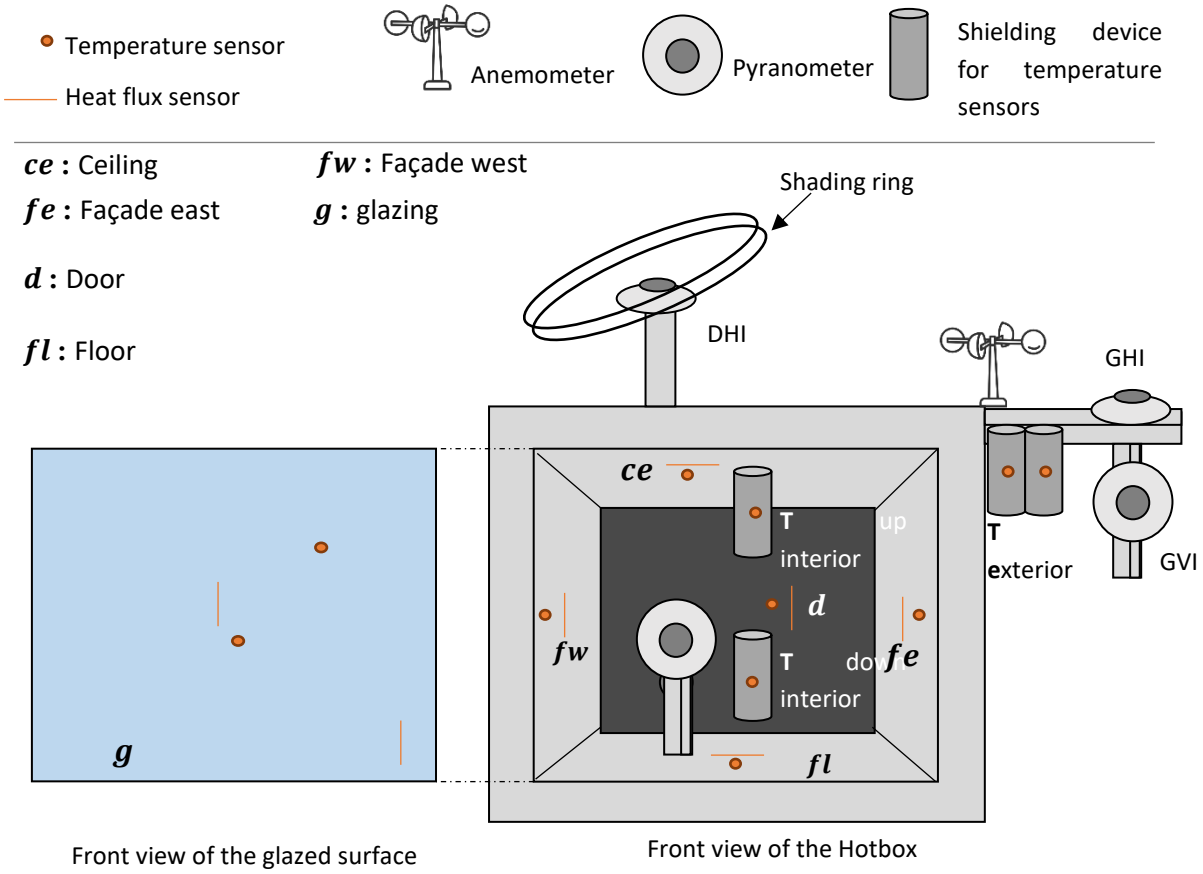

Figure 3-40 Front view of the test cell and used sensors

The sensors types, measured variable, and positioning is listed in Table 3-6 for the following elements: Meteorological station, glazing and the Hotbox opaque envelope. Although heat flux sensors and exterior surface temperature of the glazing were deployed, however, those measurements were not used in the RC model.

Table 3-6: Position of experiment sensors

	Sensor type	Measured variable	Position in the Hotbox
Meteorological station	Pyranometer n°1	Global horizontal irradiance (GHI)	Horizontal and closer to roof
	Pyranometer n°2	Global vertical irradiance (GVI)	Vertical and parallel to glazing in outside
	Pyranometer n°3	Diffuse horizontal irradiance (DHI)	Horizontal and equipped with a shading ring, the installation details are in Annex B
	Anemometer	Wind speed	Closer to roof
	2 thermocouples	Outdoor air temperature	Outside test cell, shielded
Glazing	Pyranometer	Global vertical irradiance	Vertical and fixed behind the interior face of glazing
	Thermocouple	Surface temperature	Shielded and positioned in the inner face of glazing as shown in Figure 3-41
	Thermocouple	Surface temperature	Shielded and positioned in the outer face of glazing
	Plate heat flux sensor	Heat flux	Centre of inner face of glazing
	Plate heat flux sensor	Heat flux	Corner of inner face of the glazing
Hotbox	Surface thermocouple	Surface temperature	Center of interior façade west $\boldsymbol{fw}$
	Surface thermocouple	Surface temperature	Center of interior façade east $\boldsymbol{fe}$
	Surface thermocouple	Surface temperature	Center of ceiling $\boldsymbol{ce}$
	Surface thermocouple	Surface temperature	Center of door $\boldsymbol{d}$
	3 surface thermocouples	Surface temperature	Floor temperature is measured using 3 thermocouples positioned mainly in the eastern zone as shown in Figure 3-42 to capture the irradiance received afternoon
	2 thermocouples	Indoor air temperature	In two positions: up and down, both are shielded with a distance from the glazing as shown in Figure 3-43
	Plate heat flux sensors	Heat flux	Center of façade west

	Plate heat flux sensor	Heat flux	Center of façade east
	2 Plate heat flux sensors	Heat flux	Center of ceiling
	Plate heat flux sensor	Heat flux	Center of floor
	Plate heat flux sensor	Heat flux	Center of door

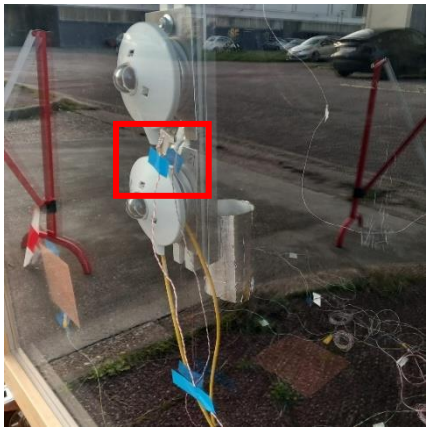

Figure 3-41: Glazing temperature sensors positioning

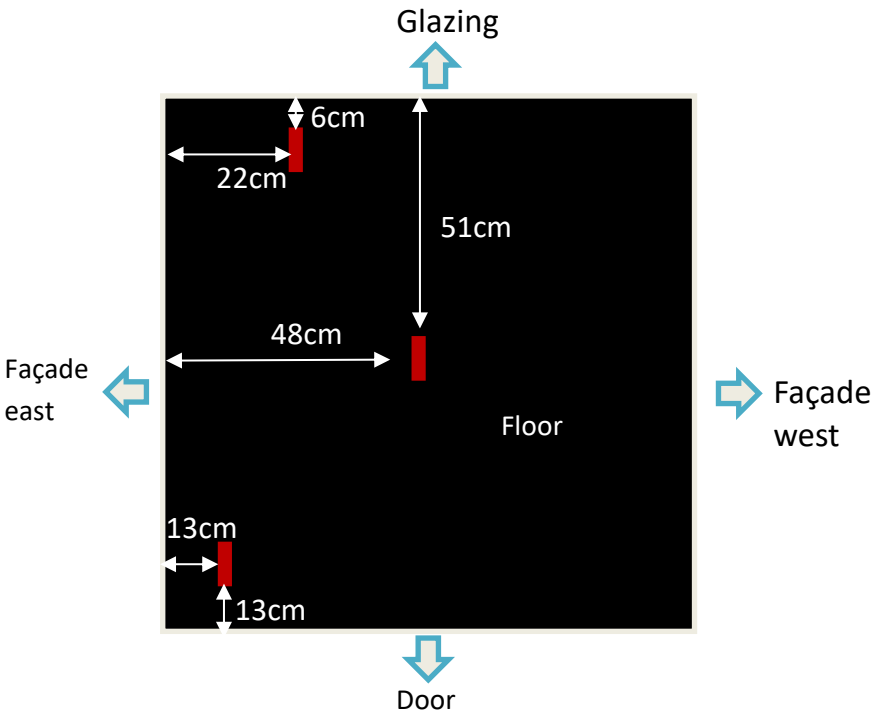

Figure 3-42: Floor temperature sensors positioning on eastern zone

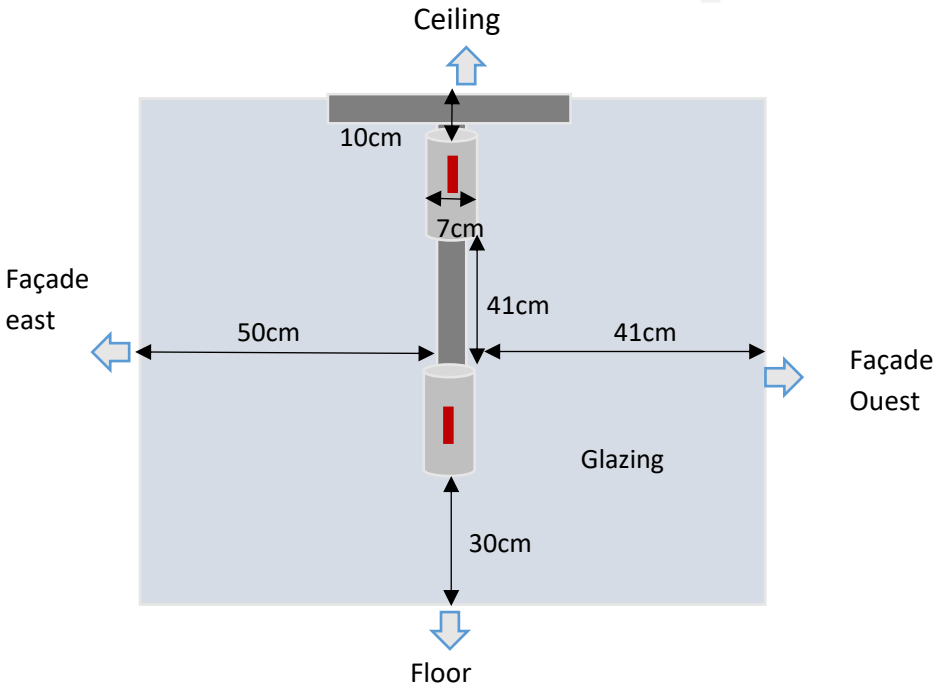

Figure 3-43: Indoor air temperature sensors placement

3.2.4.3 The RC model validation steps

The objective is to assess the ability of the model to reproduce the indoor air and surface envelope temperatures under different solar conditions. At first, the model will be tested excluding the solar gain term, by placing the Hotbox in indoor conditions. The objective is to partially validate the independent terms from solar gain, and to ensure that the terms are well modelled. In second step, the Hotbox is placed in the outdoor with a specific orientation that highlights the solar gain, in this case, a theoretical solar gain is introduced to the RC model, the capacity of the model to recover the amplitude of the solar gain is evaluated. Finally, the stage where the shading is placed with the Hotbox outdoor is attended. The previous step parameters will be reused, and the model will be evaluated to compute the solar gain from temperature fluctuations and the measured irradiance. Those steps are shown in Figure 3-44.

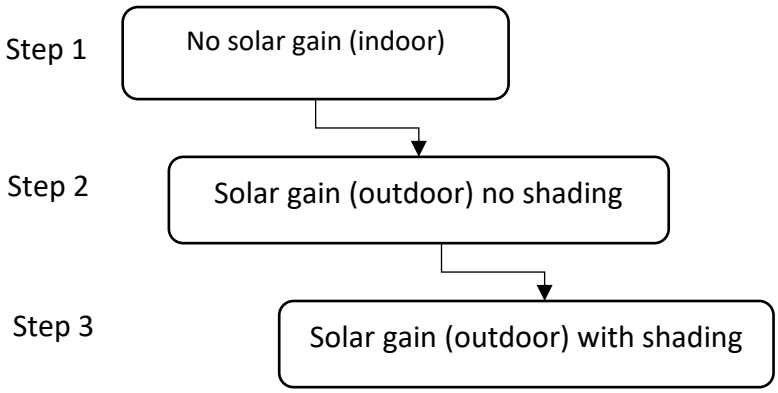

Figure 3-44: Progressive validation steps of the RC model with different experimental protocols

Indoor validation of the model without solar gain with co-heating

- **Description of the experimental campaign**

Starting with the indoor conditions without solar gain, the co-heating test is performed. As a first step, we want to characterize the Hotbox itself. The objective is to determine the heat loss coefficient HLC, and to evaluate the model ability to estimate the indoor air and surface envelope temperatures. In order to do so, a sufficient indoor and outdoor temperature air difference is necessary [141], to increase signal-to-noise ratio. That can be achieved it using a heating source. In our case it is a lamp with a constant power equal to 145 W. The data was collected with 1 min time step. For this experimental identification, to make sure the indoor air temperature is homogenous, and to reduce the uncertainty in the measurements, a mini fan is used with an air speed of $0.6\ m/s$. It can also help to avoid stratification effect. Then, a heat balance is applied to the inner volume, without consideration of the solar radiation since the experiment is carried out indoor.

The difference between indoor and outdoor air temperature is around 25°C as shown in Figure 3-45.

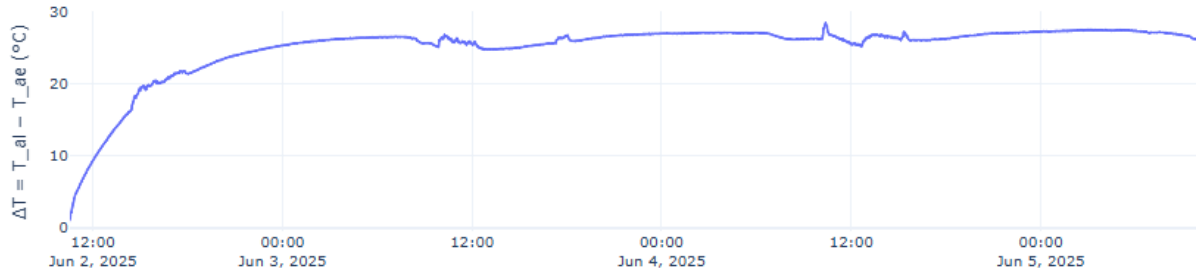

Figure 3-45: Difference between the indoor and the outdoor air temperature $T_{ai} - T_{ae}$ (Co-heating test)

To verify the stratification effect of temperature, the graph in Figure 3-46 shows a difference between the two sensors positioned in up and down inside the hotbox which ranged between 0.04°C and -0.2°C, which is a minor effect.

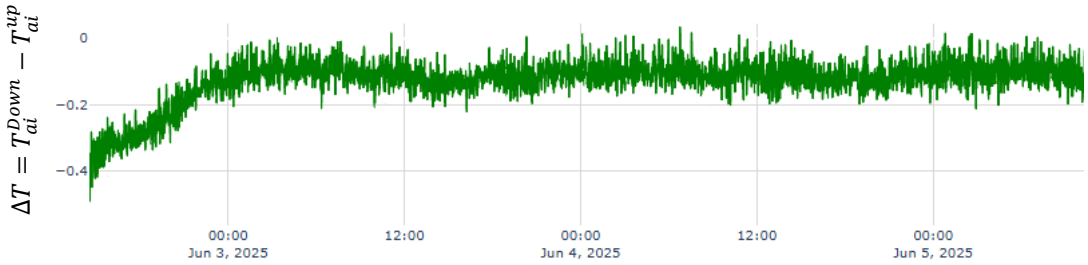

Figure 3-46: Evolution of the air temperature difference between two indoor air temperature sensors (Co-heating test)

The heat loss coefficient HLC is calculated from the air temperature difference between the indoor $T_{a,i}$ and the outdoor $T_{a,e}$ and using the supplied power P_h (Eq 3-21).

$$HLC = \frac{P_h}{T_{a,i} - T_{ae}} \left[\frac{W}{K}\right] \quad \text{Eq 3-21}$$

Using the air temperature measurements of this co-heating test and an injected power of 145 W, the heat loss coefficient calculated is $HLC = 5.67\ W/K$. This HLC value means that for every 10°C of difference between indoor and outdoor air temperature, the cell loses 56.7 W. The total surfaces $A_{env,i}$ of inner façades is $6\ m^2$, thus, to calculate the $Uvalue$ of the whole cell we can use Eq 3-22.

$$U = \frac{HLC}{A_{env,i}} \left[\frac{W}{m^2 K}\right] \quad \text{Eq 3-22}$$

Therefore, $U = 0.94\ W/m^2K$, which reflects a light insulation for an enclosure of $1\ m^3$ volume. Even though the infiltration losses cannot be isolated from $Uvalue$ and HLC terms, but the pressure decay test conclusion implies that the infiltration losses are dominant.

- **The RC model structure**

The RC model to represent the thermal behaviour for this experimental campaign is shown in Figure 3-47 , where the solar gain term is removed since the experiment was done inside a building. The injected heating power P_h is governing the exchanges in air temperature node.

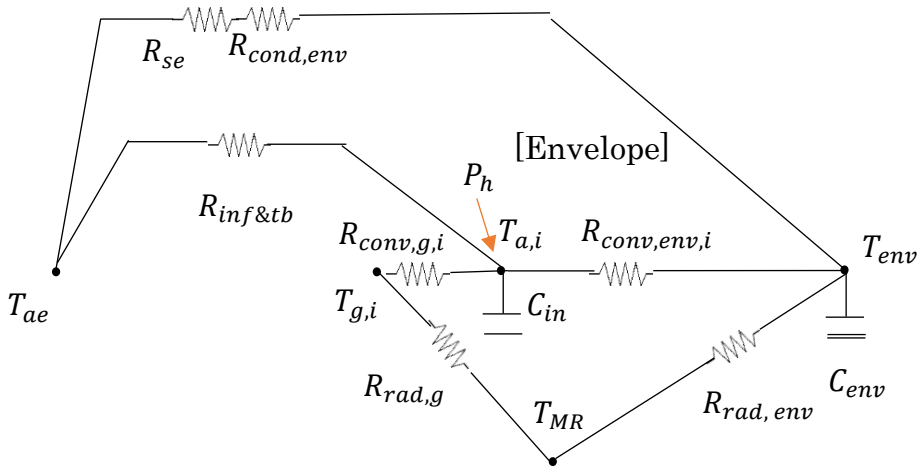

Figure 3-47: RC model for the co-heating test

The equations introduced in Section 2.1.4 are reformulated for the co-heating case by removing solar input in envelope temperature node, and injecting a heating power to the air temperature node as in Eq 3-23.

$$C_{in}\frac{dT_{ai}[t]}{dt} = \left(\frac{T_{env}[t]-T_{ai}[t]}{R_{conv,env,i}}\right) + P_h + \left(\frac{T_{gi}[t]-T_{ai}[t]}{R_{conv,gi}}\right) + \left(\frac{T_{ae}[t]-T_{ai}[t]}{R_{inf\&tb}}\right) \quad \text{Eq 3-23}$$

It should be noted that T_{gi} and T_{ae} measurements are inputs for the model. The evolution of T_{gi} for this experimental campaign is in Figure 9-3, Annex D.

- **Sensitivity analysis**

The RC model above have 9 parameters including the thermal resistances and capacitances. To find the best fitting model with this large number of parameters requires exploring a high-dimensional space. Therefore, it is relevant to limit the optimizer exploring space to the parameters that drive most of the variance of the calculated outputs of the model which are T_{ai} and T_{env}. To answer the question 'which parameter explain the output?', a practical diagnosis step of the RC model that can be done before the optimization is the sensitivity analysis. The variance of the output $V(Y)$ is decomposed from the contribution of each parameter input X_i variance $V(E(Y/X_i))$. Thus, to understand the effect of each parameter, one can change a parameter at time and fix the others, that is the core of Sobol global method. A first order Sobol index for an input parameter is then defined as in Eq 3-24.

$$S_i = \frac{V(E((Y|X_i)))}{V(Y)} \quad \text{Eq 3-24}$$

Where $E(Y/X_i)$ is the esperance of Y knowing X_i.

To account for the combination effect of parameters i and j on the output variance, beyond their individual variance, the second order Sobol index can be defined with Eq 3-25.

$$S_{i,j} = \frac{V(E((Y|X_i, X_j)))}{V(Y)} \quad \text{Eq 3-25}$$

The total Sobol index represent the overall contribution of all parameters, including first and second Sobol index, thus it can be expressed as Eq 3-26.

$$S_T = \sum S_i + \sum S_{i,j} \quad \text{Eq 3-26}$$

The influence of each RC model parameters on T_{ai} and T_{env} nodes, is temporally variable. One single averaged Sobol index of an input parameter S_i for the whole campaign time series is not sufficient. To explain the temporal influence of the parameter on the output, it must be considered that this influence can be environmentally conditioned. For example, a parameter can be influent only during the day, when the solar gain is important. As a result, a time-resolving sensitivity analysis must be conducted to reveal the dynamic influence of each parameter on both temperature nodes.

To perform those analysis, the variation space of each input parameter X_i should be defined according to a certain scaling factor. Considering that the model is reduced order, and the error can be not only the uncertainties of the parameters but also the complexity of other physical phenomena that could not be accounted, a scaling factor of $a = 0.7$ is used to define the upper and lower bound for each parameter P using $[P \times (1-a), P \times (1+a)]$. This scaling factor value is used due to the fact that the model is simplified and the real parameters values were not measured. The open source library in Python SALIB was used with Saltelli [142] sampling method. The number of input parameters is n = 9, and the base sample is $N = 256$, thus, the number of simulations is $N \times (n+2) = 2816$.

Therefore, the according bounds of the 9 RC model parameters are listed in Table 3-7

Table 3-7: Bounds for each parameter in sensitivity analysis

Parameter	Unit	Theoretical /Initial value	Lower bound	Upper bound
$R_{conv,env,i}$		0.025	0.0075	0.042
R_{se}		0.0062	0.00186	0.010

$R_{\text{cond,env}}$	K/W	0.7	0.21	1.19
$R_{conv,g,i}$		0.138	0.0414	0.23
$R_{inf\&tb}$		1.27	0.38	2.15
$R_{\text{ray,env}}$		0.038	0.0114	0.064
$R_{\text{ray},g}$		0.2	0.06	0.34
C_{env}	kJ/K	67.24	20.172	114.3
C_{in}		3612	1083.6	6140.4

The dynamic Sobol indices of RC model parameters influencing T_{ai} are shown in Figure 3-48. After the transient phase, T_{ai} is mainly influenced by $R_{conv,g,i}$, with a low contribution of $R_{\ inf\&tb}$ and $R_{cond,env}$, and relative minor effect of thermal capacitances C_{in}, C_{env} and radiative resistances $R_{ray,g}$ and $R_{ray,env}$.

On the other hand, dynamic Sobol indices for each RC model parameter influencing T_{env} in Figure 3-49, and after the transient effect, $R_{conv,g,i}$, and R_{conde} are more influential. $R_{inf\&tb}$ have less influence here then on T_{ai} , and same relative minor effect of thermal capacitances C_{in}, C_{env}, radiative resistances $R_{\text{ray},g}$ and $R_{\text{ray,env}}$ as the same case for the dynamic sensitivity analysis on T_{ai}.

Both dynamic sensitivity analysis cumulative graphs, attend a total Sobol index closer to 0.89, means most of output variance is explained by first order indices. Thus, the contribution of parameters interaction effects is limited, and therefore, calculating second order Sobol index is not necessary.

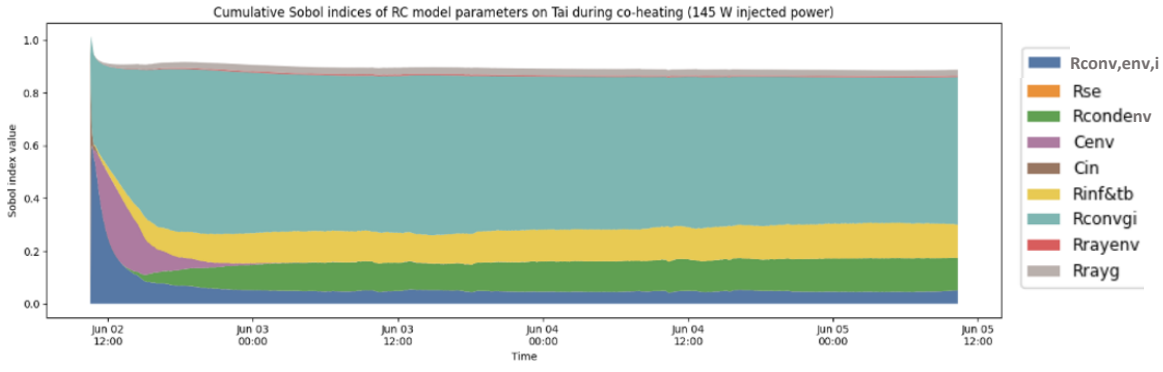

Figure 3-48: Total dynamic Sobol indices of RC model parameters influencing T_{ai} (Co-heating test)

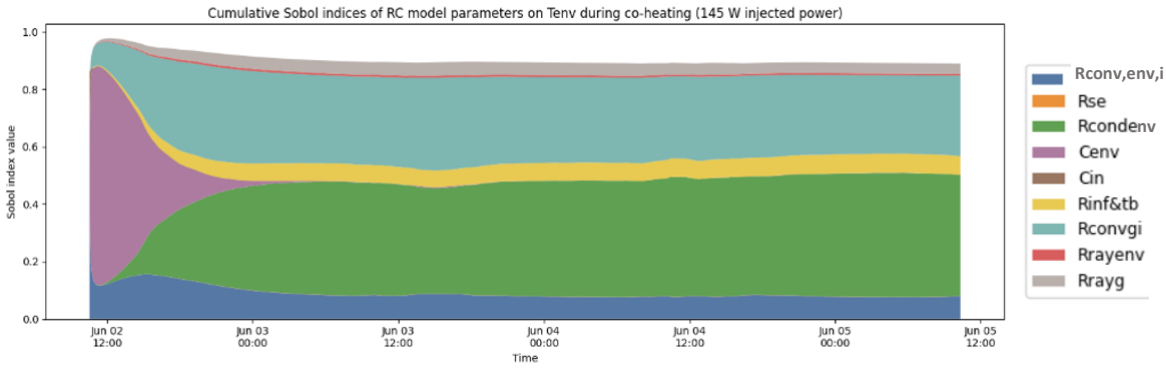

Figure 3-49: Total dynamic Sobol indices of RC model parameters influencing T_{env} (Co-heating test)

The sensitivity analysis shows that both temperatures (T_{ai} and T_{env}) are influenced by the envelope conductive resistance ($R_{condenv}$), the convection-related resistances R_{convgi} and $R_{conv,env,i}$, and the resistance associated with air infiltration and thermal bridges. The parameters related to conduction and convection phenomena are generally well known (e.g., material properties, layer thicknesses, and air velocity), whereas the resistance associated with air infiltration and thermal bridges is much more uncertain. Therefore, we propose to use this experimental campaign to identify the resistance associated with air infiltration and thermal bridges $R_{inf\&tb}$.

- **RC model calibration: Thermal parameter identification**

The objective in this part is to identify the infiltration and thermal bridges losses $R_{inf\&tb}$ by minimizing the error between the estimated and measured T_{ai} and T_{env}. The CV(RMSE) cost function was chosen to determine this error, and is defined in Eq 3-27

$$CV(RMSE) = \frac{\sqrt{\frac{1}{n}\sum_{t=1}^{n}(\hat{y}_t - y_t)^2}}{\bar{y}} \times 100 \qquad \text{Eq 3-27}$$

With:

- $\hat{y}_t$ is the calculated output at time step t;
- y_t is the measured output at time step t;
- $\bar{y}$ is the mean of the measured output;
- n is the number of observations.

Therefore, the total CV(RMSE) for both temperature nodes with an assumed equal weighting can be defined with Eq 3-28.

$$CV(RMSE) = CV(RMSE)(\widehat{T_{ai,t}}, T_{ai,t}) + CV(RMSE)(\widehat{T_{env,t}}, T_{env,t}) \qquad \text{Eq 3-28}$$

The optimization is performed using the algorithm Powell from Scipy library in Python. The initial guess of $R_{inf\&tb}$ was set to $1\ K/W$ and the bounds were defined with $[0.3; 2.83]$. Finally, the obtained optimal value is $R_{inf\&tb} = 0.88\ K/W$. The corresponding T_{ai} and T_{env}

using this optimal value while fixing the rest of the parameters of the model are presented in Figure 3-50 and Figure 3-51. In steady state, for T_{ai} graph the error of the model ranges between -0.4°C and 0.02°C. For T_{env} the error of the model ranges between -0.2°C and 0.3°C.

The quality of the evaluation process for this scenario is evaluated with two metrics as recommended by ASHRAE Guideline 14-2002 [143], using CV(RMSE) defined in Eq 3-27, and the Normalized Mean Bias Error NMBE in Eq 3-29, which evaluates the average bias of the model, p is the number of adjusted parameters of the model. A positive value indicates underestimation, and a negative value indicates an overestimation of the model. Usually NMBE is not enough as a calibration metric since is subjected to cancellation errors [144], thus, it must be associated with CV(RMSE).

$$NMBE = \frac{1}{\bar{y}} \times \frac{\sum_{t=1}^{n}(\hat{y}_t - y_t)}{n - p} \times 100 \qquad \text{Eq 3-29}$$

ASHRAE Guideline 14-2002 recommended hourly values of CV(RMSE) and NMBE to consider that a model is calibrated, those values are listed in the following with the obtained hourly values for this co-heating test model in Table 3-8, where p=1 since only $R_{inf\&tb}$was adjusted.

Table 3-8: Obtained metrics values CV(RMSE) and NMBE for co-heating with the ASHRAE guideline hourly metrics criteria for a well calibrated model

Index (hourly)	ASHRAE guideline 14-2002 [144]	Co-heating model	
CV(RMSE) %	30	T_{ai}	0.78
		T_{env}	0.43
NMBE%	±10	T_{ai}	0.67
		T_{env}	0.055

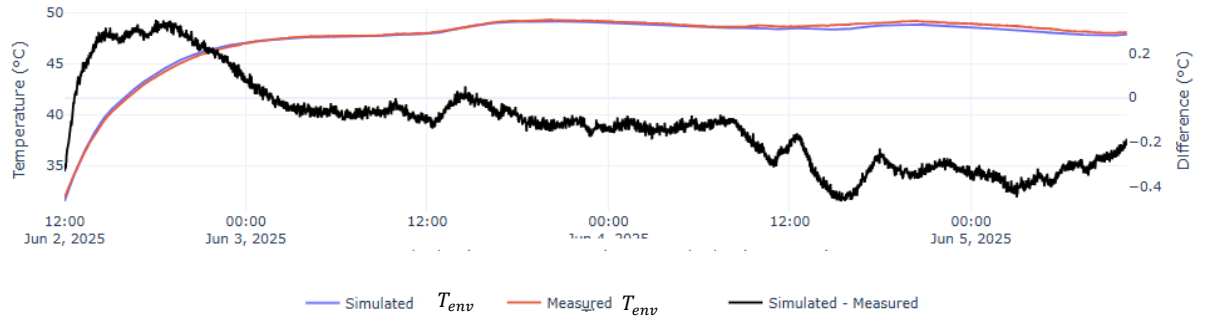

Figure 3-50: Measured vs calculated indoor air temperature using the identified value of $R_{inf\&tb}$ (Co-heating test)

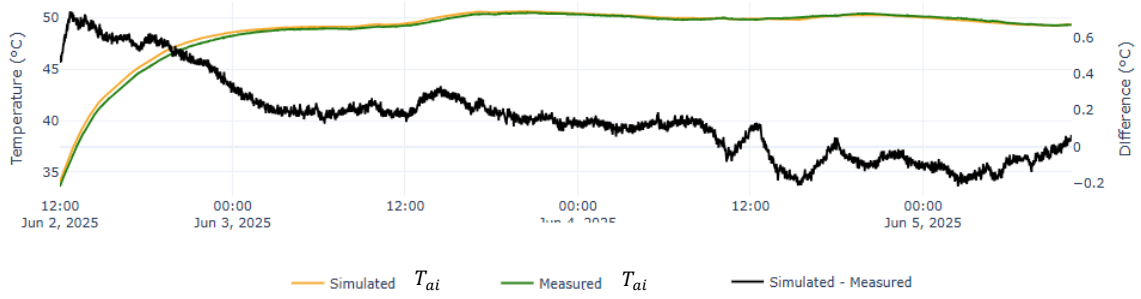

Figure 3-51: Measured vs calculated indoor surface envelope temperature using the identified value of $R_{inf\&tb}$ (Co-heating test)

To sum up, the model CV(RMSE) error is low for both calculated temperature nodes, using the identified $R_{inf\&tb}$, and compared to the recommended values by ASHRAE guideline 14 [143] listed in Table 3-8, thus, the RC model represents well the thermal behaviour of this test. Nevertheless, the result is meaningful for an indoor experiment without the solar radiation input impact. Therefore, the following parts aims at verifying its performance for outdoor environmental conditions.

<u>Outdoor experiments without the shading</u>

- **Description of the experimental campaign**

The experimental test cell was installed in outdoor site located at Bordeaux city (France) with latitude l = 44.8° and longitude L = -0.6°. The experiment was done without the shading and it was oriented with its mainly glazed façade toward the South with a surface azimuth of $\gamma = 180°$ as illustrated in Figure 3-52 and Figure 3-53.

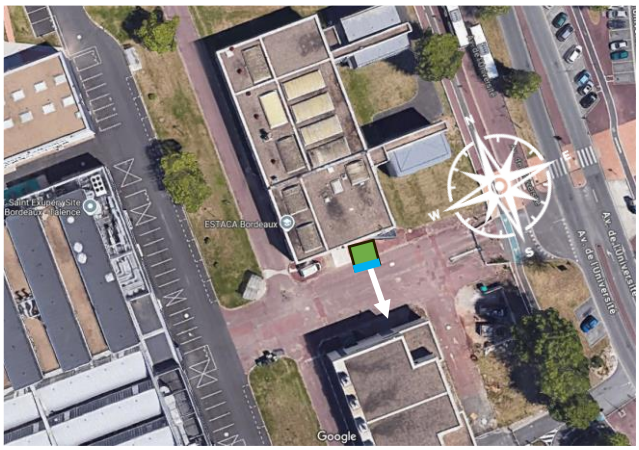

Figure 3-52: Geographical location of the experimental site



Figure 3-53: Picture of the experiment without the shading

The instrumental equipment's that were listed in Figure 3-40 are used. The data was collected with 1 min time step from 6 to 10 October 2025. The variation of global vertical irradiance (GVI) measured for the glazed façade exposer, and the diffuse horizontal irradiance (DHI) are shown in Figure 3-54. The glazed façade received a maximum irradiance of 800 W/m² for this period which is a suitable environmental condition to perform solar gain model estimations. A shading mask is appearing in the start and the end of the day, it was due to the shading of a closer building to the Hotbox site.

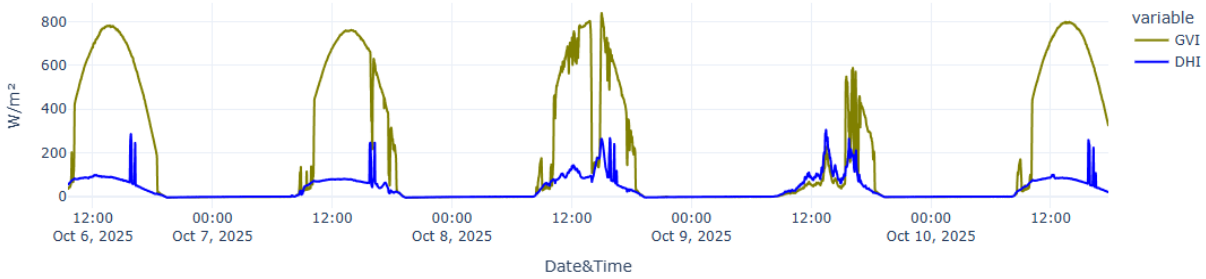

Figure 3-54: Global vertical irradiance (GVI) and diffuse horizontal irradiance (DHI) over time (Outdoor test without shading)

The Figure 3-55 shows the indoor and outdoor air temperature variation without the shading. The indoor air temperature reaches a maximum value of 80°C, while the outdoor temperature maximum is equal to 28°C. The indoor envelope surface is painted in black and the glazing has an air-filled cavity, this contributes to an important transmittance of solar gain leading to a high indoor temperature.

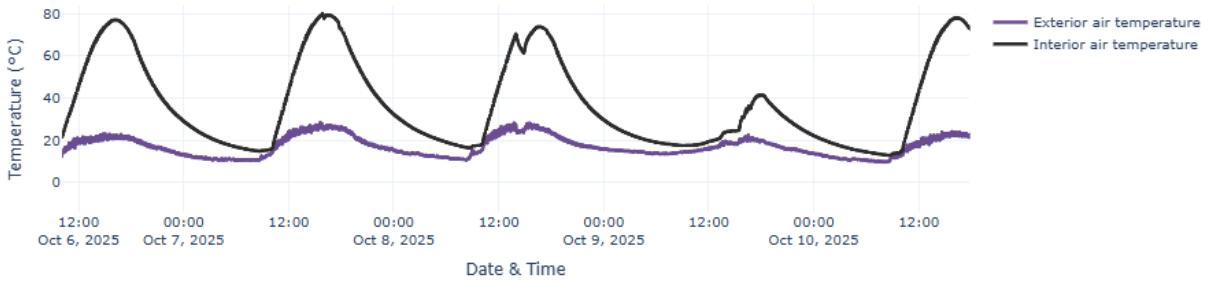

Figure 3-55: Interior and exterior air temperature variation (Outdoor test without shading)

The indoor air temperature is obtained using the mean temperature of two sensors inside the cell that were fixed in two positions: up and down, one at 30cm above the floor and the other one 10 cm below the ceiling, both centred horizontally (40cm from each wall). To evaluate the stratification effect, the difference of the temperature measured by both sensors is illustrated in Figure 3-56. A difference ranging between -2°C and +3°C is observed between both positions, which is mainly due to the effect of the projection of solar rays on the Hotbox floor.

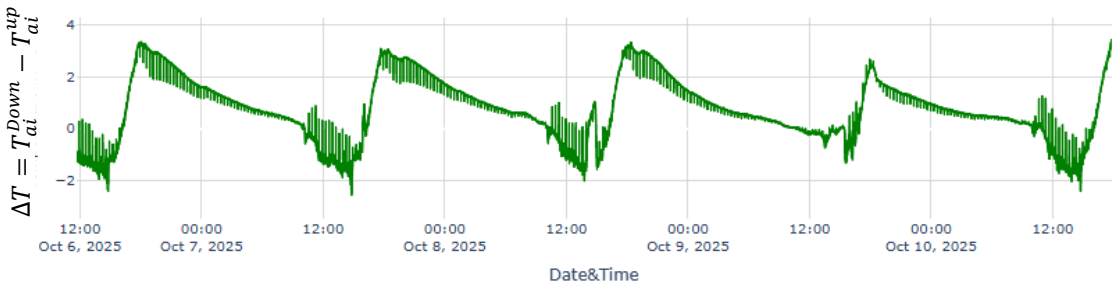

Figure 3-56: Evaluation of indoor air temperature stratification (Outdoor test without shading)

i. RC model

The RC model for this outdoor experiment is shown in Figure 3-57, with a solar gain input injected on the T_{env} temperature node.

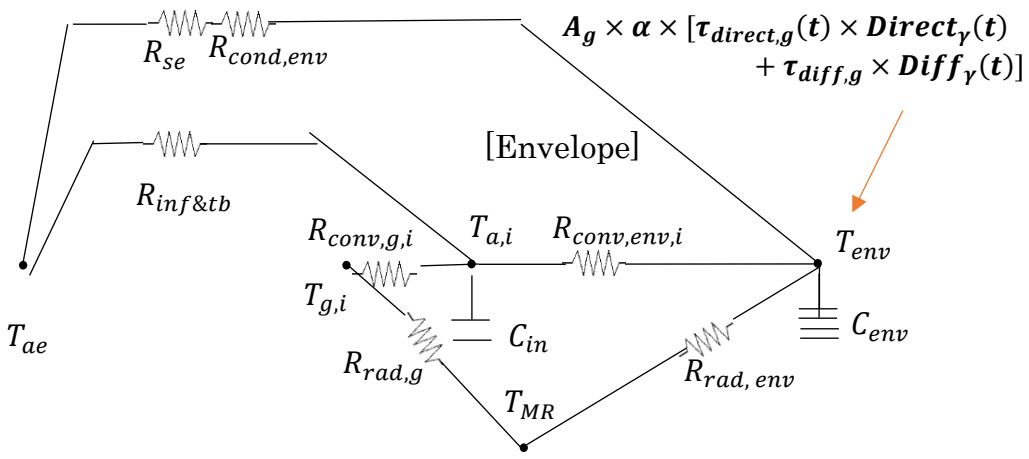

Figure 3-57: RC model for outdoor experiment without shading

The equations remain the same as Eq 3-8 except for the addition of the solar gain term, which incorporates the theoretical direct transmittance of the double glazing $\tau_{direct,g}$ from Window LBNL [128] calculations. A factor called $calibsolar$ is introduced in the T_{env} temperature node in Eq 3-30 , it serves to evaluate the time-varying influence of the direct solar gain term.

$$C_{env}\frac{dT_{env}}{dt} = \left(\frac{T_{ai}-T_{env}}{R_{conv,env,i}} + \frac{T_{ae}-T_{env}}{R_{cond,env}+R_{se,env}} + A_g \times \alpha \right.$$
$$* \left(calibsolar \times Direct_{180} \times \tau_{direct,g} + Diffus_{180} \times \tau_{diff,g}\right) \quad \text{Eq 3-30}$$
$$\left. + \frac{T_{RM}-T_{env}}{R_{ray,env}}\right)$$

ii. Sensitivity analysis

We need to select the factor of interest to be used after for the calibration of the model, the parameters that are less influent will be considered constant during the optimization process. In order to perform sensitivity analysis, Sobol method is used with Saltelli sampling method [142] similar to the co-heating test. A uniform distribution was chosen with a corresponding range $\pm 70\%$ of the baseline parameter value.

Table 3-9 gives the lower and upper bound values for each parameter.

Table 3-9: Parameters and their variation for sensitivity analysis

Parameter	Unity	Theoretical /Initial value	Lower bound	Upper bound
$calibsolar$		1	0.1	1
$R_{conv,env,i}$	K/W	0.076	0.022	0.13
R_{se}		0.0062	0.00186	0.010
$R_{cond,env}$		0.7	0.21	1.19
$R_{conv,g,i}$		0.4	0.12	0.68
$R_{inf\&tb}$		1.27	0.3	2.15
$R_{\mathrm{ray,env}}$		0.038	0.0114	0.064
$R_{\mathrm{ray},g}$		0.2	0.06	0.34
C_{env}	kJ/K	67.24	20.172	114.3
C_{in}		3612	1083.6	6140.4

After performing the dynamic sensitivity analysis on both temperature nodes, the dynamic Sobol indices for RC model parameters influencing T_{ai} are shown in Figure 3-48. T_{ai} is mainly influenced by the envelope thermal capacitance C_{env}, with a medium contribution of $calibsolar$. $R_{cond,env}$ and the remaining parameters have a relative minor effect. On the other hand, dynamic Sobol indices for each RC model parameter influencing T_{env} shown in Figure 3-59, have the same variance dynamics as for T_{ai}, except that $R_{inf\&tb}$ which have less influence here than on T_{ai}. As shown by the solar irradiance evolution in Figure 9-1 Annex D, the decrease in the Sobol index of the envelope capacitance C_{env} occurred during a cloudy period characterized by low and fluctuating irradiance. This suggests that the reduced solar excitation made the thermal inertia of the envelope less influential on the predicted indoor response.

Both dynamic sensitivity analysis cumulative graphs, gets a total Sobol index ranging between 0.98 and 0.8, meaning that the mutual interactions between parameters is limited. Thus, it is not necessary to perform second order Sobol index calculations to evaluate the effect of input parameters on each other. As a conclusion, three parameters must be identified in the optimization process namely C_{env}, $calibsolar$ as well as $R_{inf\&tb}$. This later, which is a loss

resistance (even though it has a minor influence compared to other parameters) is still a physical unknown quantity that depends on each experiment conditions.

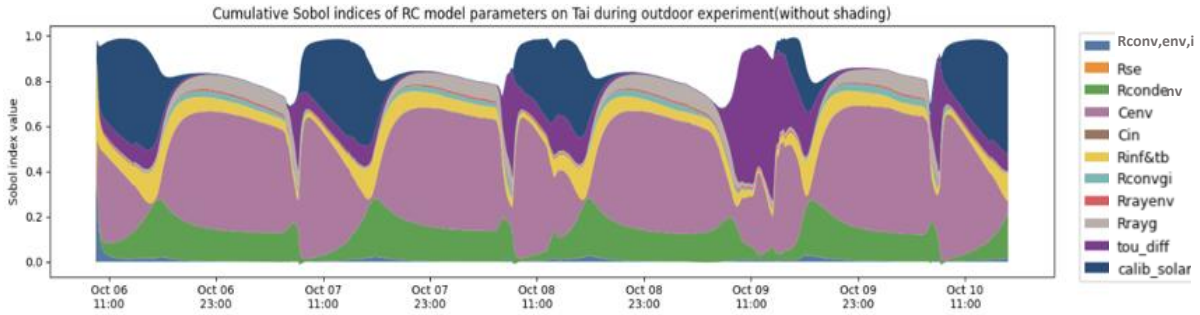

Figure 3-58: Total dynamic sensitivity analysis of RC model parameters influencing T_{ai} (Outdoor test without shading).

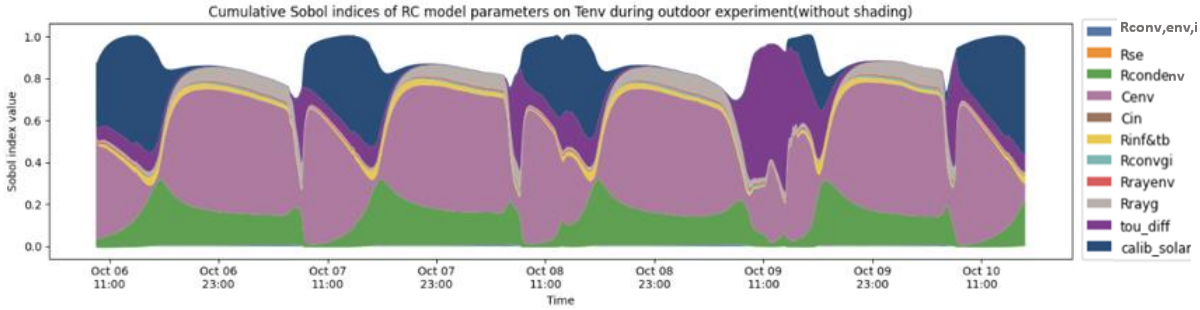

Figure 3-59: Total dynamic sensitivity analysis of RC model parameters influencing T_{env} (Outdoor test without shading)

iii. RC model calibration: Thermal parameter identification

Based on the above analysis, the identification of three parameters will be performed: C_{env}, $calibsolar$ as well as $R_{inf\&tb}$. However, C_{env}, $and\ calibsolar$ are highly correlated, since the thermal capacitance of the envelope depends on the applied solar gain excitation. Thus, a two steps optimization approach can be used:

- Step1: By fixing all parameters, and identify only C_{env} and $R_{inf\&tb}$ while considering $calibsolar = 1$;
- Step2: Use as an input the identified C_{env} and $R_{inf\&tb}$, and search for the optimal $calibsolar$.

A filter is applied in the second step to consider optimization only when vertical direct irradiance is above the threshold $Direct_{180} > 50\ W/m^2$, since that the Sobol index of $calibsolar$ appears only during the day. This identified coefficient represents the amplitude of $\tau_{direct,g}$ identified by the optimization of the model.

The total CV(RMSE) for both temperature nodes with an assumed equal weighting is used as a cost function be defined with Eq 3-31.

$$CV(RMSE) = CV(RMSE)(\widehat{T_{ai,t}}, T_{ai,t}) + CV(RMSE)(\widehat{T_{env,t}}, T_{env,t}) \quad \text{Eq 3-31}$$

The optimization is performed using the algorithm Powell from Scipy library in Python. The initial guess, the bounds, condition and the identified values of $R_{inf\&tb}$ C_{env} as a first step, and $calibsolar$ as a second step, are listed in Table 3-10.

Table 3-10: Identified values of the parameters: $R_{inf\&tb}$, C_{env} and $calibsolar$

Step	Parameter	Initial value	Bounds	Condition	Identified value
1	C_{env}	67.24 [kJ/K]	[20.17,114.3] [kJ/K]	-	63.3 [kJ/K]
	$\mathrm{R}_{inf\&tb}$	1.61 [K/W]	[0.3,2.83] [K/W]		0.61 [K/W]
2	$calibsolar$	0.6	[0.1,1]	$Direct > 50\mathrm{W/m^2}$	0.94

From the optimization process, the identified losses resistance $\mathrm{R}_{inf\&tb}$ is lower than the identified value during the indoor co-heating test, this is mainly due to the wind absence in the indoor test. The optimal value of C_{env} is only 3 kJ/K difference with the theoretical reference value. In addition, using those optimal values, the identified $calibsolar$ in the second step reached 0.94, which means the model estimated a direct solar transmittance of $0.94 \times \tau_{direct,g}$, which is an error of 0.06. The corresponding T_{ai} and T_{env} using this optimal value while fixing the other parameters of the model are presented in Figure 3-60 and Figure 3-61. Using same calibration metrics as in the co-heating model, and a number of adjusted parameters of $p = 3$ (C_{env}, $calibsolar$, and $\mathrm{R}_{inf\&tb}$) , the obtained metrics CV(RMSE) and NMBE are listed in Table 3-11.

Table 3-11: Obtained calibration metrics alongside with ASHRAE recommended hourly values for outdoor experiment without the shading toward the South

Index (hourly)	**ASHRAE guideline 14-2002** [144]	**Without shading model**	
CV(RMSE) %	30	T_{ai}	6.5
		T_{env}	6.9
NMBE%	± 10	T_{ai}	-5.4
		T_{env}	1.13

The calculated $CV(RMSE)$ between the final calculated and measured T_{ai} is 6.5 % and for T_{env} is 6.9 %, which is a low model error. With an overestimation of T_{ai} indicated by the NMBE

negative value -5.4 %. Overall, the values of both metrics remain less than the threshold defined by ASHRAE guideline 14 [143], thus the model can be considered calibrated.

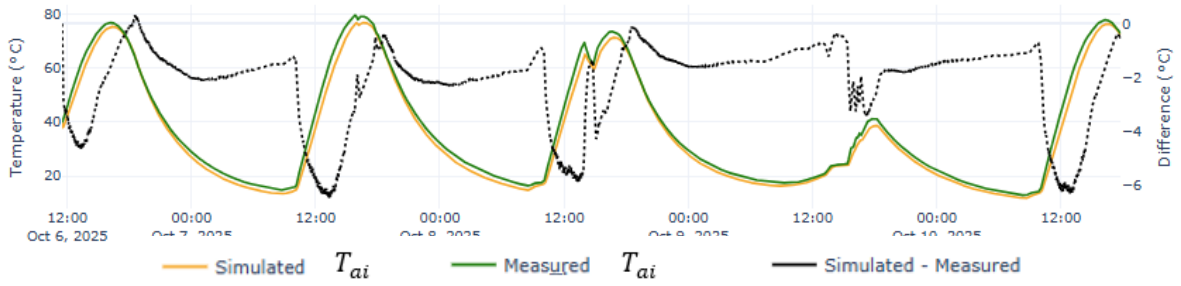

Figure 3-60:Measured vs calculated indoor air temperature with the identified parameters values (Outdoor test without shading)

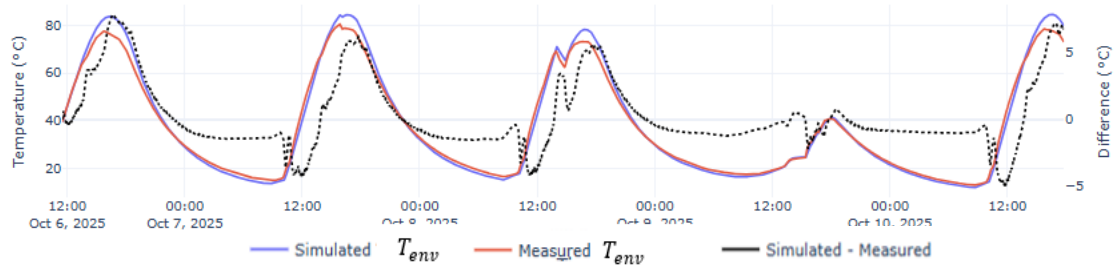

Figure 3-61: Measured vs calculated indoor surface envelope temperature with the identified parameters values (Outdoor test without shading)

Following the sequential steps of the methodology, and after verifying the model's performance excluding the solar gain, and then with the solar gain in outdoor conditions without the shading device, now we can introduce the diagonal shading in outdoor conditions to quantify its thermal performance.

<u>Outdoor experiments with the diagonal shading solution</u>

- **Experiment description**

The experiment with the shading was carried out from the 13th to the 17th of October, which was the consecutive week to the one for the measurement without the shading. This consecutive week's test choice was due to the continuously changing solar incidence angle during the day and across seasons. In order to use the RC model obtained, namely identified values of the model parameters without shading, the sun trajectory must be approximatively closer to the conditions with the shading experiment, which will allow the reuse of apparent thermal capacitance of the envelope C_{env} identified without the shading experiment. The shading is placed in front of the glazed façade. The test cell is oriented to South with a surface

azimuth of $\gamma = 180°$ as illustrated in Figure 3-62. Data was recorded for every 1 min. Same instrumental installation is used as in Figure 3-40.

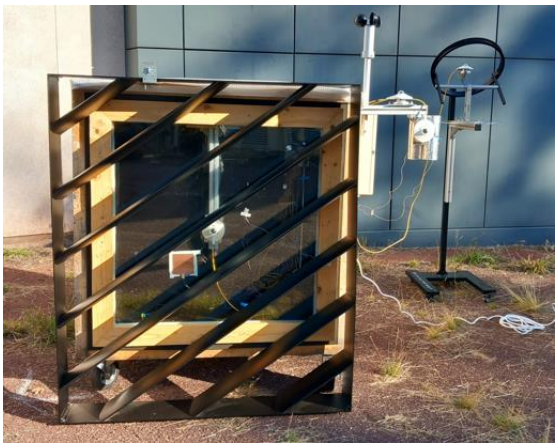

Figure 3-62: Experimental set with the shading device

The variation of global vertical irradiance (GVI) measured for the glazed façade exposer, and the diffuse horizontal irradiance (DHI) for this experiment are shown in Figure 3-63. This sunny period is also suitable for the direct solar transmittance estimation with a maximum GVI of 800 W/m². A neighbouring building acting as a shading mask affecting the start and the end of the day measurements.

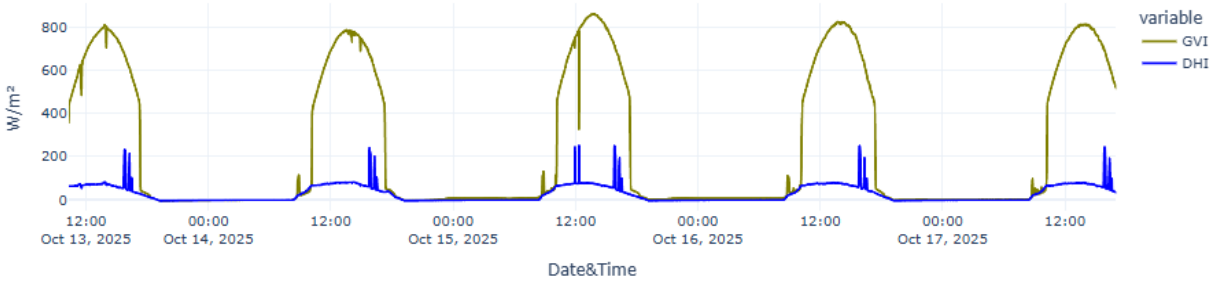

Figure 3-63: Measured global vertical irradiance (GVI) and diffuse horizontal irradiance (DHI) over time (Outdoor test with shading)

The indoor air temperature in this experiment with the shading solution installed can rise to 60°C, while the outdoor air temperature ‘s maximum is 29°C as shown in Figure 3-64. The environmental conditions recorded during this shading test are closer to the week before when the Hotbox with no shading was tested. Thus, we can conclude that the shading has reduced the indoor air temperature with around 20°C compared to no shading experiment.

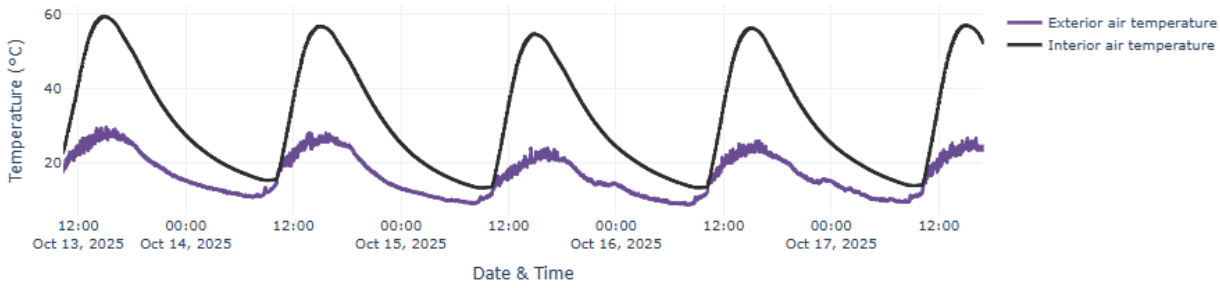

Figure 3-64: Interior and exterior air temperature variation (Outdoor test with shading)

The stratification of temperature in this campaign conditions is illustrated in Figure 3-65, the difference between the two temperature sensors range between -1°C and +2°, which is less than the previous experiment due to the diagonal shading impact.

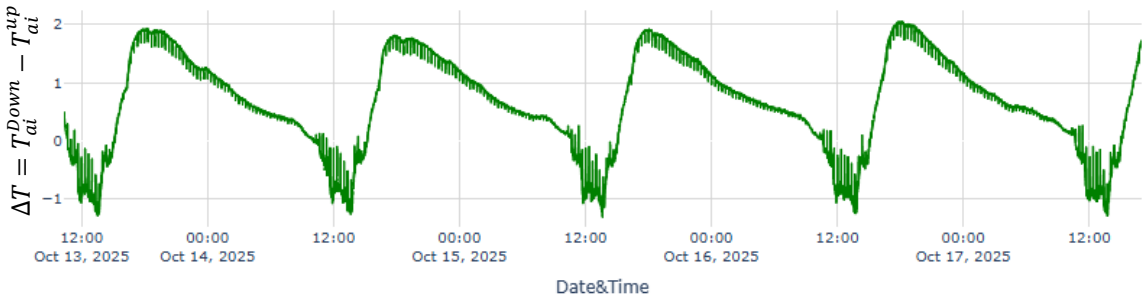

Figure 3-65: Evaluation of indoor air temperature stratification (Outdoor test with shading)

- **RC model**

The RC model for the shading experiment as shown in Figure 3-66, is the same with the one presented in Figure 3-57 with the additional term for direct solar transmittance that will be identified, and compared with theoretical solar transmittance afterward.

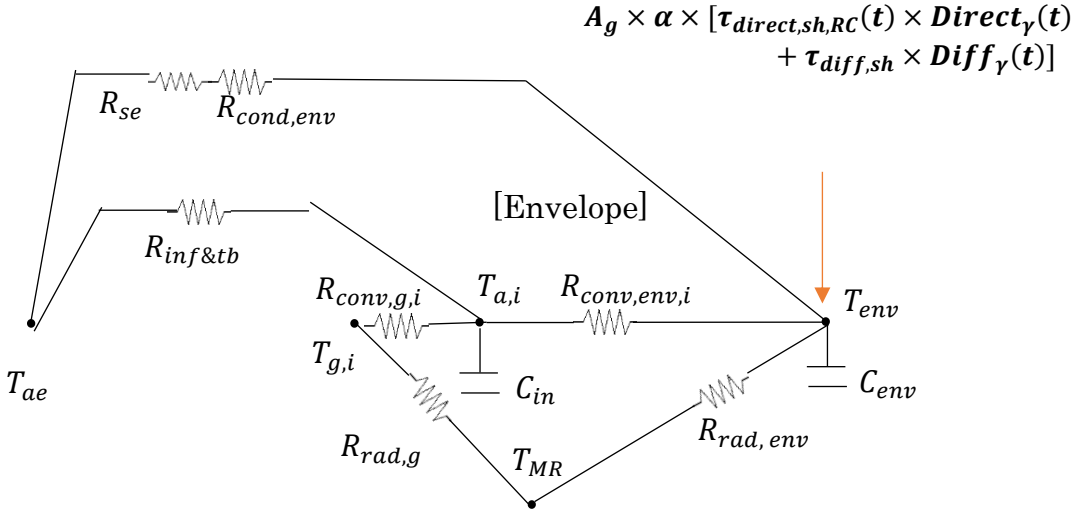

Figure 3-66: RC model for with the shading experiment

- **Identification of time-varying direct solar transmittance with RC model**

According to EA EBC Annex-71 project: 'Building energy performance assessment based on in-situ measurements' [145] the solar gain through fenestrations in general with RC model can be considered a constant to be identified with the inverse method. However, the downfall of this approach is that the solar transmittance becomes independent from sun's position. Thus, this will lead to overestimations/underestimations of the solar gain through the day. A second approach that was listed is the use of an approximative function, such as the polynomial regression or the B-Splines. Using polynomial regression may require a high polynomial order to model the dynamic solar gain behaviour [121], thus, the Splines are used for this case of study.

Splines (or spline functions) are also called piecewise polynomial with an order m, where the transition between each polynomial to another is performed by so called knots [146]. Thus, the Spline space is defined by the knots vector and the corresponding polynomial order. B-spline is a type of Splines that is defined as a linear combination of B-spline basis functions. These types of functions offer the advantage of continuity and smoothness over the knots. Hence B-spline can be written as the sum of weighted basis functions as the Eq 3-32.

$$S(t) = \sum_{i=1}^{q} C_i B_{i,m}(t) \qquad \text{Eq 3-32}$$

where $B_{i,m}$ is a pre-constructed B-spline with order (m) and number (q), and C_i is the unknown regression coefficient that must be defined by the optimizer.

Within the same Annex 71 framework [145], a study was conducted to model solar gain as a function of solar azimuth angle [146]. Following studies also proved ability of B-splines combined with RC model to capture dynamics of the solar gain [120], [121], [122], [147]. All of those studies were typically conducted on non-shaded glazing areas. In addition, the main goal is to estimate the so called '*solar aperture*' gA, which is a term referring to equivalent transparent surface transmitting the same amount of energy as the actual window [146], expressed in m^2.

However, in our case, the RC model is more detailed, and the convective and radiative heat exchanges are separated and fixed, therefore, the objective is to estimate the remaining part which is the direct transmittance. Moreover, to estimate the solar transmittance within the shading, the solar aperture approach was not considered, because the surface including the shade by the slats and the transparent areas (glazed) is already considered in the ray tracing calculations. Thus, estimating direct solar transmittance and considering same surface is coherent.

The direct transmittance depends on the two variables: solar incidence angle θ and local azimuth φ. Thus, to fit an appropriate function, it must be integrate both dimensions. Another condition to be satisfied by the function, is that the variables can be generalized through other

orientations, which is the case with (θ, φ). Consequently, a bi-variable B-spline must be defined for the RC model.

Figure 3-67 illustrates the relationship between the three angles that is to say γ_s which is the solar azimuth, measuring the angle between a reference (in our case the North) and the projection of solar rays on the horizontal plan, angle between the North reference and the façade orientation namely the surface azimuth γ, and the local azimuth φ, which defines the rotation over the normal of the glazed surface, following clockwise orientation.

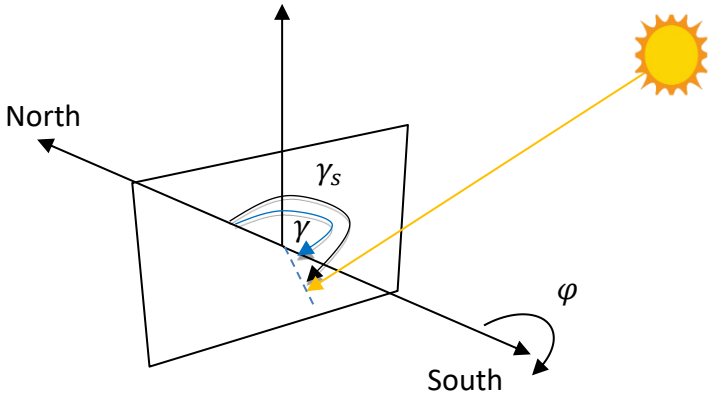

Figure 3-67: Geometric relationship between local, surface and solar azimuth angles

Thus, based on the above-mentioned definitions, a relation between the three angles can be deduced as Eq 3-33.

$$\gamma_s = \gamma - \varphi \qquad \text{Eq 3-33}$$

Therefore φ is defined with Eq 3-34.

$$\varphi = \gamma - \gamma_s \qquad \text{Eq 3-34}$$

1. $\theta(t)$ and $\varphi(t)$ values for whole outdoor experiment data

The graph in Figure 3-68 shows the variation over time of φ for the 14 October. During the day, $\varphi \in [-90°, 90°]$. At 14 h, when the solar rays are close to the normal on the glazed area of the Hotbox, θ value reaches the minimum illustrated in Figure 3-69, and corresponding φ is null.

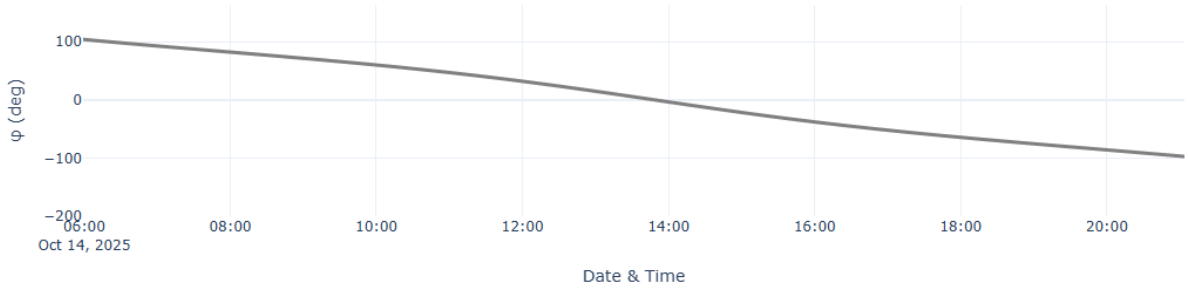

Figure 3-68:Time-varying angle φ on the 14th October with shading for South orientation

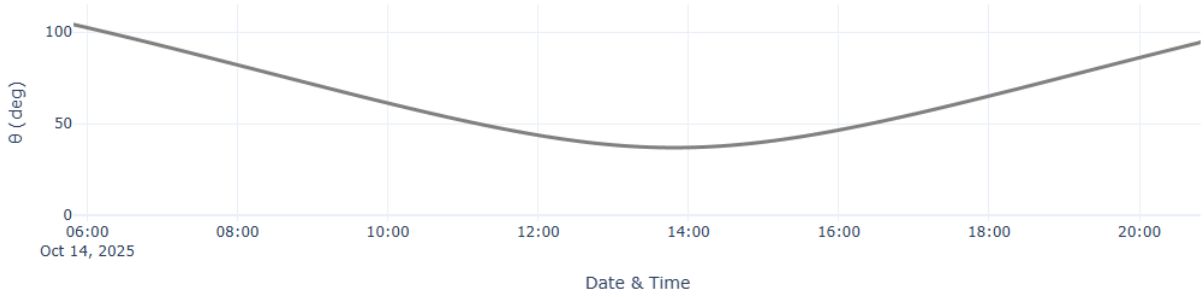

Figure 3-69: Time-varying angle θ on the 14th October with shading for South orientation

2. B spline construction

In order to construct splines the angular domain must be discretised into a finer number of points used to calculate the B-spline between them.

- **Discretization strategy**

The used discretization strategy in this work is based on defining one internal point, and two lower and upper bound points. To ensure the smoothness of the function at the bounds, the principle of open uniform vector[148] is used, where the bounds are repeated n times, where n is the B-spline number.

- **Definition of the domain**

For incidence angle θ , 34° is the minimum incidence angle which occurs around 14 h as shown in Figure 3-69, and 40° occurs around 15 h while 82° is another bound. Those angles are far from the angle where the shading is supposed to have the maximum, in order to let the optimizer, find the corresponding maximum freely. Thus, one internal knot is chosen 40°, and two bounds angles 34° and 82°, when the bounds are repeated n times which correspond to the number of B-spline then we will get the following interval with 11 values namely [34°, 34°, 34°, 34°,34°, 40°, 82°,82°, 82°, 82°, 82°].

For the local azimuth angle φ , the corresponding values for the above selected incidence angles θ are chosen, with one internal knot of 0° that occur at 14h as shown in Figure 3-68, and two bounds -82° and 90°.If those bounds are also repeated for 5 times, we will get the following interval namely [-82°, -82°, -82°, -82°, -82°, 0°, 90°,90°, 90°, 90°, 90°]

The bidimensional B-spline can be defined as the product of B-spline of each variable Eq 3-35.

$$S(\theta,\varphi) = \sum_{i=1}^{n}\sum_{j=1}^{m} C_{i,j} B_{i,m}(\theta)^{(p)} B_{j,n}(\varphi)^{(q)} \qquad \text{Eq 3-35}$$

where $B_{i,m}$ and $B_{j,n}$ are a pre-constructed B-splines with order (m) and (n) respectively, and number (q), and (p) for both variables θ and φ. $C_{i,j}$ is the unknown regression coefficient that will be obtained during the optimization.

3. Optimization of the coefficients $C_{i,j}$

In the optimization process, and using the obtained $R_{inf\&tb}$ and C_{env} optimal values identified within the experiment without the shading, a filtering regarding the direct vertical irradiance >50W/m² is applied to ensure physical consistency with sunny conditions and the transmittance is set to zero when $\theta > 82°$. The spline coefficients $C_{i,j}$ are defined on the interval $[0.1, 0.7]$ reflecting physical bounds of the transmittance, and in same time the maximum is above the theoretical transmittance, so that the optimizer is not restricted. The optimization is initialized with $C_{i,j}^{(0)} = 0.1$ for a starting point in the first morning day of the dataset. The objective function minimizes the sum of $CV(RMSE)$ of T_{ai} and T_{env}, as well as a term of regularization called Tikhonov, which can ensure a stable curve of the solar transmittance by penalizing sudden jumps between the coefficients $C_{i,j}$. This term has been introduced with a weight of 10^{-3} in order to not dominate the objective function. Those 3 steps are illustrated in Figure 3-70.

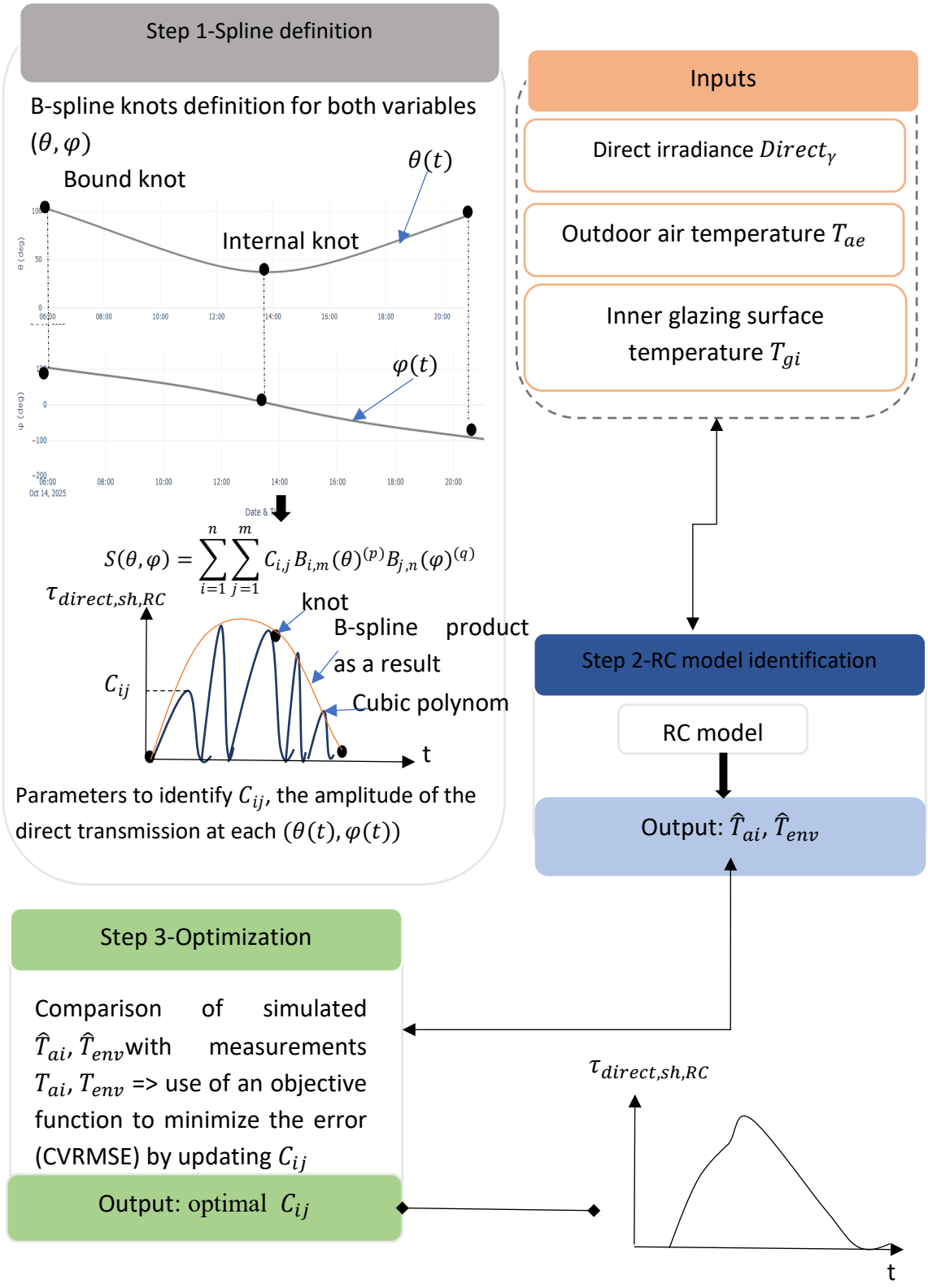

Figure 3-70: Steps to estimate $\tau_{direct,sh,RC}$ from RC model and B-spline function

The obtained $\tau_{direct,sh,RC}$ is shown in Figure 3-71. We can observe that the maximum value is before midday, and after the transmittance starts decreasing. Which aligns with the

geometrical effect of the shading solution, that let through the solar rays coming from south east (before midday) and block them from south-west (after midday).

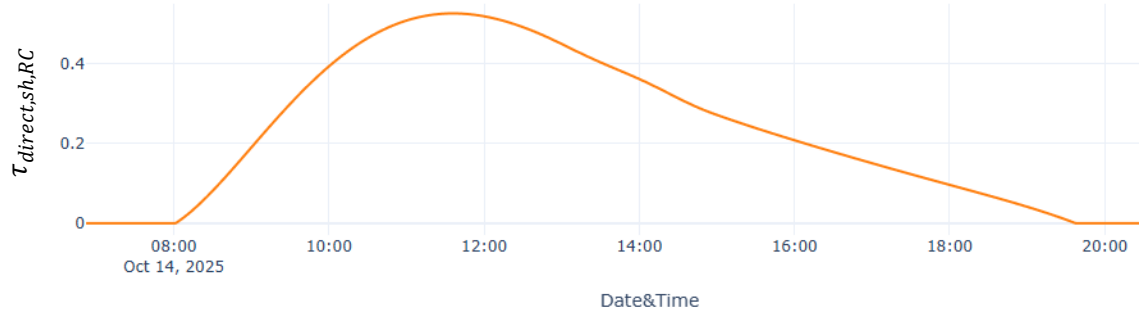

Figure 3-71: Estimation of direct transmittance $\tau_{direct,sh,RC}$ value for South orientation

The effect of the B-spline extremity knots was evaluated, while keeping the internal knots the same. The results are given in Figure 3-72. Increasing multiplied extremity knots does not improve the model accuracy. Therefore, 5 knots are kept for the rest of the comparison calculations with theoretical $\tau_{direct,sh,BSDF}$.

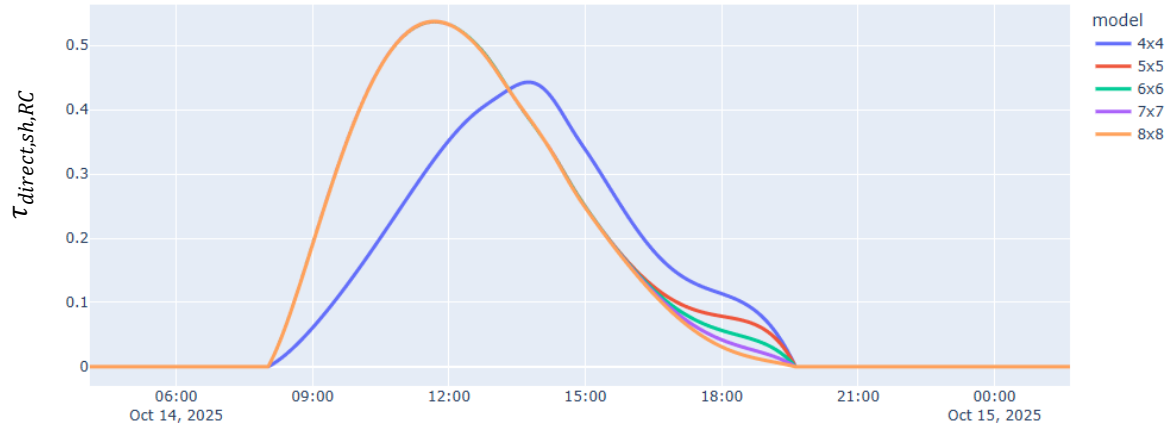

Figure 3-72: Effect of B-spline extremity knots length on the estimation of $\tau_{direct_sh_RC}(t)$ for South orientation

This methodology application was primarily destined to calculate direct transmittance of complex geometry fenestration using outdoor experimental measurements independently from geometrical model complexity. However, the diffuse transmittance $\tau_{diff,sh}$ was deduced from BSDF calculations. Thus, a local sensitivity analysis is conducted to evaluate the impact of this parameter on the model's output $\tau_{direct,sh,RC}$, the result can be seen in Figure 3-73. While varying $\tau_{diff,sh}$ from 0.1 to 0.4, the value of $\tau_{direct,sh,RC}$ had a maximum difference of 0.06 between two bounds values. Consequently, $\tau_{diff,sh}$ is not an influent parameter on

$\tau_{direct,sh,RC}$ with this experimental campaign, which is mainly due to the low diffuse irradiance received by the glazed façade compared to the direct irradiance.

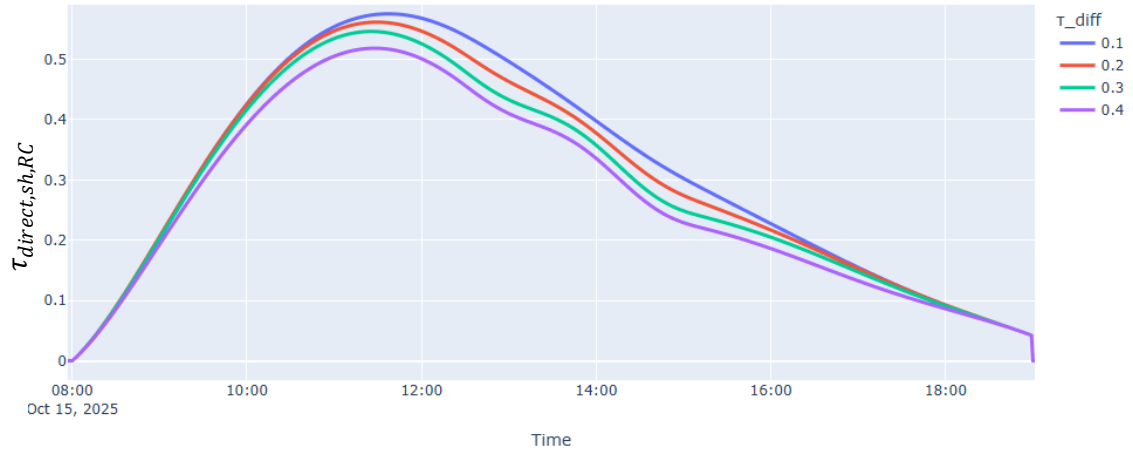

Figure 3-73: Effect of $\tau_{diff,sh}$ diffuse on the $\tau_{direct_sh_RC}(t)$ estimations for South dataset

Using the obtained $R_{inf\&tb}$ and C_{env} optimal values identified within the experiment without the shading, the estimated $\tau_{direct_sh_RC}(t)$, and a number of adjusted parameters of $p = 25$ ($C_{i,j}$ of 5 knots for a product of two splines), the obtained metrics CV(RMSE) and NMBE are listed in Table 3-12. For this experimental scenario, the model hourly error metrics CV(RMSE) and NMBE remain less than the threshold defined by ASHRAE guideline 14 [143], with an overestimation of T_{ai} indicated by the negative value of NMBE.

Table 3-12: Obtained calibration metrics alongside with ASHRAE recommended hourly values for outdoor experiment with the shading toward South

Index (hourly)	**ASHRAE guideline 14-2002** [144]	**With shading model**	
CV(RMSE) %	30	T_{ai}	7.24
		T_{env}	4.12
NMBE%	±10	T_{ai}	-8.78
		T_{env}	-0.68

The measured and calculated indoor air temperature can be shown in Figure 3-74, and the measured and calculated indoor surface envelope temperature can be shown in Figure 3-75.

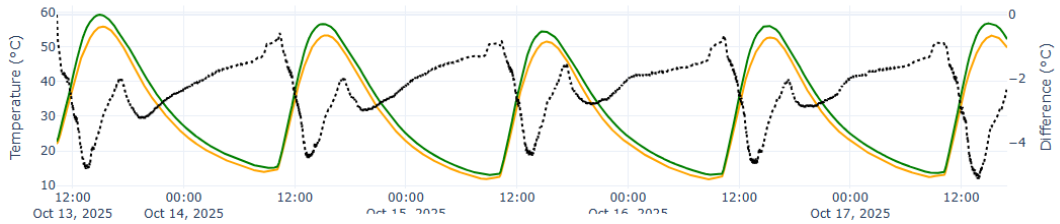

Figure 3-74: Measured and calculated indoor air temperature (Outdoor test with shading)

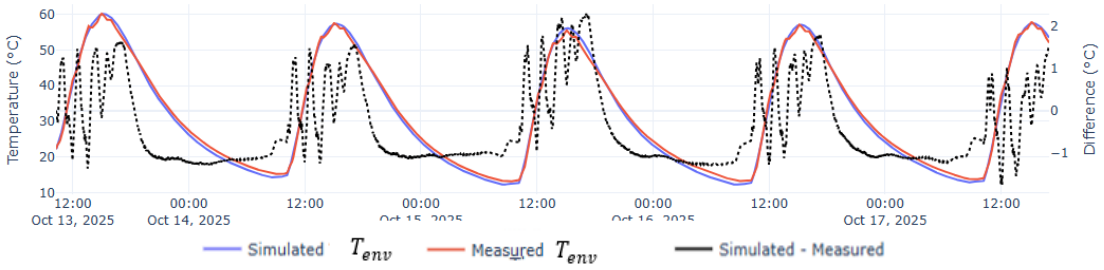

Figure 3-75: Measured and calculated indoor surface envelope temperature (Outdoor test with shading)

- **Evaluation of direct solar transmittance: Theoretical reference, shading and façade orientation impact**

The estimated solar transmittance using the RC model and B-spline function should be first compared with the direct solar transmittance derived from ray tracing with Radiance software as a first step, this will illustrate the ability of the model to reproduce the expected direct solar gain dynamic profile during the day. Secondly, the effect of the shading can be evaluated by comparing glazing-only situation with shading direct solar gain, which can lead to calculate the shading factor. Finally, solar gain is strongly influenced by façade orientation, thus, another outdoor experiment with the shading was performed for a South-Ouest orientation, and a comparison between the transmitted solar gain for both façade orientations is done to select the best orientation for the diagonal shading configuration within the experimental campaign.

A. Validation against theoretical solar transmittance

The direct solar transmittance from BSDF density data that was obtained is a function of two variables $\tau_{direct,sh,bsdf}(\theta,\varphi)$, and in order to obtain corresponding time-varying $\tau_{direct,sh,bsdf}(t)$ of each dataset, the corresponding local azimuth φ, and alongside with the solar incidence angle θ must be computed from sun position.

In order to extract the time varying direct transmittance of ray tracing from the angular $\tau_{direct_sh_BSDF}(\theta,\varphi)$, the steps are illustrated in Figure 3-76 :

1. For each time step t, and corresponding (θ,φ), search the nearest patch (θ,φ) in BSDF data.
2. Extract $\tau_{direct_sh_bsdf}$ for the selected patch, and follow the same steps for all-time series. To ensure physical consistency, for $\theta > 90°$ and negative altitude, $\tau_{direct_sh_bsdf}$ was set to zero.
3. A linear 2D interpolation step is however necessary in the angular domain, since the obtained time-varying $\tau_{direct_sh_bsdf}(t)$ can show a discrete behaviour as illustrated in Figure 3-77.

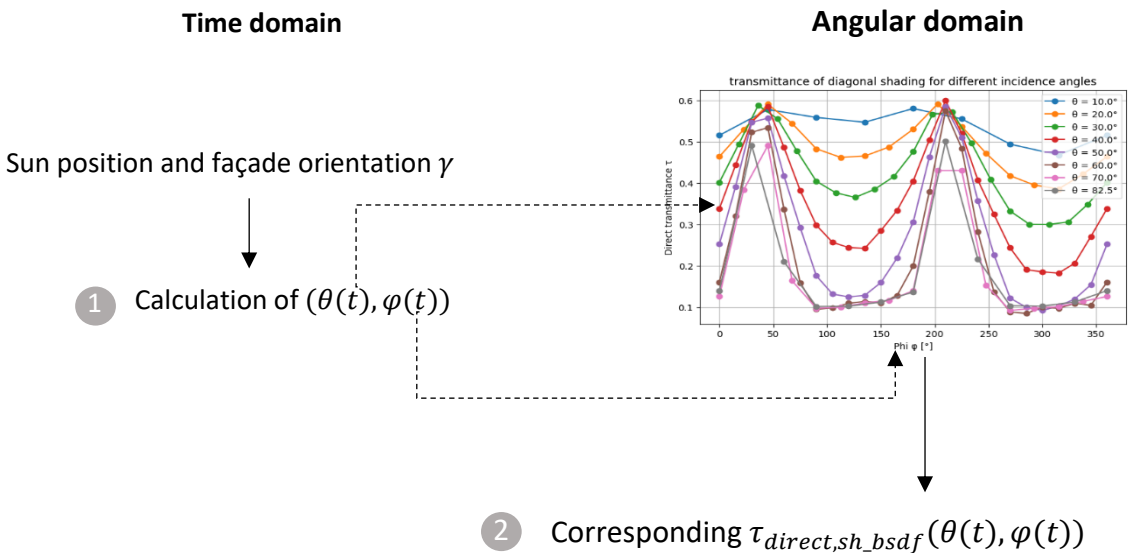

Figure 3-76: Schematic representation of the obtention of $\tau_{direct_sh_bsdf}(t)$ derived from BSDF calculations $\tau_{direct_sh_bsdf}(\theta, \varphi)$

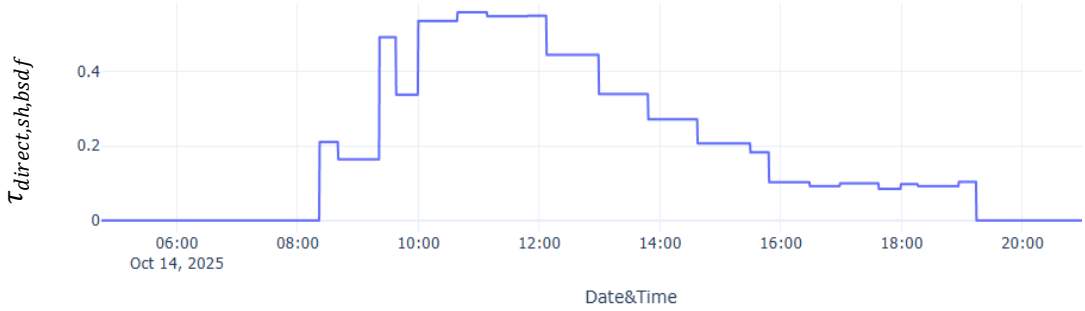

Figure 3-77: The obtained discrete $\tau_{direct_sh_bsdf}(t)$ (South orientation case)

After interpolation in the angular domain, the final smooth $\tau_{direct_sh_bsdf}(t)$ is shown in Figure 3-78. $\tau_{direct_sh_bsdf}$ can arrive to a maximum of 0.55 from 11 h to 12 h, and then start decreasing after 12h. This behaviour was expected due to the diagonal slats effect, and let the solar rays transmit when the local azimuth is aligned with the slats and blocks those rays when the local azimuth is not in same direction as the slats opening. Figure 3-79 summarizes the angular distribution of $\tau_{direct_sh_bsdf}$. A strong directional preferred rays' transmission is observed, where the maximum direct transmittance is occurring when the local azimuth is aligned with diagonal slats' inclination angle, as discussed in Section 3.2.2. The black region corresponds to the block zone of the shading, and the lighter region is the regions where rays are let through.

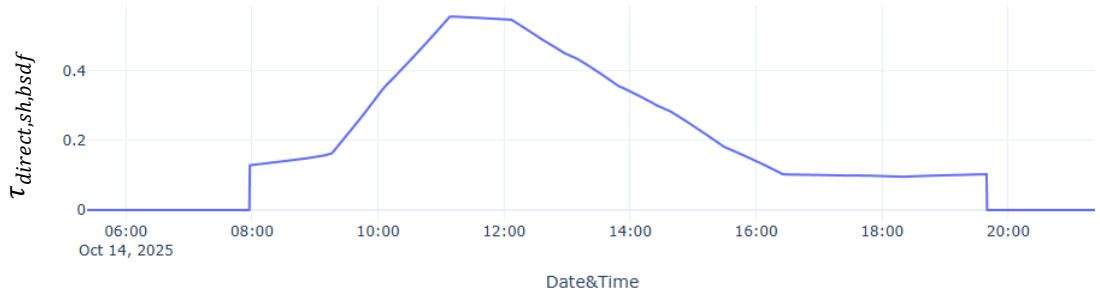

Figure 3-78: The obtained smooth $\tau_{direct_sh_bsdf}(t)$ (South orientation case)

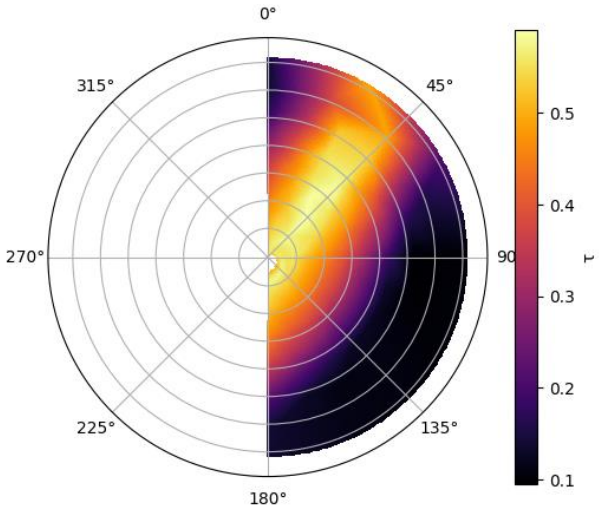

Figure 3-79: Angular distribution of theoretical direct transmittance of the glazing with shading $\tau_{direct,sh_{BSDF}}$ (South orientation case)

The obtained time varying $\tau_{direct_sh_bsdf}$ is compared with theoretical direct transmittance of the glazing alone computed with Window LBNL [128] $\tau_{direct,g}$ in Figure 3-80. This azimuthal preference is more observable when comparing with the glazing alone.

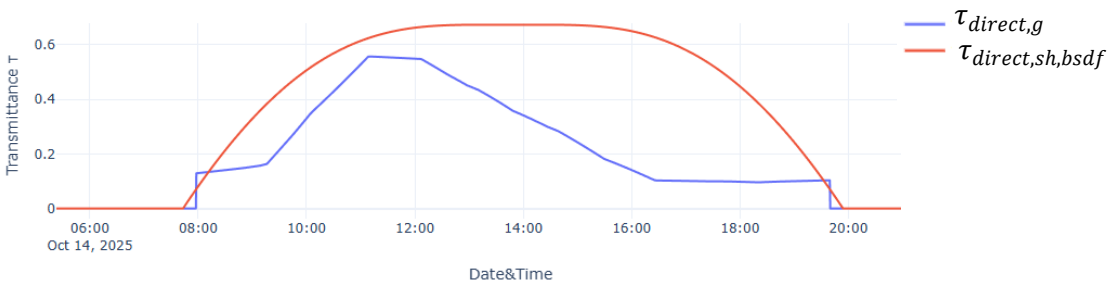

Figure 3-80: Comparison between $\tau_{direct_sh_bsdf}(t)$ and $\tau_{direct_g}(t)$ (South orientation case)

The comparison between the obtained $\tau_{direct_sh_bsdf}(t)$ and RC with B-spline solar transmittance $\tau_{direct_sh_RC}(t)$ is shown in Figure 3-81.

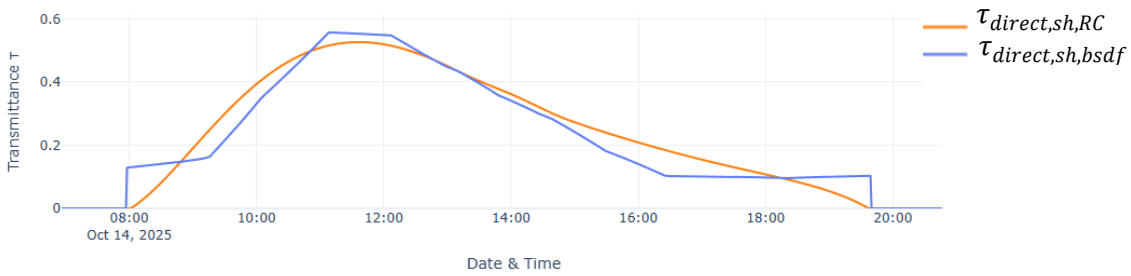

Figure 3-81: Comparison between $\tau_{direct_sh_bsdf}(t)$ and $\tau_{direct_sh_RC}(t)$ (South orientation case)

The CV(RMSE) between BSDF derived transmittance and RC with B-spline direct transmittance is 24%.

The transmitted direct solar heat flux is calculated using the estimated and theoretical solar transmittance with Eq 3-36 and Eq 3-37.

$$q_{spline}(t) = \tau_{direct_sh_RC}(t) \times Direct_{180}(t) \quad \text{Eq 3-36}$$

$$q_{bsdf}(t) = \tau_{direct_sh_BSDF}(t) \times Direct_{180}(t) \quad \text{Eq 3-37}$$

The comparison between q_{spline} and q_{bsdf} is illustrated in Figure 3-82.

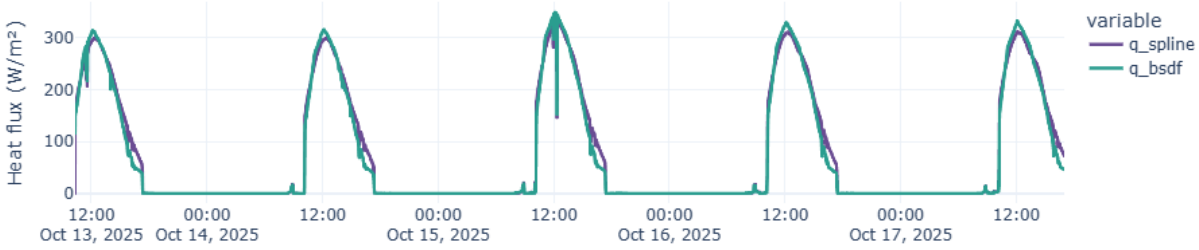

Figure 3-82: Transmitted direct heat flux using calculated and theoretical direct transmittance (South orientation case)

To calculate the cumulative absolute error between the estimated and theoretical direct solar gain, the integral absolute error (IAE) metric [149] is considered. The advantage of this metric is that it can capture the cumulative discrepancies between the two variables which may be masked if the net energy comparison is used as a metric. The IAE is expressed with Eq 3-38.

$$IAE = \int |\Delta q(t)| dt = \int \left| q_{RC,spline}(t) - q_{BSDF}(t) \right| dt \quad \text{Eq 3-38}$$

The IAE is normalized by corresponding cumulative solar direct heat flux using the theoretical BSDF transmittance, as in Eq 3-39.

$$e = \frac{IAE}{\int q_{BSDF}(t)dt} \times 100 \qquad \text{Eq 3-39}$$

The 14th of October monitoring data is selected as one sunny day for the IAE calculations. The RC model overestimate the direct solar gain comparing to BSDF calculations with a relative error of 8%. This is mainly due to the mask effect of the measured irradiance that appears in the beginning and the end of each day as shown in Figure 3-63, which in turn leads to an overestimation of direct solar transmittance factor for those time interval as a result of the compensation illustrated in Figure 3-81. The corresponding cumulative energy for each method: RC model and BSDF is calculated using Eq 3-40, both are illustrated in Figure 3-83. The net energy difference between the both methods is $60\ Wh/m^2$.

$$E_{method} = \frac{1}{3600} \times \sum q_{method}(t)\ \Delta t \quad [\mathrm{Wh/m^2}] \qquad \text{Eq 3-40}$$

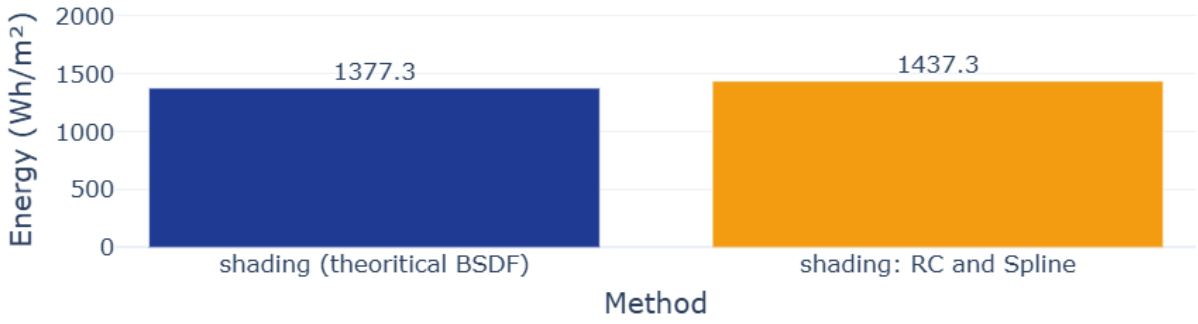

Figure 3-83: Comparison between direct transmitted solar energy using RC model and BSDF (South orientation case)

B. Impact of shading on solar transmittance

To evaluate the performance of the diagonal shading, the direct solar heat flux calculated by RC and B-spline with the shading can be compared with the direct theoretical solar gain of the glazing alone calculated using the shading factor in with Window LBNL (Eq 3-41).

$$Shading\ reduction\ factor = \frac{E_{glazing} - E_{RC,spline}}{E_{glazing}} \times 100 \qquad \text{Eq 3-41}$$

$E_{glazing}$ can be calculated using Eq 3-42 with the corresponding $q_{glazing}$ computed thanks to Eq 3-42:

$$q_{glazing}(t) = \tau_{direct,g}(t) \times Direct_{180}(t) \qquad \text{Eq 3-42}$$

The cumulative energy for shading integration and glazing only direct solar transmittance is illustrated in Figure 3-84. The corresponding shading factor is 43.5%.

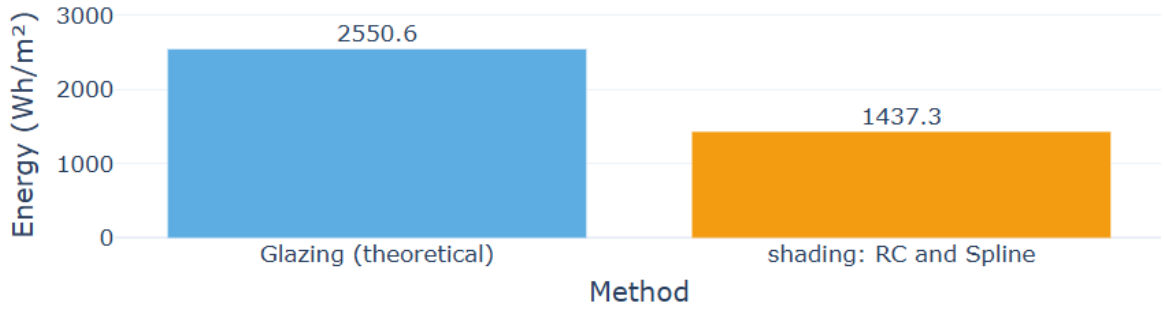

Figure 3-84: Shading integration and glazing only direct solar transmittance cumulative energy (South orientation case)

C. Influence of façade orientation: South-West case

The shaded-glazed façade is oriented toward the South-West with a surface azimuth of 270° as shown in Figure 3-85. The data is recorded for 3 days during September 2025. This data is fitted to the same RC model as South orientation case with a B-spline function defined with the according $\theta$and local azimuth φ of direct irradiance appearance for this orientation as follow:

- **Discretization strategy:**

The used discretization strategy is the same as for the South orientation dataset case, which is based on defining one internal point, and two lower and upper bound points, and an open uniform knots vector [148].

For incidence angle θ, 13° is the minimum incidence angle which occurs around 19 h, the lower bound is 28° occurring at 18 h, and the maximum bound is 88° occurring at 14 h. Thus, it results ins [13°, 13°, 13°, 13°, 13°, 28°, 88°, 88°, 88°, 88°, 88°].

For the local azimuth φ, this interval was defined according to the previously selected incidence angle interval that is to say [8°, 8°, 8°, 8°, 8°, 20°, 88°, 88°, 88°, 88°, 88°].

A different interval variation of both angles is accorded for each façade orientation. In the South-West orientation case, the glazed façade will 'see' the direct irradiance only during the end of the day, whereas the South orientation case the façade can see the direct irradiance during the day. However, the methodology of Splines construction remains the same, one internal knot and two boundary knots. The obtained direct solar transmittance using RC model is illustrated in Figure 3-86. Both, theoretical and model-based calculations have a maximum that occurs in same time. However, the profile of the splines tends to decrease at the end of the day, in contrast of the theoretical calculations.



Figure 3-85: South-West orientation experiment using the shading (Surface azimuth=270°)

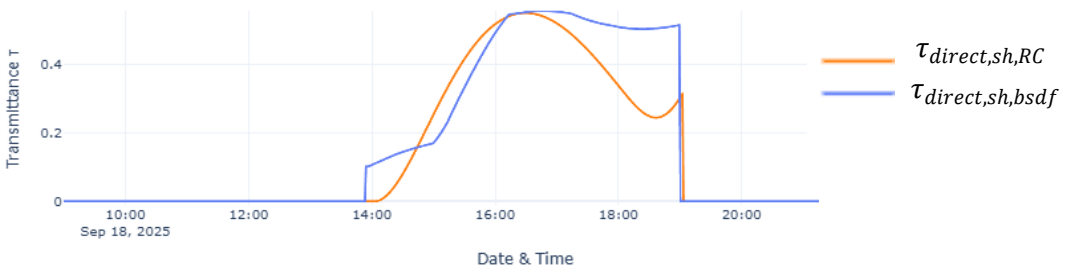

Figure 3-86: Comparison between $\tau_{direct,sh,RC}$ and $\tau_{direct,sh,bsdf}$ (South-West orientation case)

One sunny day is chosen also for this dataset, and the obtained cumulative energy for both methods is illustrated in Figure 3-87. A relative error of -20 % and a shading factor of 24 % are obtained as shown in Figure 3-88. These results show that the model accuracy is less compared to South orientation data. One of the reasons is mainly due to the lack of diffuse measurements data during September experiment, which leads to the use of empirical models for the decomposition and projection of the Irradiance to obtain the direct solar radiation. Comparing the shading factor for South and South-West orientation cases, the diagonal shading is more efficient with a South orientation.

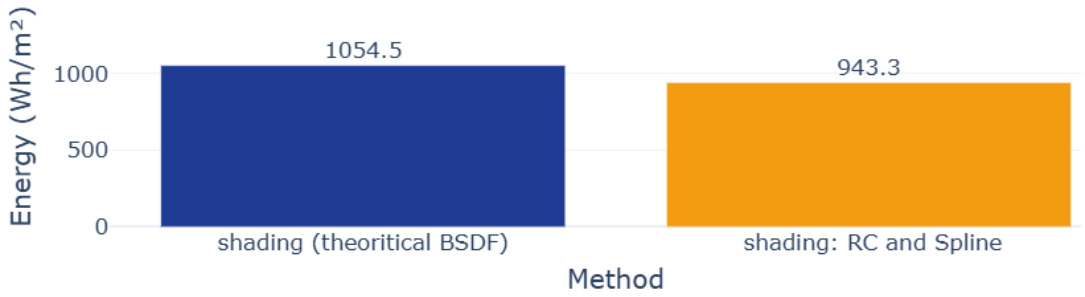

Figure 3-87: Comparison of cumulative energy using BSDF and RC model (South-West orientation case)

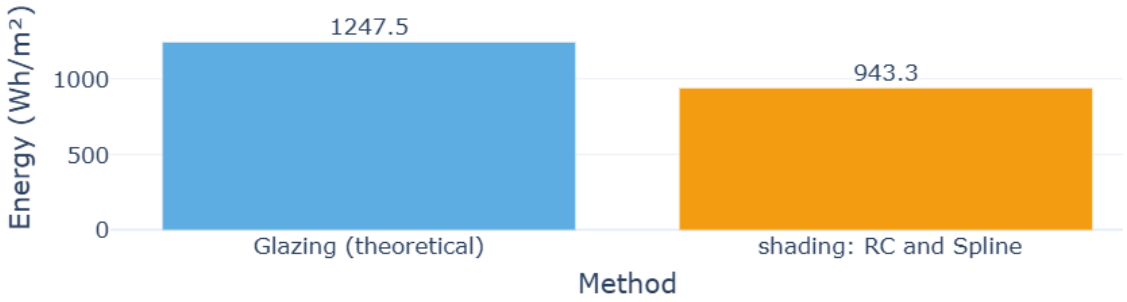

Figure 3-88: Shading integration and glazing only direct solar transmittance cumulative energy (South-West orientation case)

3.3 Conclusion

This chapter applies the proposed methodology to evaluate adaptive façade thermal performance defined in Chapter 2 to the solar gain evaluation of a complex geometry shading device using an RC model and B-spline function.

The RC model has been validated through three stages. First i) Indoor conditions with a continuously injected heating power, then ii) outdoor conditions without the shading element, and finally iii) with the shading. The RC model for two outdoor configurations conserves the same structure, since the reference façade namely the double glazing exhibits the same physical phenomena when it is equipped with the shading. The ability of the model to estimate the direct solar transmittance had been evaluated without the shading as a first step, and then this term is replaced with a B-spline function to be fitted with the measurements with the shading. Despite the infiltration losses experimental limitation, the sensitivity analysis shows a low influence of this term on the T_{ai} and specifically T_{env} relatively to other parameters.

The impact of shading is then assessed for South orientation, with the RC model and B-spline function, the relative error compared to ray tracing BSDF direct solar transmittance calculations shows a low deviation of 8%. Thus, through a cumulative energy comparison between glazing-only and the RC model methods, the results show a significant shading reduction factor of 43%, highlighting the effectiveness of the diagonal shading in this orientation.

Finally, to investigate the impact of the façade azimuth on the diagonal shading performance, a South-West orientation experiment was performed, and the results showed a higher cumulative error of -20 %, and a lower shading factor of 24 %. Consequently, the best orientation of the diagonal shading with an angle from horizontal plan of 35° and a tilt of 4° and with this experimental comaign is South orientation. In addition, this methodology can be generalized to other shading device that have a complex static geometry, since it is independent from geometrical details of the shading, and the used strategy for the B-spline function can be generalized.

3.4 Limitations

This PhD work has been focused on the thermal performance of adaptive façade, but as any other building element, before judging its performance, it is necessary to address other functions performance such as visual, acoustic, glare, etc. A holistic approach is required to consider the interference between all those building functions. Various limitations should be acknowledged regarding those results. First, the collected measurement of the outdoor experiment with the shading was characterized with a strong direct irradiance, which improves the estimation of the direct solar transmittance with the splines, but if the diffuse was dominant, this will lead to an underestimation of the coefficients. Meaning the function cannot be generalized for weather conditions when the diffuse is important. Second, the cost function used during the optimization to determine spline coefficients is the sum of $CV(RMSE)$ for T_{ai} and T_{env} estimations of the model vs measurements, which assign an equal weighting for both temperature nodes. That's an untested assumption, and physically one can be more significant than other, specially that the envelope is the part that receives first the solar gain transmitted to the indoor. Third, regarding the envelope temperature node, it was also assumed an equal weighting of 1/5 for each indoor façade, which is again, an untested assumption. Indeed, it is highly affected by the temperature sensors number, their positioning, and the homogeneity of temperature across the façade. Fourth, the vertical direct irradiance was not measured. However, the diffuse horizontal irradiance was measured in three outdoor experimental campaigns which provided the direct horizontal irradiance, and with Perez model the projection was done. Nonetheless, with the last experiment for South-West orientation, the diffuse was not calculated. Thus, the direct solar transmittance was affected. Finally, the identified RC model was calibrated and validated for a test cell of $1m^3$, and the B-spline coefficients change for each façade orientation.

General conclusion and perspectives

The aim of this PhD thesis is to provide a general methodology for façade engineers to characterize adaptive façade on the thermal performance level, using experimental and numerical methods. The core of this PhD thesis was structured into three main chapters. This final section summarises the outcomes of this thesis, by listing the sub-questions answers and limitations.

Answers to sub-research questions

Sub-questions

- ✓ *What are the limitations of existing thermal characterization methodologies for adaptive façade? (Chapter 1)*

Chapter 1 defined first the adaptive façade, and its various classifications. Furthermore, the methods to characterize passive façade were introduced, which were limited by the static assumption of KPIs. Hence, their use for adaptive façade is not suitable. In addition, the existing approaches to characterize thermal performance of adaptive façade uses a simplification of the façade state representation, particularly, when the transient states of the façade are not considered. The lack of hybrid methodology that combines experimental measurements and modelling framework was shown .

- ✓ *How to propose a generalized methodology to enhance adaptive façade thermal performance characterization under real outdoor conditions? (Chapter 2)*

The complexity of adaptive façade thermal behaviour, makes it difficult to propose a general methodology, owing to the diversity of the technologies, control operations, and impact of boundary conditions. To address these challenges, and the limitations listed in Chapter 1, Chapter 2 proposes a general methodology based on 3 steps. First step consists in an inventory of heat transfer mechanisms within the adaptive façade and the associated test cell. This step leads to the identification of the dominant modulated heat transfer path by the adaptive façade, thus, the corresponding KPI is the parameter to be estimated by the model. As a second step, a numerical model is implemented for two experimental configurations namely with a reference or 'passive façade' and an 'adaptive façade'. The purpose of using a reference façade is to provide a baseline model which can allow the comparison of thermal performance for both, and also calibrate the test cell if not done before. The model can be black, grey or white box. The third step requires both; the implemented models and the collected measurements during experiments, to estimate the corresponding KPI of the modulated heat path by the adaptive façade. If it exists, a validation step can be done using a theoretical KPI. Otherwise, the model can be tested in different adaptive façade configurations.

- ✓ *How to implement the proposed methodology to evaluate thermal performance of a shading device? (Chapter 3)*

The adapted methodology to the case study is composed of the following steps: Step1: This step consists in identifying the ongoing heat transfer paths within the test cell and the shading

prototype according to the three mechanisms: which is conduction, convection and radiation. This step also includes the choice of the passive façade, which is a double glazing in this case. The outcome of step 1 is the identification of the modulated heat transfer by the adaptive façade which is the short-wave length radiation, and specifically the direct solar transmittance, that is variable with sun path. Step2: The grey box model type is chosen for this step, and for both façades namely double-glazing with and without shading; The model structure remains the same, except the term of the solar gain that is defined as an unknown parameter to identify in the outdoor with shading scenario. Other experimental protocols were also necessary to test the credibility of the RC model alongside with sensitivity analysis. A co-heating test was performed without solar gain and outdoor test without shading was also performed, to identify the thermal capacitance and heat losses infiltration. The outcome of step 2 is a partially calibrated model using the two first experimental scenarios, an identified thermal envelope capacitance and thermal losses resistance without the shading in outdoor experiment. Those two parameters are used in step 3 to identify the direct solar transmittance using measurements of experiment with the shading for South and South West orientations. The bidirectional B-spline function is used to model the direct solar gain with solar incidence angle and the local azimuth. The choice was guided by the need to establish a generalized function that is independent from façade orientation, which can allow the reuse of the model to other façade exposures. In addition, the coefficients of this function are identified during the optimization process. The main outcome of this part is the estimated direct transmittance by the RC model with B-spline functions for South orientation.

- ✓ *How accurately the identified KPI reproduce the thermal behaviour of the shading device? (Chapter 3)*

An available ray tracing tool supported this validation step using as an input the 3D model of the whole system i.e., double-glazing and the shading which resulted in a bidirectional direct transmittance using the solar incidence angle and local azimuth, which is converted to time-dependant direct solar transmittance, to be compared with the B-spline based direct transmittance. Moreover, the resulted direct solar transmittance with the RC model and B-spline function was compared with the theoretical direct transmittance resulted from ray-tracing, and also with the theoretical solar transmittance without the shading. This step allows the conclusion on the performance of the shading compared to no shading, and also, with the dataset of South-West orientation, the best orientation of this shading was also concluded, which was South for this shading configuration. Overall, the model metrics are less than the threshold defined by the ASHRAE guideline 14 [143].

Limitations and suggestions for future work

Although the results are promising, various limitations were identified of this research work. Those limitations are listed below for each methodology corresponding step:

- Step 1: Inventory of heat transfer paths: Understanding the adaptive element is a critical step, when one heat path is dominant, a single KPI can be used to characterize

the thermal performance of the adaptive element. However, when multiple heat paths are modified with same amplitude, in this case a KPI that consider both is necessary, and the experimental scenarios will be complex due to the interference effect of both. It should also be noted that this diagonal shading is dominated by direct-to-direct solar rays, as shown in Section 3.1.5, however, when a shading device is more dominated by direct to diffuse solar rays, the measurements of reflectance of the shading slat becomes necessary, since it have a high influence on the solar transmittance.

- Step 2: Model formulation: The passive façade is selected and presented in this step, in our case the double glazing was chosen as the reference façade. However, a constructer or designer of a shading solution, could be more interested to compare his product with another conventional product in market. Thus, an overestimation of the performance may occur when compared to a non-shaded glazing. Regarding the KPI approximation function, in our case, we presented a preliminary analysis using the ray-tracing technic that allows the selection of B-spline as a function to be optimized in the model. However, in the general case of adaptive façade, a prior knowledge often is complex or does not exist using numerical software. Therefore, it is recommended to choose a function that can handle irregular or non-linear data, which is usually the case when using an adaptive envelope element. In addition, to make the approximative function generalized, the choice of the function variables that can calculate the KPI is also a step where we used a priori knowledge.
- Step3: KPI identification: The experimental campaign aiming at the characterization of the system must be carried out in an environmental condition that allow the identification of the KPI. The impact of the selection and location of sensors and associated hypothesis should also be noted. It is especially true for surface temperature sensors, where a sun patch on a small area of the surface can elevate temperature. In the case of study, no control operation was needed to be defined, since the shading operates in an open-loop control, meaning the geometry does not move.

For the future work, from an experimental perspective, the use of additional measurements such as the heat flux or radiative exchange can provide additional insights to the model. A validation under long time period and varying climate can also allow the evaluation of model accuracy. Different façade orientation can also be investigated, as well as different configurations comparison such as the integration of selective glazing or a comparison with a conventional shading device such as venetian blinds with a reference control scenario according to ISO52016-3 [1], in order to highlight the added value of the tested adaptive element. From a numerical perspective, the RC model complexity can be extended to capture the temperature variation phenomena, and also the KPI variables can include the tilt angles of the diagonal shading . In terms of application, the proposed method can be integrated into building simulation tool, or can be coupled with a model predictive control (MPC).

Scientific publications

a) Article in an international conference:

Moutaoikil, A., Vogt Wu, T., Recht, T., Dugué, A. , Mora, L., Inard, C. (2025). Elaboration of a methodology for estimating angle-dependant solar transmittance of static complex shading device. *Journal of Physics: Conference Series*, 3140, 072018 (CISBAT 2025). https://10.1088/1742-6596/3140/7/072018

b) Other oral communications

Oral presentation at the IEA EBC Annex 94 meeting ("Validation and Verification of In-situ Building Energy Performance Measurement Techniques"), 11-13 May 2026, Paris, France.
Title:" General *methodology for the thermal performance characterization of adaptive façade"*

Annex A: Estimation of the interior thermal capacitance of the Hotbox

The interior capacitance of the Hotbox was calculated based on the inventory of the installed equipment inside the Hotbox of $1\ m^3$ (sensors and their support…). Using tabulated values from ISO 10456 [126]

Table 6-1: Inventory of equipment inside the hotbox and their thermal capacitance

Equipment	Materiel	C_p $[J.kg^{-1}.K^{-1}]$	Weight [kg]	Capacitance $[J.K^{-1}]$
Kipp & Zonen pyranometer [150]	Aluminium	880	0.6	528
Metal support	Aluminium (0.5m and diameter of 4cm)	880	Estimated 0.5	528
Terminal blocks of data logger	Plastic and metal contacts	1400	Estimated 0.3	420
Pyranometer cables [150]	Coiled, about 10m, PVC + copper	400	0.4	160
Air	Air	1008	1.2	1209
Total [J/K]				2845
Ratio with Cair [-]				2.35

From Table 6-1, the ratio of total equipment's capacitance with air capacitance is 2.35, therefore a conservative value of 3× C_{air} is considered for interior capacitance in the RC model to account for the uncertainties in the estimated thermal capacitances of equipment (thermocouples thermal capacitances was not included in the inventory), thus $C_{in} = 3627\ J/K$.

Annex B: Shading ring installation for the pyranometer

Diffuse horizontal irradiance is measured using a pyranometer equipped with a shading ring, which blocks direct solar radiation from reaching the sensor. As a result, the instrument records only the diffuse component of the solar irradiance.



Figure 7-1: Shading ring adjustment to measure the diffuse horizontal irradiance DHI

The alignment was periodically verified and adjusted to account for seasonal variations in solar declination according to the correction factors listed in Table 7-1. During October measurements, the value -43° is considered.

Table 7-1: Adjustment table for shading ring [151]

| Start date | End date | setting [mm] | Declination (negative for southern hemisphere) | | |

Annex C: Irradiance transposition

If the diffuse and direct horizontal irradiance are not known, which was the case for South-West orientation dataset calculations, the relationship for solar radiation transposition model can be used, presented in this appendix from Eq 8-1 to Eq 8-4.

First, the horizontal extra-terrestrial radiation $G_{ext,h}$ [W/m²] for a Julian day n using the zenith solar angle θ_z is calculated with Eq 8-1 [132].

$$G_{ext,h} = 1353 \times (1 + 0.033 \cos\left(\frac{360n}{356}\right)) \times cos\theta_z \qquad \text{Eq 8-1}$$

Second, the clearness index k_T is expressed as the ratio between exterior global horizontal irradiance GHI [W/m²] and the horizontal extra-terrestrial irradiance$G_{ext,h}$ [W/m²] with Eq 8-2.

$$k_T = \frac{GHI}{G_{ext,h}} \qquad \text{Eq 8-2}$$

Finally, the direct and diffuse horizontal irradiance Direct and DHI [W/m²] can be calculated from the diffuse fraction index k_d [152].

$$DHI(t) = k_d(t) \times DHI(t) \qquad Direct(t) = \frac{GHI(t) - DHI(t)}{\cos\theta_z(t)} \qquad \text{Eq 8-3}$$

$$k_d = \begin{cases} 1 - 0.24k_T & if\ k_T < 0.35 \\ 1.55 - 1.84k_T & if\ 0.35 < k_T < 0.75 \\ 0.177 & if\ k_T > 0.75 \end{cases} \qquad \text{Eq 8-4}$$

Annex D: Glazing and envelope surface temperatures and solar irradiance measurements

This appendix provides the experimental measurements of the outdoor experimental campaign without the shading of: solar irradiance (Figure 9-1), the inner-surface temperatures of the opaque envelope (Figure 9-2) and the glazing surface temperature (Figure 9-3).

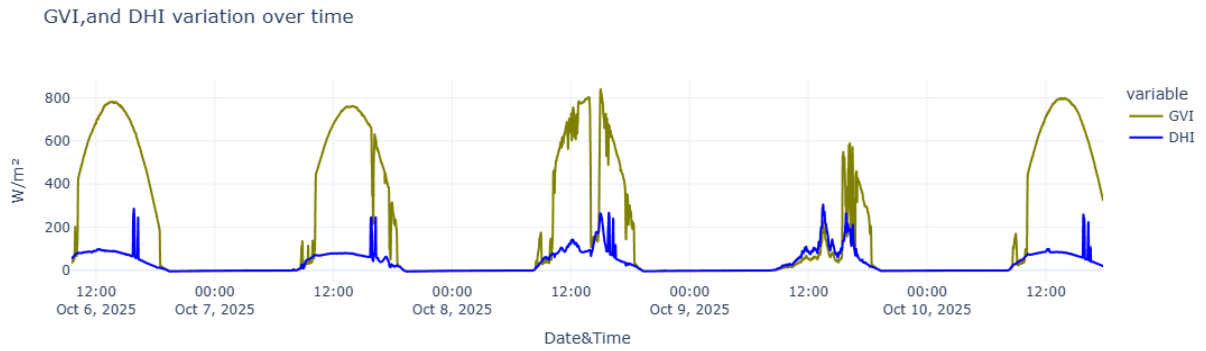

Figure 9-1: Global vertical and horizontal irradiance over time (without shading experiment toward the south)

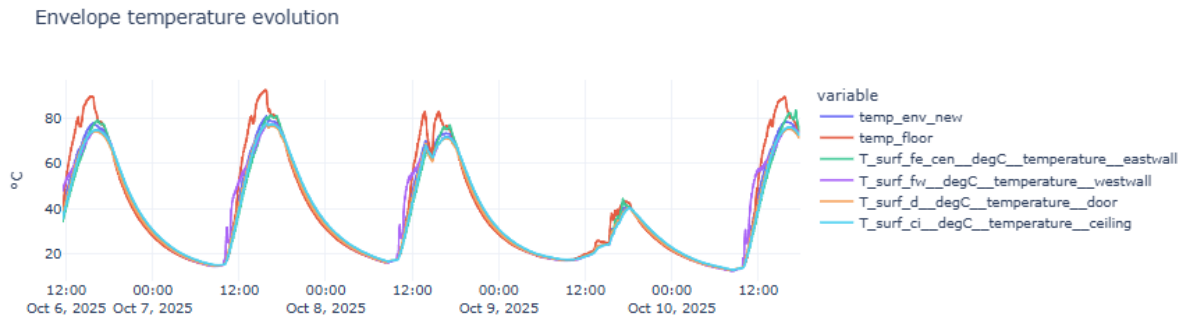

Figure 9-2: Evolution of inner surface temperature for each opaque façade

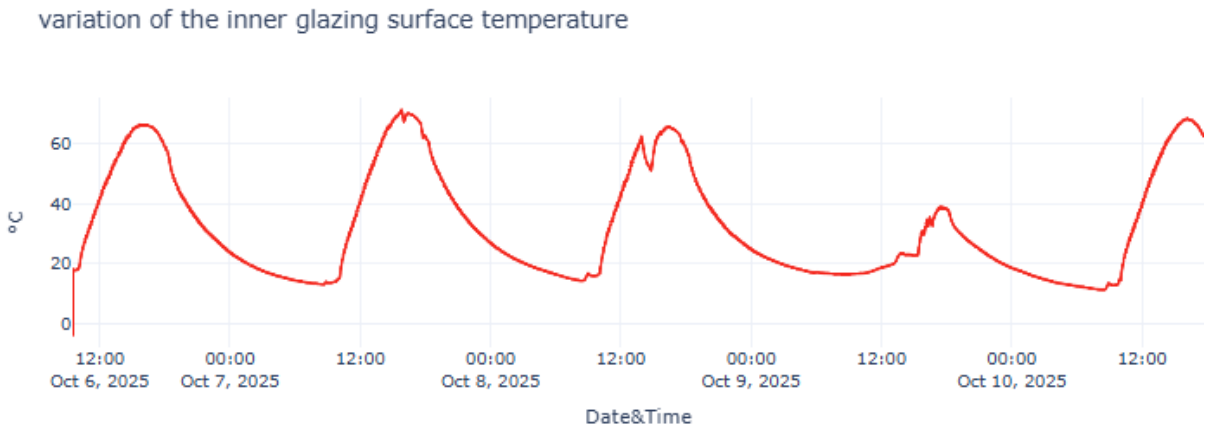

Figure 9-3: Evolution of inner glazing surface temperature

References

[1] 'ISO 52016-3 2023Energy performance of buildings - Energy needs for heating and cooling, internal temperatures and sensible and latent heat loads - Part 3 : calculation procedures regarding adaptive building envelope elements', ISO. [Online]. Available: https://www.iso.org/fr/standard/75395.html

[2] 'Energy Performance of Buildings Directive'. Accessed: Aug. 31, 2025. [Online]. Available: https://energy.ec.europa.eu/topics/energy-efficiency/energy-performance-buildings/energy-performance-buildings-directive_en

[3] Eurostat, 'Disaggregated final energy consumption in households - quantities'. Eurostat, 2022. doi: 10.2908/NRG_D_HHQ.

[4] A. G. Kitous and J. Després, 'Assessment of the impact of climate change on residential energy demand for heating and cooling', JRC Publications Repository. Accessed: Apr. 27, 2026. [Online]. Available: https://publications.jrc.ec.europa.eu/repository/handle/JRC110191

[5] S. B. Sadineni, S. Madala, and R. F. Boehm, 'Passive building energy savings: A review of building envelope components', *Renew. Sustain. Energy Rev.*, vol. 15, no. 8, pp. 3617–3631, Oct. 2011, doi: 10.1016/j.rser.2011.07.014.

[6] S. Barbosa and K. Ip, 'Perspectives of double skin façades for naturally ventilated buildings: A review', *Renew. Sustain. Energy Rev.*, vol. 40, pp. 1019–1029, Dec. 2014, doi: 10.1016/j.rser.2014.07.192.

[7] D. Aelenei, L. Aelenei, and C. Vieira, 'Adaptive Façade: Concept, Applications, Research Questions':, *Energy Procedia*, vol. 91, pp. 269–275, Jun. 2016, doi: 10.1016/j.egypro.2016.06.218.

[8] H. Alkhatib, P. Lemarchand, B. Norton, and D. T. J. O'Sullivan, 'Deployment and control of adaptive building facades for energy generation, thermal insulation, ventilation and daylighting: A review', *Appl. Therm. Eng.*, vol. 185, p. 116331, Feb. 2021, doi: 10.1016/j.applthermaleng.2020.116331.

[9] S. Attia, F. Favoino, R. Loonen, A. Petrovski, and A. Monge-Barrio, 'Adaptive Façades System Assessment: An initial review', Nov. 2015. Accessed: May 03, 2026. [Online]. Available: https://www.semanticscholar.org/paper/Adaptive-Fa%C3%A7ades-System-Assessment%3A-An-initial-Attia-Favoino/acb5870320a5653dfa5ea58ff195a0590861fe8c

[10] R. Bakhshoodeh, C. Ocampo, and C. Oldham, 'Thermal performance of green façades: Review and analysis of published data', *Renew. Sustain. Energy Rev.*, vol. 155, p. 111744, Mar. 2022, doi: 10.1016/j.rser.2021.111744.

[11] Y. Lin, L. Xu, W. Yang, L. Tian, and M. Chan, 'A Systematic Review on the Research and Development of Adaptive Buildings', *Buildings*, vol. 15, no. 10, p. 1593, Jan. 2025, doi: 10.3390/buildings15101593.

[12] R. C. G. M. Loonen, M. Trčka, D. Cóstola, and J. L. M. Hensen, 'Climate adaptive building shells: State-of-the-art and future challenges', *Renew. Sustain. Energy Rev.*, vol. 25, pp. 483–493, Sep. 2013, doi: 10.1016/j.rser.2013.04.016.

[13] R. Loonen *et al.*, 'Design for façade adaptability: Towards a unified and systematic characterization', Nov. 2015. Accessed: Apr. 27, 2026. [Online]. Available: https://www.semanticscholar.org/paper/Design-for-fa%C3%A7ade-adaptability%3A-Towards-a-unified-Loonen-Rico-Mart%C3%ADnez/6b8887257aa80bffea4c56dc7cc944813c93b75b

[14] T. Mols, A. Blumberga, and I. Karklina, 'Evaluation of climate adaptive building shells: multi-criteria analysis', *Energy Procedia*, vol. 128, pp. 292–296, Sep. 2017, doi: 10.1016/j.egypro.2017.09.077.

[15] A. Zarzycki and M. Decker, 'Climate-adaptive buildings: Systems and materials', *Int. J. Archit. Comput.*, vol. 17, no. 2, pp. 166–184, Jun. 2019, doi: 10.1177/1478077119852707.

[16] 'IEA - ECBCS Annex 44-Integrating Environmentally Responsive Elements in Buildings', Aalborg University's Research Portal. Accessed: Apr. 27, 2026. [Online]. Available: https://vbn.aau.dk/en/projects/iea-ecbcs-annex-44-integrating-environmentally-responsive-element/

[17] M. Jafari and A. Alipour, 'Review of approaches, opportunities, and future directions for improving aerodynamics of tall buildings with smart facades', *Sustain. Cities Soc.*, vol. 72, p. 102979, Sep. 2021, doi: 10.1016/j.scs.2021.102979.

[18] O. Omar, 'Intelligent building, definitions, factors and evaluation criteria of selection', *Alex. Eng. J.*, vol. 57, no. 4, pp. 2903–2910, Dec. 2018, doi: 10.1016/j.aej.2018.07.004.

[19] S. O. Sadegh, E. Gasparri, A. Brambilla, and A. Globa, 'Kinetic facades: An evolutionary-based performance evaluation framework', *J. Build. Eng.*, vol. 53, p. 104408, Aug. 2022, doi: 10.1016/j.jobe.2022.104408.

[20] M. Hosseini, M. Mohammadi, T. Schroeder, and O. Santin, 'Integrating interactive kinetic façade design with colored glass to improve daylight performance based on occupants' position', *J. Build. Eng.*, vol. 31, p. 101404, Apr. 2020, doi: 10.1016/j.jobe.2020.101404.

[21] L. Valentin, M. Dabbagh, and M. Krarti, 'Benefits of switchable insulation systems for residential buildings in France', *Energy Build.*, vol. 259, p. 111868, Mar. 2022, doi: 10.1016/j.enbuild.2022.111868.

[22] S. W. Tong, W. P. Goh, X. Huang, and C. Jiang, 'A review of transparent-reflective switchable glass technologies for building facades', *Renew. Sustain. Energy Rev.*, vol. 152, p. 111615, Dec. 2021, doi: 10.1016/j.rser.2021.111615.

[23] D. S. Panya, T. Kim, and S. Choo, 'A Methodology of Interactive Motion Facades Design through Parametric Strategies', *Appl. Sci.*, vol. 10, no. 4, p. 1218, Jan. 2020, doi: 10.3390/app10041218.

[24] E. Cruz *et al.*, 'Design processes and multi-regulation of biomimetic building skins: A comparative analysis', *Energy Build.*, vol. 246, p. 111034, Sep. 2021, doi: 10.1016/j.enbuild.2021.111034.

[25] R. Loonen, P.-J. Hoes, and J. Hensen, 'Performance prediction of buildings with responsive building elements challenges and solutions: 2nd IBPSA-England Conference on Building Simulation and Optimization (BSO 2014)', in *Proceedings of the 2014 Building Simulation and Optimization Conference (BSO14), 23-24 June 2014, London, United Kingdom*, Jun. 2014.

[26] X. Xu and S. V. Dessel, 'Evaluation of an Active Building Envelope window-system', *Build. Environ.*, vol. 43, no. 11, pp. 1785–1791, Nov. 2008, doi: 10.1016/j.buildenv.2007.10.013.

[27] C. Ochoa and G. Capeluto, 'Strategic decision-making for intelligent buildings: Comparative impact of passive design strategies and active features in a hot climate', *Build. Environ.*, vol. 43, pp. 1829–1839, Nov. 2008, doi: 10.1016/j.buildenv.2007.10.018.
[28] R. Romano, L. Aelenei, D. Aelenei, and E. Mazzucchelli, 'What is an Adaptive Façade? Analysis of Recent Terms and Definitions from an International Perspective', *J. Facade Des. Eng.*, vol. 6, pp. 65–76, Nov. 2018, doi: 10.7480/jfde.2018.3.2478.
[29] A. Tabadkani, A. Roetzel, H. X. Li, and A. Tsangrassoulis, 'Design approaches and typologies of adaptive facades: A review', *Autom. Constr.*, vol. 121, p. 103450, Jan. 2021, doi: 10.1016/j.autcon.2020.103450.
[30] M. Morales-Beltran and P. Teuffel, 'Towards smart building structures: adaptive structures in earthquake and wind loading control response – a review', *Intell. Build. Int.*, vol. 5, no. 2, pp. 83–100, Apr. 2013, doi: 10.1080/17508975.2013.778193.
[31] R. Velasco, A. P. Brakke, and D. Chavarro, 'Dynamic façades and computation: 16th International Conference on Computer-Aided Architectural Design, CAAD 2015', *Commun. Comput. Inf. Sci.*, vol. 527, pp. 172–191, 2015, doi: 10.1007/978-3-662-47386-3_10.
[32] 'Final Booklet Series COST TU1403 – COST Action TU1403 – Adaptive Facades Network'. Accessed: Feb. 21, 2023. [Online]. Available: http://tu1403.eu/?page_id=1562
[33] C. Bedon *et al.*, 'Key Structural Aspects for Adaptive Facades - Activity Progress from the EU-COST Action TU1403 "Structural" Task Group', vol. 2, pp. 135–154, Jun. 2018, doi: 10.3844/sgamrsp.2018.135.154.
[34] A. Tabadkani, A. Roetzel, H. X. Li, and A. Tsangrassoulis, 'A review of automatic control strategies based on simulations for adaptive facades', *Build. Environ.*, vol. 175, p. 106801, May 2020, doi: 10.1016/j.buildenv.2020.106801.
[35] H. Thieblemont, F. Haghighat, R. Ooka, and A. Moreau, 'Predictive control strategies based on weather forecast in buildings with energy storage system: A review of the state-of-the art', *Energy Build.*, vol. 153, pp. 485–500, Oct. 2017, doi: 10.1016/j.enbuild.2017.08.010.
[36] L. Badarnah Kadri, 'Towards the LIVING envelope: Biomimetics for building envelope adaptation', Delft University of Technology, 2012. doi: 10.4233/UUID:4128B611-9B48-4C8D-B52F-38A59AD5DE65.
[37] G. Cattarin, F. Causone, A. Kindinis, and L. Pagliano, 'Outdoor test cells for building envelope experimental characterisation – A literature review', *Renew. Sustain. Energy Rev.*, vol. 54, pp. 606–625, Feb. 2016, doi: 10.1016/j.rser.2015.10.012.
[38] A. Erkoreka, J. J. Bloem, C. Escudero, K. Martin, and J. M. Sala, 'Optimizing Full Scale Dynamic Testing of Building Components: Measurement Sensors and Monitoring Systems', *Energy Procedia*, vol. 78, pp. 1738–1743, Nov. 2015, doi: 10.1016/j.egypro.2015.11.285.
[39] M. Rendu, 'Méthodologies pour la caractérisation des performances thermiques d'éléments de façades à échelle réelle', phdthesis, Université de La Rochelle, 2021. Accessed: Apr. 26, 2026. [Online]. Available: https://theses.hal.science/tel-03511281
[40] S. Mohammadi, A. Weersink, J. van 't Ende, and C. Struck, 'Rotatable Smart TinyLab, a platform for testing integrated façades and indoor climate', *IOP Conf. Ser. Earth Environ. Sci.*, vol. 1085, no. 1, p. 012055, Sep. 2022, doi: 10.1088/1755-1315/1085/1/012055.
[41] G. Cattarin, F. Causone, A. Kindinis, and L. Pagliano, 'Outdoor test cells for building envelope experimental characterisation – A literature review', *Renew. Sustain. Energy Rev.*, vol. 54, pp. 606–625, Feb. 2016, doi: 10.1016/j.rser.2015.10.012.

[42] C. Bedon *et al.*, 'Structural characterisation of adaptive facades in Europe - Part II: Validity of conventional experimental testing methods and key issues', *J. Build. Eng.*, vol. 25, p. 100797, Sep. 2019, doi: 10.1016/j.jobe.2019.100797.
[43] Y. Yang, 'Innovative non-destructive methodology for energy diagnosis of building envelope', phdthesis, Université de Bordeaux, 2017. Accessed: Apr. 26, 2026. [Online]. Available: https://theses.hal.science/tel-01719261
[44] 'ISO 6946:2017-Building components and building elements — Thermal resistance and thermal transmittance — Calculation methods', ISO. Accessed: Apr. 26, 2026. [Online]. Available: https://www.iso.org/standard/65708.html
[45] L. Evangelisti, C. Guattari, P. Gori, and R. De Lieto Vollaro, 'In situ thermal transmittance measurements for investigating differences between wall models and actual building performance', *Sustain. Switz.*, vol. 7, no. 8, pp. 10388–10398, 2015, doi: 10.3390/su70810388.
[46] 'ISO 7345:2018 -Thermal performance of buildings and building components - Physical quantities and definitions'. Accessed: Aug. 04, 2025. [Online]. Available: https://viewerbdc-afnor-org.docelec.u-bordeaux.fr/pdf/viewer/24MrgnNOkSE1?proxy=true
[47] 'ISO 9869-1:2014-Thermal insulation - Building elements - In-situ measurement of thermal resistance and thermal transmittance - Part 1 : heat flow meter method'. Accessed: Aug. 04, 2025. [Online]. Available: https://cobaz-afnor-org.docelec.u-bordeaux.fr/notice/norme/iso-9869-12014/XS125521?rechercheID=35509136&searchIndex=10&activeTab=all
[48] 'ISO 10878:2013 Non-destructive testing — Infrared thermography — Vocabulary', ISO. Accessed: Apr. 26, 2026. [Online]. Available: https://www.iso.org/standard/46265.html
[49] P. A. Fokaides and S. A. Kalogirou, 'Application of infrared thermography for the determination of the overall heat transfer coefficient (U-Value) in building envelopes', *Appl. Energy*, vol. 88, no. 12, pp. 4358–4365, Dec. 2011, doi: 10.1016/j.apenergy.2011.05.014.
[50] B. Tejedor, M. Casals, M. Gangolells, and X. Roca, 'Quantitative internal infrared thermography for determining in-situ thermal behaviour of façades', *Energy Build.*, vol. 151, pp. 187–197, Sep. 2017, doi: 10.1016/j.enbuild.2017.06.040.
[51] R. Albatici, A. M. Tonelli, and M. Chiogna, 'A comprehensive experimental approach for the validation of quantitative infrared thermography in the evaluation of building thermal transmittance', *Appl. Energy*, vol. 141, pp. 218–228, Mar. 2015, doi: 10.1016/j.apenergy.2014.12.035.
[52] S. Sfarra, A. Cicone, B. Yousefi, C. Ibarra-Castanedo, S. Perilli, and X. Maldague, 'Improving the detection of thermal bridges in buildings via on-site infrared thermography: The potentialities of innovative mathematical tools', *Energy Build.*, vol. 182, pp. 159–171, Jan. 2019, doi: 10.1016/j.enbuild.2018.10.017.
[53] 'ISO 8990:1994-Thermal insulation — Determination of steady-state thermal transmission properties — Calibrated and guarded hot box', ISO. Accessed: Apr. 26, 2026. [Online]. Available: https://www.iso.org/standard/16519.html
[54] A. Shea, K. Wall, and P. Walker, 'Evaluation of the thermal performance of an innovative prefabricated natural plant fibre building system', *Build. Serv. Eng. Res. Technol.*, vol. 34, no. 4, pp. 369–380, Nov. 2013, doi: 10.1177/0143624412450023.

[55] ‘ISO 12569:2017-Thermal performance of buildings and materials - Determination of specific airflow rate in buildings - Tracer gas dilution method’. [Online]. Available: https://www.iso.org/obp/ui/#iso:std:iso:12569:ed-3:v1:fr
[56] A. Jankovic, G. Gennaro, G. Chaudhary, F. Goia, and F. Favoino, ‘Tracer gas techniques for airflow characterization in double skin facades’, *Build. Environ.*, vol. 212, p. 108803, Mar. 2022, doi: 10.1016/j.buildenv.2022.108803.
[57] D. H. W. Li, J. C. Lam, and S. L. Wong, ‘Daylighting and its effects on peak load determination’, *Energy*, vol. 30, no. 10, pp. 1817–1831, Jul. 2005, doi: 10.1016/j.energy.2004.09.009.
[58] ‘ISO/CIE 10916:2024-Light and lighting - Energy performance of lighting in buildings - Calculation of the impact of daylight utilization’.
[59] A. Luna-Navarro, G. R. Hunt, and M. Overend, ‘Dynamic façades – An exploratory campaign to assess occupant multi-domain environmental satisfaction and façade interaction’, *Build. Environ.*, vol. 211, p. 108703, Mar. 2022, doi: 10.1016/j.buildenv.2021.108703.
[60] ‘ISO 16823:2025(en), Non-destructive testing — Ultrasonic testing — Through-transmission technique’. Accessed: Apr. 26, 2026. [Online]. Available: https://www.iso.org/obp/ui/en/#iso:std:iso:16823:ed-2:v1:en
[61] ‘ISO 12354-3:2017-Acoustique du bâtiment — Calcul de la performance acoustique des bâtiments à partir de la performance des éléments — Partie 3: Isolement aux bruits aériens venus de l’extérieur’, ISO. Accessed: Apr. 26, 2026. [Online]. Available: https://www.iso.org/fr/standard/70244.html
[62] N. Granzotto and E. Piana, ‘Evaluation Method for Façade Acoustic Insulation for a Corner Room: Discussion on the Results Obtained as a Function of the Source Position’, *Appl. Sci.*, vol. 10, p. 7434, Oct. 2020, doi: 10.3390/app10217434.
[63] ‘ISO/TR 9705-2:2001-Reaction-to-fire tests — Full-scale room tests for surface products — Part 2: Technical background and guidance’, ISO. Accessed: Apr. 26, 2026. [Online]. Available: https://www.iso.org/standard/24937.html
[64] M. Gholami Rostam and A. Abbasi, ‘Dynamic climate-adaptive design: A key to realizing future-proof energy efficiency in building sector’, *Appl. Energy*, vol. 341, p. 121146, Jul. 2023, doi: 10.1016/j.apenergy.2023.121146.
[65] F. Roberts, S. Yang, H. Du, and R. Yang, ‘Effect of semi-transparent a-Si PV glazing within double-skin façades on visual and energy performances under the UK climate condition’, *Renew. Energy*, vol. 207, pp. 601–610, May 2023, doi: 10.1016/j.renene.2023.03.023.
[66] F. Favoino, ‘Building performance simulation of adaptive facades’, Cambridge University, 2016.
[67] F. Goia, M. Perino, and V. Serra, ‘Experimental analysis of the energy performance of a full-scale PCM glazing prototype’, *Sol. Energy*, vol. 100, pp. 217–233, Feb. 2014, doi: 10.1016/j.solener.2013.12.002.
[68] A. Pugsley, A. Zacharopoulos, J. Deb Mondol, and M. Smyth, ‘Vertical Planar Liquid-Vapour Thermal Diodes (PLVTD) and their application in building façade energy systems’, *Appl. Therm. Eng.*, vol. 179, p. 115641, Oct. 2020, doi: 10.1016/j.applthermaleng.2020.115641.
[69] L. J. Claros-Marfil, V. Zetola, J. F. Padial, and B. Lauret, ‘Experimental-simulation methodology for estimation of thermal parameters of adaptive facades in mild climate

conditions: A water-flow glazing case study', *J. Build. Eng.*, vol. 45, p. 103384, Jan. 2022, doi: 10.1016/j.jobe.2021.103384.

[70] R. Loonen, F. Favoino, J. Hensen, and M. Overend, 'Current status, requirements and opportunities for building performance simulation of adaptive facades', 2018, pp. 21–47. [Online]. Available: https://www.semanticscholar.org/paper/Review-of-current-status%2C-requirements-and-for-of-Loonen-Favoino/93a302e8b6e457427207da8cac579ac6ddd35c74

[71] F. Goia, M. Perino, and M. Haase, 'A numerical model to evaluate the thermal behaviour of PCM glazing system configurations', *Energy Build.*, vol. 54, pp. 141–153, Nov. 2012, doi: 10.1016/j.enbuild.2012.07.036.

[72] A. Luna-Navarro, R. Loonen, M. Juaristi, A. Monge-Barrio, S. Attia, and M. Overend, 'Occupant-Facade interaction: a review and classification scheme', *Build. Environ.*, vol. 177, p. 106880, Jun. 2020, doi: 10.1016/j.buildenv.2020.106880.

[73] H. B. Gunay, W. O'Brien, and I. Beausoleil-Morrison, 'A critical review of observation studies, modeling, and simulation of adaptive occupant behaviors in offices', *Build. Environ.*, vol. 70, pp. 31–47, Dec. 2013, doi: 10.1016/j.buildenv.2013.07.020.

[74] W. Tian, 'A review of sensitivity analysis methods in building energy analysis', *Renew. Sustain. Energy Rev.*, vol. 20, pp. 411–419, Apr. 2013, doi: 10.1016/j.rser.2012.12.014.

[75] N. DeForest *et al.*, 'Regional performance targets for transparent near-infrared switching electrochromic window glazings', *Build. Environ.*, vol. 61, pp. 160–168, Mar. 2013, doi: 10.1016/j.buildenv.2012.12.004.

[76] L. Shen and Y. Han, 'Optimizing the modular adaptive façade control strategy in open office space using integer programming and surrogate modelling', *Energy Build.*, vol. 254, p. 111546, Jan. 2022, doi: 10.1016/j.enbuild.2021.111546.

[77] S. P. Corgnati, M. Perino, and V. Serra, 'Experimental assessment of the performance of an active transparent façade during actual operating conditions', *Sol. Energy*, vol. 81, no. 8, pp. 993–1013, Aug. 2007, doi: 10.1016/j.solener.2006.12.004.

[78] L. Bianco *et al.*, 'Towards New Metrics for the Characterisation of the Dynamic Performance of Adaptive Façade Systems', *J. Facade Des. Eng.*, vol. 6, no. 3, pp. 175–196, Nov. 2018, doi: 10.7480/jfde.2018.3.2564.

[79] M. Voigt, D. Roth, and H. Binz, 'Challenges with adaptive facades - a life cycle perspective', Oct. 2021.

[80] J. J. Bloem, 'System identification applied to building performance data', *Eur. Comm. Jt. Res. Cent.*, 1994.

[81] Q. Zhu, A. Li, J. Xie, W. Li, and X. Xu, 'Experimental validation of a semi-dynamic simplified model of active pipe-embedded building envelope', *Int. J. Therm. Sci.*, vol. 108, pp. 70–80, Oct. 2016, doi: 10.1016/j.ijthermalsci.2016.05.004.

[82] Y. He, H. Yu, A. Ozaki, N. Dong, and S. Zheng, 'A detailed investigation of thermal behavior of green envelope under urban canopy scale in summer: A case study in Shanghai area', *Energy Build.*, vol. 148, pp. 142–154, Aug. 2017, doi: 10.1016/j.enbuild.2017.03.014.

[83] H. Viot, 'Modélisation et instrumentation d'un bâtiment et de ses systèmes pour optimiser sa gestion énergétique', thesis, Bordeaux, 2016. Accessed: Sep. 16, 2025. [Online]. Available: https://theses.fr/2016BORD0349

[84] S. P. Corgnati, M. Perino, and V. Serra, 'Experimental assessment of the performance of an active transparent façade during actual operating conditions', *Sol. Energy*, vol. 81, no. 8, pp. 993–1013, Aug. 2007, doi: 10.1016/j.solener.2006.12.004.

[85] G. Pernigotto, I. Ballarini, F. Patuzzi, A. Prada, V. Corrado, and A. Gasparella, 'Simulative Applications of Novel Indicators for the Characterization and Performance Evaluation of Transparent Facades', 2025, *bu,press*. doi: 10.13124/9788860462022.
[86] W. Braham and Y. K. Yi, 'White box, Black box, Gray-box modelling of building energy use: An overview'.
[87] T. Berthou, 'Développement de modèles de bâtiment pour la prévision de charge de climatisation et l'élaboration de stratégies d'optimisation énergétique et d'effacement', phdthesis, Ecole Nationale Supérieure des Mines de Paris, 2013. Accessed: Sep. 15, 2025. [Online]. Available: https://pastel.hal.science/pastel-00935434
[88] G. Sidebotham, *Heat Transfer Modeling: An Inductive Approach*. Springer, 2015.
[89] D. Bienvenido-Huertas and C. Rubio-Bellido, *Optimization of the Characterization of the Thermal Properties of the Building Envelope: Analysis of the Characterization of the Façades using Artificial Intelligence*. in SpringerBriefs in Applied Sciences and Technology. Cham: Springer International Publishing, 2021. doi: 10.1007/978-3-030-63629-6.
[90] D. D. Johnston, D. Miles-Shenton, D. Farmer, and D. J. Wingfield, 'Whole House Heat Loss Test Method (Coheating)', 2013. [Online]. Available: https://www.leedsbeckett.ac.uk/-/media/files/research/leeds-sustainability-institute/coheating-method-for-whole-house-heat-loss/lsi_cebe_coheating_test_method_june2013.pdf
[91] S. Thébault and R. Bouchié, 'Refinement of the ISABELE method regarding uncertainty quantification and thermal dynamics modelling', *Energy Build.*, vol. 178, pp. 182–205, 2018, doi: 10.1016/j.enbuild.2018.08.047.
[92] F. Alzetto, G. Pandraud, R. Fitton, I. Heusler, and H. Sinnesbichler, 'QUB: A fast dynamic method for in-situ measurement of the whole building heat loss', *Energy Build.*, vol. 174, pp. 124–133, Sep. 2018, doi: 10.1016/j.enbuild.2018.06.002.
[93] S. Hammarsten, D. Van Hattem, H. Bloem, and R. Colombo, 'Passive solar component testing with identification methods', *Sol. Energy*, vol. 41, no. 1, pp. 5–13, 1988, doi: 10.1016/0038-092X(88)90108-9.
[94] 'ISO 9972:2015-Thermal performance of buildings — Determination of air permeability of buildings — Fan pressurization method', ISO. Accessed: Apr. 26, 2026. [Online]. Available: https://www.iso.org/standard/55718.html
[95] B. Mattsson and J. Claesson, 'A Transient Pressurization Method for Measurements of Airtightness', *J. Build. Phys.*, vol. 31, no. 1, pp. 35–53, Jul. 2007, doi: 10.1177/1744259107079021.
[96] E. B. Møller, T. V. Rasmussen, and A. Nicolajsen, 'A Simplified Method Using Compressed Air to Determine Air Leakage', [Online]. Available: https://web.ornl.gov/sci/buildings/conf-archive/2010%20B11%20papers/57_Moller.pdf
[97] 'ISO 10211:2017-Thermal bridges in building construction — Heat flows and surface temperatures — Detailed calculations', ISO. Accessed: Apr. 26, 2026. [Online]. Available: https://www.iso.org/standard/65710.html
[98] 'ISO 6781-3:2015(en), Performance of buildings — Detection of heat, air and moisture irregularities in buildings by infrared methods — Part 3: Qualifications of equipment operators, data analysts and report writers'. Accessed: Apr. 26, 2026. [Online]. Available: https://www.iso.org/obp/ui/en/#iso:std:iso:6781:-3:ed-1:v1:en

[99] A. Saltelli, Ed., *Sensitivity analysis in practice: a guide to assessing scientific models*. Hoboken, NJ: Wiley, 2004.
[100] A. Norouziasas *et al.*, 'Implementation of ISO/DIS 52016-3 for adaptive façades: A case study of an office building', *Build. Environ.*, vol. 235, p. 110195, May 2023, doi: 10.1016/j.buildenv.2023.110195.
[101] E. Cuce and S. B. Riffat, 'A state-of-the-art review on innovative glazing technologies', *Renew. Sustain. Energy Rev.*, vol. 41, pp. 695–714, Jan. 2015, doi: 10.1016/j.rser.2014.08.084.
[102] M. Thalfeldt, E. Pikas, J. Kurnitski, and H. Voll, 'Facade design principles for nearly zero energy buildings in a cold climate', *Energy Build.*, vol. 67, pp. 309–321, Dec. 2013, doi: 10.1016/j.enbuild.2013.08.027.
[103] P. D. Robinson and M. G Hutchins, 'Advanced glazing technology for low energy buildings in the UK', *Renew. Energy*, vol. 5, no. 1, pp. 298–309, Aug. 1994, doi: 10.1016/0960-1481(94)90387-5.
[104] K. Al-Obaidi, M. Ismail, and A. M. A. Rahman, 'A Review of Skylight Glazing Materials in Architectural Designs for a Better Indoor Environment', *Mod. Appl. Sci.*, vol. 8, no. 1, Art. no. 1, Dec. 2013, doi: 10.5539/mas.v8n1p68.
[105] Y. Misawa, S. Hikone, M. Nakamura, S. Iwamoto, and M. Iwata, 'Diagonally arranged louvers in integrated facade systems - effects on the interior lighting environment', *J. Facade Des. Eng.*, vol. 2, no. 3–4, pp. 163–182, May 2015, doi: 10.3233/FDE-150018.
[106] Y. Grobman, G. Austern, Y. Hatiel, and I. Capeluto, 'Evaluating the Influence of Varied External Shading Elements on Internal Daylight Illuminances', *Buildings*, vol. 10, no. 2, p. 22, Feb. 2020, doi: 10.3390/buildings10020022.
[107] Y. Misawa, K. Azuma, W. Cho, S. Iwamoto, and M. Iwata, 'Simulation study on energy conservation performance for integrated external louver facades', *J. Facade Des. Eng.*, vol. 3, no. 3–4, pp. 237–252, Jun. 2016, doi: 10.3233/FDE-160043.
[108] A. Laouadi and A. Parekh, 'Optical models of complex fenestration systems', *Light. Res. Technol.*, vol. 39, no. 2, pp. 123–145, Jun. 2007, doi: 10.1177/1365782806072671.
[109] G. De Michele *et al.*, 'Opportunities and Challenges for Performance Prediction of Dynamic Complex Fenestration Systems (CFS)', *J. Facade Des. Eng.*, pp. 101-115 Pages, Nov. 2018, doi: 10.7480/JFDE.2018.3.2531.
[110] 'ISO 15099:2003. (2003). Thermal performance of windows, doors, and shading devices – Calculation of thermal transmittance (ISO 15099:2003). International Organization for Standardization', ISO. Accessed: Apr. 08, 2025. [Online]. Available: https://www.iso.org/standard/26425.html
[111] M. G. Gomes, A. J. Santos, and A. M. Rodrigues, 'Solar and visible optical properties of glazing systems with venetian blinds: Numerical, experimental and blind control study', *Build. Environ.*, vol. 71, pp. 47–59, Jan. 2014, doi: 10.1016/j.buildenv.2013.09.003.
[112] S. Chaiyapinunt and S. Worasinchai, 'Development of a mathematical model for a curved slat venetian blind with thickness', *Sol. Energy*, vol. 83, no. 7, pp. 1093–1113, Jul. 2009, doi: 10.1016/j.solener.2009.01.013.
[113] J. Klems, 'A New Method for Predicting the Solar Heat Gain of Complex Fenestration Systems II. Detailed Description of the Matrix Layer Calculation', *ASHRAE Trans.*, vol. 100, no. 1, 1993.
[114] P. Apian-Bennewitz *et al.*, 'Analysis and evaluation of BSDF characterization of daylighting systems', IEA SHC Task 61, Oct. 2021. doi: 10.18777/ieashc-task61-2021-0012.

[115] M. G. Gomes, A. M. Rodrigues, and J. A. Bogas, 'Numerical and experimental study of the optical properties of venetian blinds', *J. Build. Phys.*, vol. 36, no. 1, pp. 7–34, Jul. 2012, doi: 10.1177/1744259112444022.
[116] M. G. Gomes, A. J. Santos, and M. Calhau, 'Experimental study on the impact of double tilted Venetian blinds on indoor daylight conditions', *Build. Environ.*, vol. 225, p. 109675, Nov. 2022, doi: 10.1016/j.buildenv.2022.109675.
[117] C. Chantrasrisalai, 'Optical and thermal fenestration models for building cooling load calculations', Oklahoma State University, 2007.
[118] T. Hubert, 'Bio-inspiration et enveloppe du bâtiment : proposition d'une méthode de conception et application expérimentale. Mécanique [physics]. Université de Bordeaux, 2022.', vol. 246, p. 111034.
[119] 'ISO 9050:2003-Glass in building — Determination of light transmittance, solar direct transmittance, total solar energy transmittance, ultraviolet transmittance and related glazing factors', ISO. Accessed: Apr. 26, 2026. [Online]. Available: https://www.iso.org/standard/35062.html
[120] X. Zhang, C. Rasmussen, D. Saelens, and S. Roels, 'Time-dependent solar aperture estimation of a building: Comparing grey-box and white-box approaches', *Renew. Sustain. Energy Rev.*, vol. 161, p. 112337, Jun. 2022, doi: 10.1016/j.rser.2022.112337.
[121] X. Zhang, D. Saelens, and S. Roels, 'Quantifying dynamic solar gains in buildings: Measurement, simulation and data-driven modelling', *Renew. Sustain. Energy Rev.*, vol. 212, p. 115221, Apr. 2025, doi: 10.1016/j.rser.2024.115221.
[122] X. Zhang, D. Saelens, and S. Roels, 'Data-driven estimation of time-dependent solar gain coefficient in a two-zone building with synthetic occupants: Two B-splines integrated grey-box modeling approaches', *Build. Environ.*, vol. 244, p. 110311, Oct. 2023, doi: 10.1016/j.buildenv.2023.110311.
[123] *ASHRAE HANDBOOK 2001*. Accessed: Jul. 17, 2025. [Online]. Available: http://archive.org/details/ashrae-handbook-2001
[124] 'ISO 6946: 2017- Building components and building elements - Thermal resistance and thermal transmittance - Calculation methods'.
[125] T. Hubert, 'Bio-inspiration et enveloppe du bâtiment : proposition d'une méthode de conception et application expérimentale', Theses, Université de Bordeaux, 2022. Accessed: Apr. 01, 2026. [Online]. Available: https://theses.hal.science/tel-03892809
[126] 'ISO 10456:2007-Building materials and products — Hygrothermal properties — Tabulated design values and procedures for determining declared and design thermal values', ISO. Accessed: Apr. 28, 2026. [Online]. Available: https://www.iso.org/standard/40966.html
[127] 'ISO 13789:2017 -Thermal performance of buildings — Transmission and ventilation heat transfer coefficients — Calculation method'. Accessed: Jul. 08, 2025. [Online]. Available: https://viewerbdc-afnor-org.docelec.u-bordeaux.fr/pdf/viewer/69MVSD9mLW41?proxy=true
[128] 'WINDOW | Documentation | Windows & Daylighting'. Accessed: Apr. 26, 2026. [Online]. Available: https://windows.lbl.gov/window-documentation
[129] 'NF EN ISO 14683 | Juillet 2017 Thermal bridges in building construction - Linear thermal transmittance - Simplified methods and default values'.
[130] M. H. Sherman and M. P. Modera, 'Signal attenuation due to cavity leakage', *J. Acoust. Soc. Am.*, vol. 84, no. 6, pp. 2163–2169, Dec. 1988, doi: 10.1121/1.397062.

[131] ‘Building ventilation: The state of the art, building airtightness: Research and practice’, ResearchGate. Accessed: Sep. 08, 2025. [Online]. Available: https://www.researchgate.net/publication/284044637_Building_ventilation_The_state_of_the_art_building_airtightness_Research_and_practice
[132] J. Duffie and W. Beckman, *Solar Engineering of Thermal Processes*. 2006. doi: 10.1002/9781118671603.
[133] ‘NFRC 100A-2010: Procedure for Determining Fenestration Attachment Product U-factors’, National Fenestration Rating Council (NFRC). Accessed: Apr. 01, 2026. [Online]. Available: https://nfrccommunity.org/store/viewproduct.aspx?id=1403208&hhSearchTerms=%22NFRC+and+100-2010%22
[134] ‘Window Calculation Module: Engineering Reference — EnergyPlus 8.0’. Accessed: Nov. 24, 2023. [Online]. Available: https://bigladdersoftware.com/epx/docs/8-0/engineering-reference/page-043.html
[135] D. Geisler-Moroder *et al.*, ‘BSDF Generation Procedures for Daylighting Systems’, IEA SHC Task 61, Jan. 2021. doi: 10.18777/ieashc-task61-2021-0001.
[136] A. McNeil, C. J. Jonsson, D. Appelfeld, G. Ward, and E. S. Lee, ‘A validation of a ray-tracing tool used to generate bi-directional scattering distribution functions for complex fenestration systems’, *Sol. Energy*, vol. 98, pp. 404–414, Dec. 2013, doi: 10.1016/j.solener.2013.09.032.
[137] G. Ward, ‘Computing and applying variable-resolution data for bidirectional scattering distribution functions’, 2011.
[138] S. Park and N. Baek, ‘A Shader-Based Ray Tracing Engine’, *Appl. Sci.*, vol. 11, p. 3264, Apr. 2021, doi: 10.3390/app11073264.
[139] ‘Coating Arsonsisi’s catalog’, ARSONSISI. Accessed: May 26, 2026. [Online]. Available: https://fr.arsonsisi.com/
[140] S. Roels, P. Bacher, G. Bauwens, H. Madsen, and M. J. Jiménez, ‘Characterising the Actual Thermal Performance of Buildings: Current Results of Common Exercises Performed in the Framework of the IEA EBC Annex 58-Project’, *Energy Procedia*, vol. 78, pp. 3282–3287, Nov. 2015, doi: 10.1016/j.egypro.2015.11.726.
[141] G. Bauwens and S. Roels, ‘Co-heating test: A state-of-the-art’, *Energy Build.*, vol. 82, pp. 163–172, Oct. 2014, doi: 10.1016/j.enbuild.2014.04.039.
[142] A. Saltelli, ‘Making best use of model evaluations to compute sensitivity indices’, *Comput. Phys. Commun.*, vol. 145, no. 2, pp. 280–297, May 2002, doi: 10.1016/S0010-4655(02)00280-1.
[143] ‘ASHRAE Guideline 14-2002 Measurement of Energy and Demand Savings’. [Online]. Available: https://www.eeperformance.org/uploads/8/6/5/0/8650231/ashrae_guideline_14-2002_measurement_of_energy_and_demand_saving.pdf
[144] G. R. Ruiz and C. F. Bandera, ‘Validation of Calibrated Energy Models: Common Errors’, *Energies*, vol. 10, no. 10, Art. no. 10, Oct. 2017, doi: 10.3390/en10101587.
[145] ‘IEA EBC Annex 71-Building energy performance assessment based on in-situ measurements-Physical parameter identification’. [Online]. Available: https://www.iea-ebc.org/publications/
[146] C. Rasmussen, L. Frölke, P. Bacher, H. Madsen, and C. Rode, ‘Semi-parametric modelling of sun position dependent solar gain using B-splines in grey-box models’, *Sol. Energy*, vol. 195, pp. 249–258, Jan. 2020, doi: 10.1016/j.solener.2019.11.023.

[147] X. Zhang, D. Saelens, and S. Roels, ‘Estimating dynamic solar gains from on-site measured data: An ARX modelling approach’, *Appl. Energy*, vol. 321, p. 119278, Sep. 2022, doi: 10.1016/j.apenergy.2022.119278.
[148] C. de Boor, ‘A Practical Guide to Splines’.
[149] S. B. Joseph, E. G. Dada, A. Abidemi, D. O. Oyewola, and B. M. Khammas, ‘Metaheuristic algorithms for PID controller parameters tuning: review, approaches and open problems’, *Heliyon*, vol. 8, no. 5, p. e09399, May 2022, doi: 10.1016/j.heliyon.2022.e09399.
[150] ‘SMP11 Pyranometer User Manual’, Kipp & Zonen. [Online]. Available: https://www.kippzonen.com/Product/557/SMP10x-Pyranometer
[151] ‘Hukx pyranometer shading ring SHR02 user manual’. Accessed: Apr. 26, 2026. [Online]. Available: https://www.hukx.com/uploads/Hukx-SHR02-user-manual.pdf?v=1764066745
[152] D. G. Erbs, S. A. Klein, and J. A. Duffie, ‘Estimation of the diffuse radiation fraction for hourly, daily and monthly-average global radiation’, *Sol. Energy*, vol. 28, no. 4, pp. 293–302, Jan. 1982, doi: 10.1016/0038-092X(82)90302-4.